PROTON IRRADIATION AND GAMMA-RAY IRRADIATION TESTING
STUDIES ON THE COMMERCIAL GRADE GANFETS TO INVESTIGATE
THEIR CHARACTERISTICS UNDER THE SPACE RADIATION
ENVIRONMENT

A THESIS SUBMITTED TO
THE GRADUATE SCHOOL OF NATURAL AND APPLIED SCIENCES
OF
MIDDLE EAST TECHNICAL UNIVERSITY

BY

LÜTFİ BOYACI

IN PARTIAL FULFILLMENT OF THE REQUIREMENTS
FOR
THE DEGREE OF MASTER OF SCIENCE
IN
ELECTRICAL AND ELECTRONICS ENGINEERING

SEPTEMBER 2019

Approval of the thesis:

PROTON IRRADIATION AND GAMMA-RAY IRRADIATION TESTING STUDIES ON THE COMMERCIAL GRADE GANFETS TO INVESTIGATE THEIR CHARACTERISTICS UNDER THE SPACE RADIATION ENVIRONMENT

Submitted by **Lütfi Boyacı** in partial fulfillment of the requirements for the degree of **Master of Science in Electrical and Electronics Engineering Department, Middle East Technical University** by,

Prof. Dr. Halil Kalıpçılar
Dean, Graduate School of **Natural and Applied Sciences**   _____

Prof. Dr. İlkay Ulusoy
Head of Department, **Electrical and Electronics Eng.**   _____

Assist. Prof. Dr. Ozan Keysan
Supervisor, **Electrical and Electronics Eng. METU**   _____

Examining Committee Members:

Assist. Prof. Dr. Emine Bostancı
Electrical and Electronics Engineering, METU   _____

Assist. Prof. Dr. Ozan Keysan
Electrical and Electronics Engineering, METU   _____

Assist. Prof. Dr. Taner Göktaş
Electrical and Electronics Engineering, İnönü University   _____

Assist. Prof. Dr. Selçuk Yerci
Electrical and Electronics Engineering, METU   _____

Prof. Dr. Mehmet Timur Aydemir
Electrical and Electronics Engineering, Gazi University   _____

Date: 10.09.2019

I hereby declare that all information in this document has been obtained and presented in accordance with academic rules and ethical conduct. I also declare that, as required by these rules and conduct, I have fully cited and referenced all material and results that are not original to this work.

Name, Surname: Lütfi Boyacı

Signature:

ABSTRACT

PROTON IRRADIATION AND GAMMA-RAY IRRADIATION TESTING STUDIES ON THE COMMERCIAL GRADE GANFETS TO INVESTIGATE THEIR CHARACTERISTICS UNDER THE SPACE RADIATION ENVIRONMENT

Boyacı, Lütfi
M. Sc., Department of Electrical and Electronics Engineering
Supervisor: Assist. Prof. Dr. Ozan Keysan

September 2019, 110 pages

In this thesis, the radiation performances of the commercial GaNFETs were investigated for the possible future integration of these devices to the power subsystems of the satellites as a main switching power element instead of the Silicon MOSFET. Two main irradiation tests were applied to the GaNFETs, namely proton irradiation test, and gamma-ray irradiation test. By these tests, tough space radiation environment was simulated to understand the GaNFET's radiation performances.

In the proton irradiation test, it is aimed to investigate the device's performance of the Single Event Effect (SEE) which is the failure caused by the strike of the single high energetic particle. A GaNFET EPC2034 (200V, 48A) from Efficient Power Conversion Corporation (EPC) was chosen as a test sample considering the fact that it could be a possible candidate of the switch for the 100 V space bus designs. Four test samples were positioned on two test cards. They were irradiated with the 30 MeV protons while the devices are switching. A flux of 8.2×10^9 protons/cm^2/s is applied for 12.5 seconds for both test cards to reach ultimate fluence of 10^{11} protons/cm^2 as declared in ESCC Specification No. 25100. Real-time measurements were taken. V_{gs} - I_{ds} characteristics are measured and recorded for each device before, during and

after irradiation. It is observed that the devices retained their functionally. All the devices remained healthy and continued to operate. No failure was observed. Further irradiation is applied for one of the test cards (having two GaNFETs) with a destructive purpose. Same flux level is applied for 30 minutes up to a total fluence level of 1.476×10^{13} protons/cm^2 which is quite higher level than that of appointed in the ESCC standard. It is observed that the GaNFETs stayed fully functional under this elevated level of radiation and no destructive events and irreversible failures took place for transistors. This study showed that the irradiated GaNFETs are reasonably resistant to applied proton radiation.

In the gamma-ray irradiation test, the objective was to investigate the Total Ionizing Dose (TID), which corresponds to the cumulative radiation effect, performance of the devices. Two test samples were chosen, EPC2034 and GS61004B (100 V - 45 A) from GaN Systems, respectively. GS61004B was considered as a possible candidate of switch for the 28 V or 50 V power system buses. Nine irradiation test samples for each brand were assembled to two irradiation boards separately. In each board, three of the devices were biased from gate to source, three of them were biased from drain to source and the remaining three were unbiased to observe the bias effects on the device's radiation performance. The radiation dose was adjusted to 12,5 kRad (Si)/hour. Measurements were taken for the levels of 12.5, 25, 50 and 100 kRad respectively between the 1, 1, 2, and 4 hours of gamma-ray irradiation intervals. Gate to source voltages, drain to source voltages and drain current waveforms were recorded for the switching periods. Gate to source threshold voltages, gate to source plateau voltages, gate to source rise and fall times, and drain to source rise and fall times were analyzed for each device under test in detail. All the 18 devices stayed healthy and fully operational. No irreversible or destructive effects were observed. No meaningful or one-way change was noticed on the devices' gate to source threshold voltages and plateau voltages or rise and fall times. Characteristics and the performances of the devices have not changed. It was clearly observed that the

irradiated samples were radiation-resistant up to a total dose level of 100 kRad regardless of the bias condition.

ÖZ

UZAY RADYASYON ORTAMINDAKİ KARAKTERLERİNİ GÖZLEMLEMEK ÜZERE TİCARİ SINIF GANFETLER ÜZERİNDE PROTON IŞINLAMASI VE GAMA IŞINLAMASI TEST ÇALIŞMALARI

Boyacı, Lütfi
Yüksek Lisans, Elektrik ve Elektronik Mühendisliği Bölümü
Tez Danışmanı: Yrd. Doç. Dr. Ozan Keysan

Eylül 2019, 110 sayfa

Bu tezde, gelecekteki uyduların güç alt sistemlerinde, temel anahtarlama elemanı olarak silikon tabanlı MOSFET'ler yerine entegre edilebilmesi amacıyla, ticari sınıf GaNFET'lerin radyasyon altındaki performansı incelenmiştir. Proton ışınlama ve Gama ışınlama testleri olmak üzere GaNFET'ler üzerinde iki ana ışınlama testi yapılmıştır. GaNFET'lerin radyasyon performansının anlaşılabilmesi için uzayın zorlu radyasyon ortamı bu testler ile simule edilmiştir. Proton ışınlaması testinde, yüksek enerjili parça isabet etmesi sonucu oluşan tek olay etkilerine karşı komponentin performansının incelenmesi hedeflenmiştir. 100 V baralı uydu güç alt sistemleri için anahtar olarak kullanılması ihtimali göz önünde bulundurularak Efficient Power Conversion Corporation (EPC) firmasından EPC2034 (200V, 48A) GaNFET'i seçilmiştir. İki test kartı üzerine dört adet test örneği yerleştirilmiştir. Bu komponentler anahtarlama yaparken, 30 MeV enerjili hızlandırılmış protonlarla ışınlanmıştır. İlgili ESCC standardında işaret edilmiş olan 10^{11} protons/cm^2 toplam akı değerine ulaşmak için 12.5 saniye süre ile 8.2×10^9 protons/cm^2/s fluks uygulanmıştır. Işınlama öncesinde, esnasında ve sonrasında gerçek zamanlı olarak V_{gs}-I_{ds} karakterleri ölçülmüş ve kaydedilmiştir. Tüm komponentlerin fonksiyonelliğini koruduğu gözlemlenmiştir. Tüm komponentler sağlıklı kalmış ve

çalışmaya devam etmektedir. Herhangi bir hata gözlenmemiştir. Test kartlarından bir tanesi için bozucu olması amacıyla 30 dakika süre ile ilave ışınlama gerçekleştirilmiştir. Fluks seviyesi korunarak ESCC standardında belirlenen değerden oldukça yüksek olan $1.476x10^{13}$ protons/cm^2 toplam akı değerine ulaşılmıştır. Test edilen parçalar, oldukça yüksek bu radyasyon seviyesi altında tamamen fonksiyonel olarak kalmıştır ve yıkıcı veya kalıcı bir hata meydana gelmemiştir. Bu çalışma, ışınlanan GaNFET'lerin uygulanan proton radyasyonuna dayanıklı olduğunu açıkça ortaya koymuştur. Gama ışınlaması testinde, zaman içinde biriken etki olan toplam iyonlaşan doza karşı komponentin performansının incelenmesi amaçlanmıştır. EPC2034 ve GaN Systems firmasından GS61004B (100 V-45 A) olmak üzere iki farklı test örneği seçilmiştir. Test örneklerinden GS61004B, 28 V veya 50 V uydu güç baraları için muhtemel anahtar adayı olarak düşünülmüştür. Her markadan 9 adet test örneği iki farklı test kartına ayrı olarak yerleştirilmiştir. Işınlama esnasında, her test kartında, gerilimin parçanın radyasyon performansına etkisinin de gözlenebilmesi amacıyla, test örneklerinden üçünde kapı-kaynak pinleri arasına, diğer üçünde akaç-kaynak pinleri arasına gerilim uygulanmış, kalan üçü de gerilimsiz halde bırakılmıştır. Radyasyon dozu 12.5 kRad (Si)/hour olarak ayarlanmıştır. 12.5, 25, 50 ve 100 kRad seviyelerinde ölçümler alınmıştır. Bu ölçümlerde kapı-kaynak gerilimleri, akaç-kaynak gerilimleri ve akaç akımları dalga şekilleri anahtarlama periyotları için kaydedilmiştir. Test altındaki her malzeme için kapı-kaynak eşik gerilimi, kapı-kaynak plato gerilimi, kapı-kaynak yükselme ve düşme süreleri ve akaç-kaynak yükselme ve düşme süreleri detaylıca analiz edilmiştir. Test edilen 18 parçanın tamamı sağlığını korumuş ve işlevsel kalmıştır. Komponentlerin kapı-kaynak eşik değerlerinde, plato gerilimlerinde, yükselme ve düşme sürelerinde anlamlı veya tek yönde bir değişim tespit edilmemiştir. Parçaların karakterleri veya performansları değişmemiştir. Test edilen komponentlerin, uygulanan gerilim koşullarından bağımsız olarak 100 kRad'a toplam iyonize dozuna dayanıklı olduğu açık şekilde gözlenmiştir.

Anahtar Kelimeler: GaNFET, Proton Işınlama Testi, Gama Işınlama Testi, Tek Olay Etkileri, Toplam İyonize Dozu

x

Dedicated to my father with eternal gratitude

ACKNOWLEDGMENTS

TABLE OF CONTENTS

LIST OF TABLES

LIST OF FIGURES

FIGURES

xix

LIST OF ABBREVIATIONS

ABBREVIATIONS

BCR	Battery Charge Regulator
BDR	Battery Discharge Regulator
CME	Coronal Mass Ejections
COTs	Commercial of the Shelf
DD	Displacement Damage
DUT	Device Under Test
ECSS	European Cooperation for Space Standardization
EM	Engineering Model
EPS	Electrical Power System
ESCC	European Space Components Coordination
FM	Flight Model
GaN	Gallium Nitride
GaNFET	Gallium Nitride Field Effect Transistor
GCR	Galactic Cosmic Ray
GEO	Geosynchronous Orbit
IC	Integrated Circuit
I$_{ds}$	Drain to Source Current
LEO	Low Earth Orbit
LET	Linear Energy Transfer
MEO	Medium Earth Orbit
MOSFET	Metal Oxide Semiconductor Field Effect Transistor
NASA	National Aeronautics and Space Administration
PCU	Power Conditioning Unit
PDU	Power Distribution Unit
SEB	Single Event Burnout

SEE	Single Event Effect
SEGR	Single Event Gate Rupture
Si	Silicon
TAEA	Turkish Atomic Energy Agency
TID	Total Ionizing Dose
V_{gs}	Gate to Source Voltage
V_{ds}	Drain to Source Voltage
2DEG	Two Dimensional Electron Gas

CHAPTER 1

INTRODUCTION

1.1. About Spacecrafts and Power Systems

A satellite means an object launched to space and orbiting around the earth or another space object. A satellite needs to escape from the atmospheric conditions of the earth to be in an orbit. Today, thousands of human-made satellites orbit the earth for different purposes. According to "Online Index of Objects Launched into Outer Space" of the United Nations Office for Outer Space Affairs (UNOOSA), a total of 8545 objects launched to space in the past and currently, 5102 of them are at the orbit. A chart showing the yearly launch number distributions can be investigated from Figure 1.1.
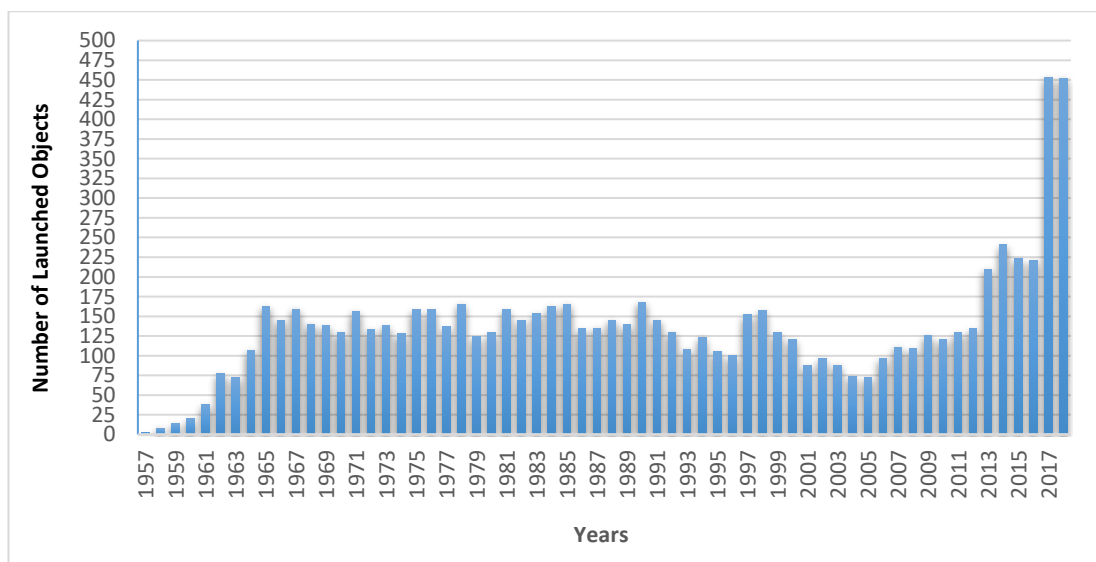
Figure 1.1 Number of launched objects per year (UNOOSA data, May-2019)

Various satellites orbit the earth at different altitudes, paths, and speeds depending on their missions. The three most common orbit types are low Earth orbit (LEO), medium Earth orbit, and Geosynchronous orbit (GEO) which can be listed as in [1]:

> ➢ Low Earth Orbit (LEO): an altitude which is less than 1500 km
> ➢ Medium (altitude) Earth Orbit (MEO): an altitude between 8000 – 25000 km
> ➢ Geosynchronous Earth Orbit (GEO): an altitude between 25000 – 60000 km (typically 36000 km)

Figure 1.2 Main orbits, [credit: Robert Simmon, NASA]

A satellite consists of various subsystems to fulfill its operational duties. The power system is one of the principal subsystems belonging to the bus in terms of its complexity, cost, mass, and volume. According to [2], the power system constitutes between 25% (for LEO satellites) and 45% (for GEO satellites) of the satellite dry mass. It consists of main equipment named power generation unit (solar arrays), energy storage unit (battery), power conditioning unit (PCU), and power distribution unit (PDU). A typical block diagram of the power system having a regulated bus philosophy can be seen in Figure 1.3. A real satellite PCU equipment example of the Airbus can be seen in Figure 1.4.

2
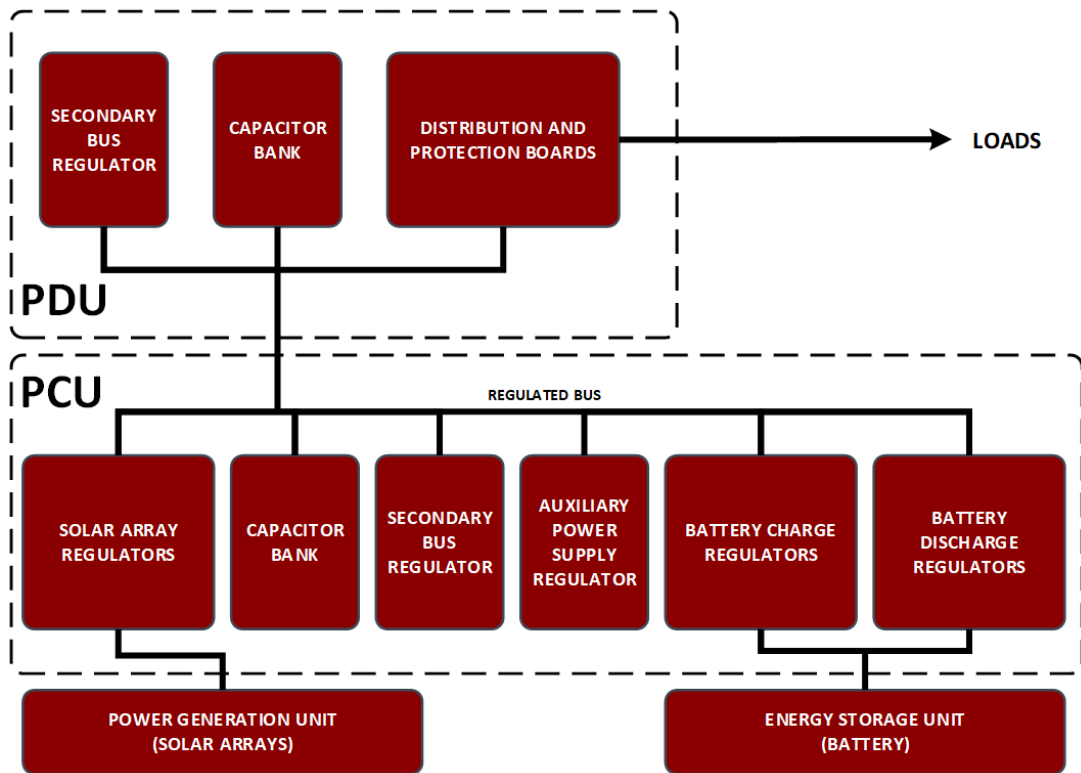
Figure 1.3 Example power system block diagram
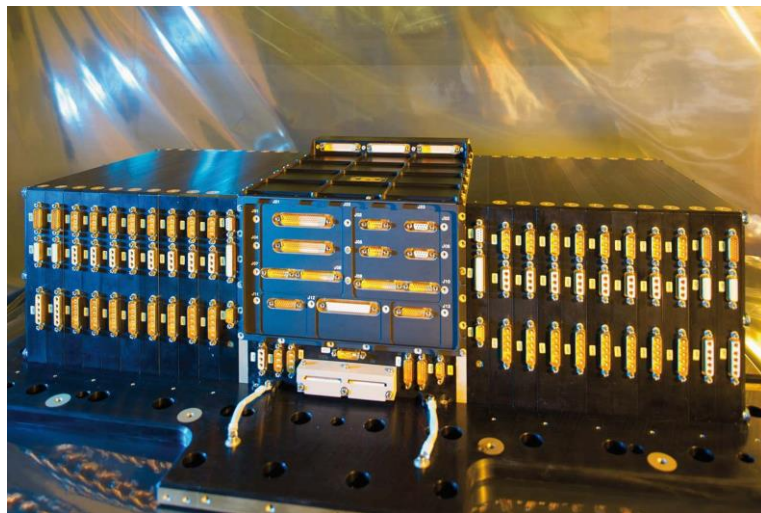
Figure 1.4 PCU equipment of the Airbus for regulated bus systems

3

In space, the external source of energy is the available solar radiation. In the eclipse period and when the arrays are under the shadow, the energy needed by spacecraft loads is supplied by the discharge of the energy store unit, the battery. Discharge is performed by the battery discharge regulators of PCU. Battery management units, including special protection circuits, are used to avoid undervoltage or overvoltage on the chemical Li-ion battery cells for their health. Battery charge regulators are responsible for converting the bus or panel voltage (according to power system configuration) to battery voltage with different charge mode options, constant voltage, constant current, etc. Apart from battery charge and discharge boards, PCU contains many functions and units. Solar panel regulators are one of them and used to regulate the power bus voltage by transferring the power in the solar panels to the bus by checking the solar panels' surplus power. Low-level voltages required by logical and control circuits and secondary bus voltage needed by the particular equipment are generated on the specific converter boards in the PCU or PDU.

1.2. Problem Definition

In NASA's current study [3], power systems are investigated for various space missions. In this study, the cost and the mass data of the radioisotope power systems (RPS) in which the energy is produced by the nuclear source and the solar EPS in which the power source is sun are collected. In Figure 1.5, the power system's cost percentage on the spacecraft, and in Figure 1.6, the mass percentage on the spacecraft bus can be seen. In brief, an average of different missions, power system constitutes 27 % and 24 % of the total bus mass for nuclear and solar EPS, respectively. Likewise, the power system constitutes 26 % and 11 % of the overall spacecraft cost for nuclear and solar EPS respectively.
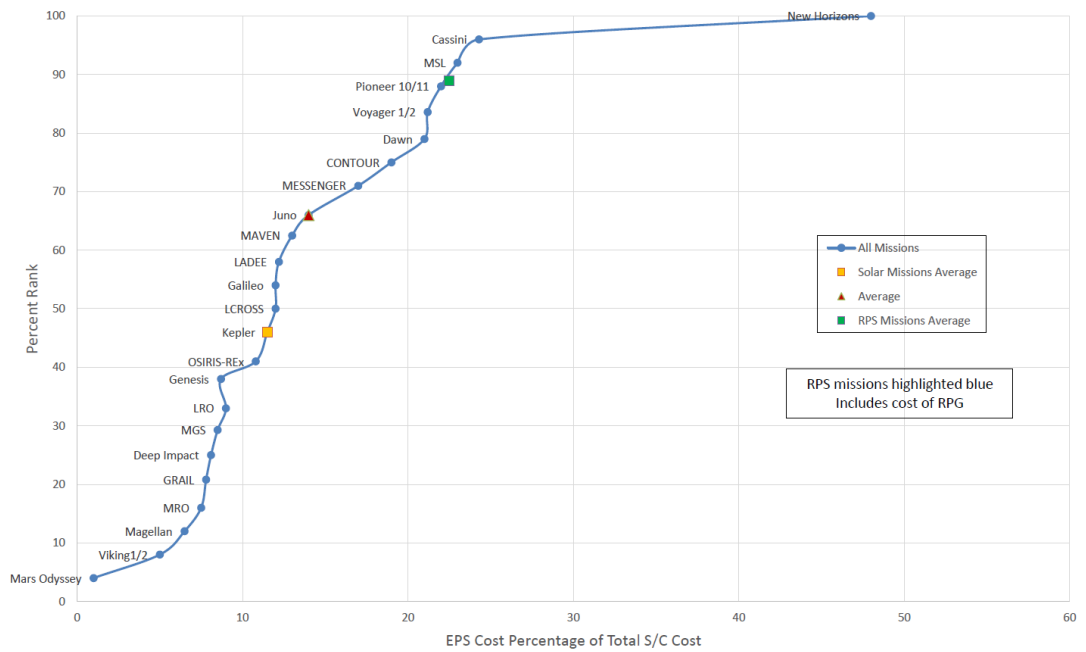
Figure 1.5 Cost percentage of the power system on the total system cost for various missions [3]
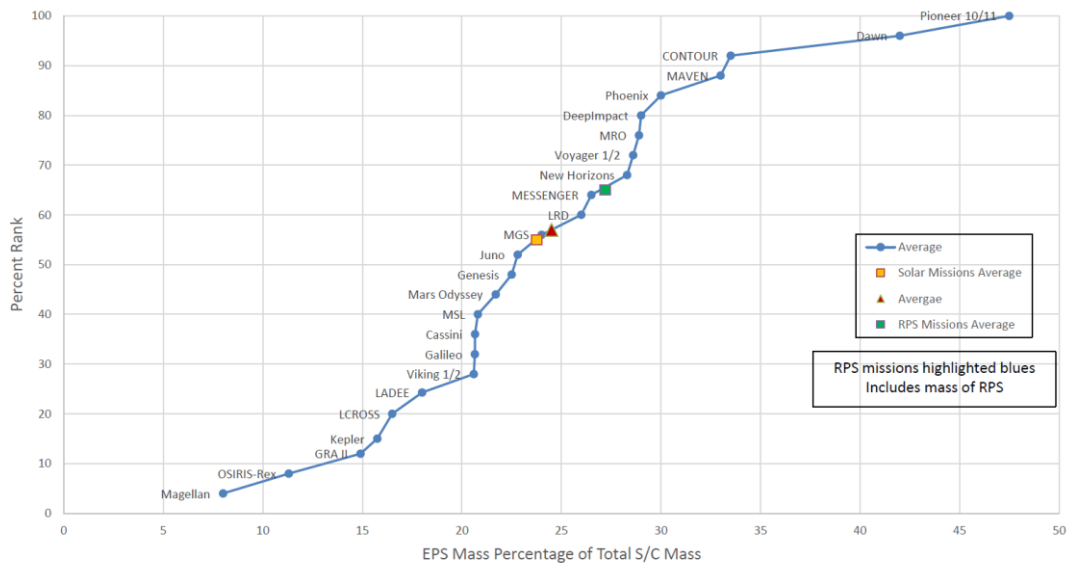
Figure 1.6 Mass percentage of the power system on the total bus mass of spacecraft for various missions [3]

It is obvious that an effort to make the power subsystem low-cost will directly affect the total spacecraft expenditure. Besides, the mass percentage of the power subsystems

over the total spacecraft bus mass is above 25% for several missions as can be seen in Figure 1.6. Struggles to reduce the mass of the power subsystem will certainly lead to the reduction of the mass of the system, resulting in a reduction in the launch cost. In a space area, increasing efforts are underway to reduce the cost of launching. In [2], It is reported that the average cost of putting one kilogram of the spacecraft into low earth orbit is around $ 10000, and it is $ 50000 for geostationary orbit missions.

In light of the above information, it is clear that the reduction of the power system cost significantly affects the total system cost in a positive way. Besides, a reduction in the power system mass considerably reduces the total launching cost. Thus, a quite remarkable question arises: "how can the mass and cost of the power system be reduced?"

1.2.1. How to Reduce the Mass, Volume, and Cost of the Power System?

Power controller unit (PCU) of the power system is mainly composed of the necessary converter boards, such as battery charge regulator, battery discharge regulators, solar array regulators, built-in power supplies, etc. as can be seen in Figure 1.7. All of the mentioned converters need necessary filter components both at their output and input to filter out noise or ripple, reduce the EMI, limit inrush current, avoid transients, etc. These components are mainly composed of inductors and capacitors as seen in Figure 1.7. Roughly, they constitute 50-80% of the total weight of the electronic elements on the board. As can be seen from the example board pictures, these parts take up quite a lot space on the cards and it is clear that they are reasonably massive compared to other electrical components. On the other hand, some cards, such as the capacitor bank in PCU and PDU equipment, are almost merely capacitors and are very heavy, e.g. 3-5 kg each.
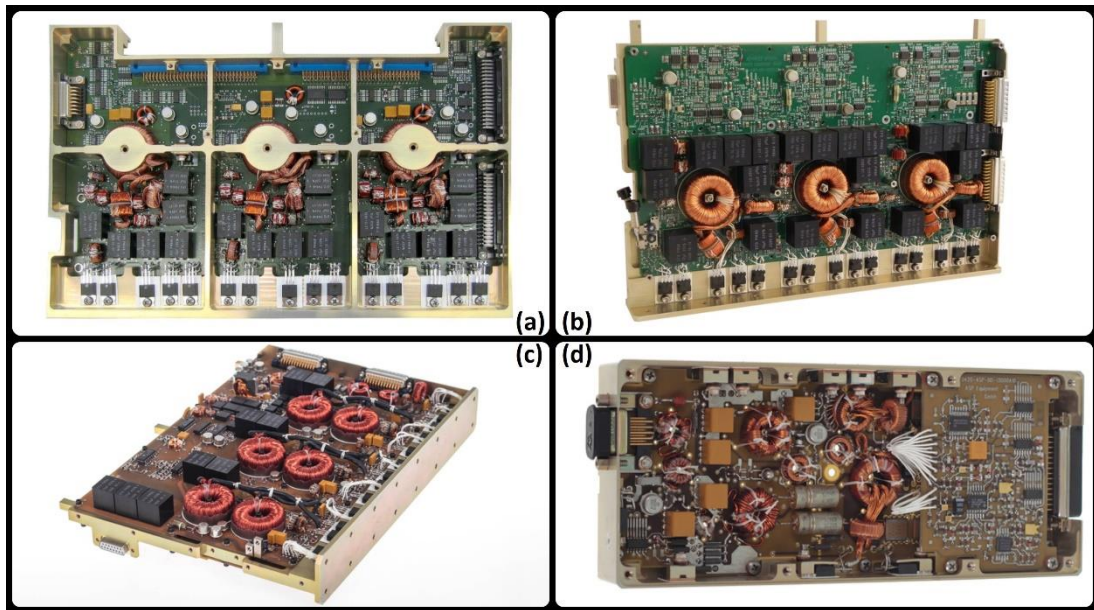
Figure 1.7 ASP, Advanced Space Power Equipment GmbH's space power boards: (a):Solar array regulator, (b): Buck-Boost regulator, (c): MPPT power control unit, (d): High-efficiency DC-DC converter

Capacitance and the inductance values of these filter components are inversely proportional to the switching frequency of the converter. For instance, the output LC low pass filter of the buck converter has the cut-off frequency of $\frac{1}{2\pi\sqrt{LC}}$ [4]. Assuming that a designer is decided to put the cut-off frequency of the output filter to the one-twentieth of the switching frequency, and if the switching frequency is 100 kHz, low pass filter cut-off frequency is supposed to be 5kz. For example, if she can somehow shift the switching frequency to 500 kHz, the cut-off frequency of the filter becomes 25 kHz. In this way, the product of the inductance and the capacitance values (LC) could become 4% of the previous design. Shrinkage of the packages of the filter components has two main advantages. The first one is the direct reduction of their mass. The second is the reduction in the weight of the aluminum tray on which the cards are mounted. The basic elements that determine the tray height are usually the highest ones which are generally the filter components as seen in Figure 1.7. Besides, the thickness of the aluminum support walls between the two sides of the tray is directly dependent on the weight of the board. It should be noted that lower value filter elements will be low-cost compared to ones with higher values. As a sum of all, as the

7

mass of the PCU equipment decreases, the satellite mass will also decrease, and the launching cost will be reduced.

However, increasing the switching frequency to the 500 kHz is not so realistic, since that much high level brings some other problems with it. Today, the basic switching element commonly used in these space power circuits is Silicon (Si) based radiation-hardened MOSFET. For the MOSFET, increasing the switching frequency above a certain optimum value significantly increases the switching losses. Turn-on and turn-off losses, gate drive loss, and output capacitance loss are directly proportional to the frequency [5], [6]. Therefore, increasing the frequency after a specific value causes a loss of efficiency. Further, excessive loss on the MOSFETs will also cause heating problems. Even without high switching frequency (250 kHz - 1 MHz), heating is a major problem for MOSFETs in space power designs and the bottom of the tray is used as an aluminum heat sink for them to get rid of heat as shown in Figure 1.7 (a),(b), and (c). Even in this case, one of the main electronic parts limiting the qualification temperature of the equipment is the MOSFET.

In the light of all, the option to raise the frequency and reduce the mass and cost does not seem to be possible with today's MOSFETs. Since the MOSFET is the mature technology, today's space power boards are at their limit in terms of frequency, efficiency and etc. Therefore, it is needed to use and integrate another technology instead of MOSFET as the main switching element to realize all these improvements by frequency increasing. Wide bandgap semiconductors, that go beyond the limits of Si-based MOSFETs would be new options owing to their superior switching performances. Especially the GaNFETs are the principal candidate in this context, with their fast switching capabilities.

1.2.2. Space vs. Industrial Power Components

Since there is no repair or maintenance option for the spacecraft in its operation lifetime, it is supposed to be free of critical failures. Therefore, reliability is a primary

concern for space designs. Since the space environment is harsh with its radiation sources, vacuum condition and wide operational temperature ranges, space electronic components are supposed to be insusceptible to these tough conditions. Therefore, in the aerospace industry, special components that are more reliable due to their extensive testing/screening, materials, technology, packaging, processes, etc. are used. These materials are both less produced and more tested compared to their counterparts in the commercial industry. As a result, there is an extraordinary price difference between industrial and space components. One can investigate the typical costs of the N-channel and P-channel commercial and space MOSFETs in Table 1.1.

Today, a new trend is to use the commercial of the shelf (COTs) components instead of the space-qualified parts if it is possible depending on the missions and equipment. For example, NASA and several other space agencies have a heritage of using commercial components in the spacecraft even for the mission-critical functions [7], [8]. They regularly conduct studies on the availability of commercial components in space [8].

Of course, using the COTs components has both advantages and disadvantages. First, the biggest advantage is their being low-cost as shown in Table 1.1 for other electronic components. Secondly, they have higher-performance compared to space equivalent versions. Furthermore, they are more advantageous from the logistic perspective, since the purchase lead times for the space-qualified components are extremely high for some components – some have lead time around a year. As there is an unreasonable minimum order quantity in some space products; sometimes, unnecessary purchase more than needed has to be done. However, the main deficit of the COTs components is that they are less reliable than the space-qualified parts because the space parts have strict specifications and test methods and periodically audited by the related agencies. Vibration, humidity, oxidation, and radiation capabilities are stronger as well for the space-parts. One needs to take the risk if it is desired to use the COTs instead of radiation-hardened and space-qualified equivalent for its benefits, especially the cost, and the performance.

9

Table 1.1 Example price comparison for commercial and space-qualified MOSFETs

MOSFET	V_{ds}-I_{ds}	Price	Type
Brand-A	200V, 45A	$ 3	N-channel, Commercial
Brand-B	200V, 42/45A	$ 1250	N-channel,100 kRad Radiation Hardened
Brand-C	200V, 42/45A	$ 1900	N-channel,100 kRad Radiation Hardened
Brand-D	-200V, -11A	$ 2	P-channel, Commercial
Brand-B	-200V, -8/8.5A	$ 830	P-channel,100 kRad Radiation Hardened
Brand-C	-200V, -8/8.5A	$ 1000	P-channel,100 kRad Radiation Hardened

It is obvious that there is an extraordinary price difference -over 400 times- between commercial and radiation-hardened space MOSFETs with similar ratings. This price difference is mainly due to the reliability difference between two parts since the space parts are subjected to extra tests and finely screened. Besides, they are manufactured with different technologies to improve radiation performance and packaged with special materials for radiation shielding and hermeticity [9]. Space-qualified and radiation-hardened MOSFET is used as the basic switching element in the satellite power subsystem. Almost all of the converter boards extensively use it as seen in Figure 1.7. Most of the distribution boards in the PDU equipment use the MOSFET very common and it is at the top of the basic cost items of the PDU equipment. The total cost of these components is very high for PCU and PDU equipment. Using the commercial MOSFET instead of the radiation-hardened ones will significantly reduce the cost of PCU and the PDU equipment, however, it is not practically possible for the spacecraft with a significant operational lifetime without proven radiation performance of the device even if the detailed upscreening/testing is done for it.

The electrical properties and the functionality of the MOSFET deteriorates over the years in the space environment which is full of the radiation sources. The commercial MOSFETs are especially weak in terms of their radiation performances. The most

common radiation-induced problem is the falling of the V_{gs-th} voltage of the MOSFET even below to 0V which means the loss of the device's controllability. Trapped charges created by the ionizing radiation in the gate oxide layer, cause a negative shift on gate-to-source turn-on threshold voltage of the MOSFET. If this shift becomes remarkably high, the MOSFET cannot be turned off even if no bias voltage is applied to gate-source. Thus, MOSFET fails and becomes a normally-on type (or depletion mode).

Utilizing the commercial MOSFET instead of the radiation-hardened version in the spacecraft design is not reliable as obvious due to their weak radiation performances. Instead of the commercial MOSFET, another component with the same function can be considered to replace the radiation-hardened MOSFET to decrease down the PCU and PDU equipment's cost and to improve the electrical performance. New wide-bandgap technologies, Silicon-Carbide (SiC) based and Gallium-Nitride (GaN) based transistors, can be regarded as the counterpart of the MOSFET in terms of device's function. Silicon Carbide (SiC) is a wide bandgap material and SiC power MOSFET is a relatively new technology comparing to silicon-based ones. In favor of their high electric field breakdown and advantageous thermal properties, SiC MOSFETs are more favorable, especially for high voltages (>800V) in proportion to Si MOSFETs. However, the generally accepted bus voltages of the satellites are at around 120V as maximum, depending on the satellite power requirement. Therefore, the GaN-based Transistors (GaNFETs) would be a more suitable option to replace the MOSFET.

1.3. Performance Comparison of Silicon and GaN-Based Power Transistors

In section 1.2.1, the importance of the power system for a satellite in terms of the total system mass and the budget is discussed. In this section, a method is proposed to reduce the total cost and the mass of the power subsystem and thus to reduce the launching costs by substantially decreasing the weight of the overall system. This method is increasing the switching frequency as possible reminding that the current

11

Si-based MOSFET technology is mature enough and at the edge of its limits to increase the frequency level to the high value that will make a significant difference. In section 1.2.2, it is examined how effective the total MOSFET cost over the total power subsystem cost. Then, it is proposed to use commercial (considering the possible risk) or technology as a replacement of the radiation-hardened space-qualified MOSFET. These two fundamental ideas of change are putting the GaNFETs as an option.

Silicon-based MOSFET is generally accepted and used switching element both for the commercial power industry and space power industry. Over three-decades, from 1976 to 2010, there have been many developments for MOSFET in terms of device technology and structure [10]. However, the improvements today are slowing down and almost reaching the theoretical performance limit [10], [11] for Si-MOSFETs. On the other hand, the first enhancement-type gallium nitride on silicon (eGaN) field effect transistor (FET) was introduced as the replacement of power MOSFETs by the Efficient Power Conversion Corporation (EPC) in 2009 [10]. GaNFETs behave quite similar to MOSFET with some exceptions. First, it is a gate-voltage controlled device, and it needs to be enhanced by positive gate voltage in a similar manner as MOSFET. The basic difference is that the proper gate drive voltage is supposed to be 4-5 V for GaNFETs, and it is inconvenient to exceed 6V. Gate threshold voltages are also around 1 V which is smaller than that of the MOSFET. GaNFETs have a short path between drain and source, therefore the die size is much smaller than that of MOSFET and on-resistance is lower as well, thanks to smaller conduction path. Thus, they are advantageous over the MOSFET in terms of conduction losses. In fact, the main advantage of GaNFET is its switching performances. Compact die size enables GaNFET to have smaller parasitic, such as input and output capacitances and internal inductances and therefore they have improved switching speeds compared to MOSFET. They have quite a high capacity of critical electric field compared to silicon, meaning that the much higher V_{ds} voltage withstanding capability for the same R_{ds-on} resistance [12].

Three of the main loss constituents that creates the total hard switching loss of the FET are:

- Gate Charge Loss: $Q_{gate} * V_{drive} * f_{switching}$
- Switching Transition Loss: $\frac{1}{2} * V_{drain} * I_{drain} * (T_r + T_f) * f_{switching}$
- Output Capacitance Loss: $\frac{1}{2} * C_{oss} * V_{drain}^2$

It is obvious that the gate charges, output capacitances, rise and fall times of the device are the main factors that determine the switching losses of the devices for a specific frequency. If the device has lower values for the mentioned properties, it has a lower loss and higher efficiency values for the specified frequency. In other words, the switching frequency of the device can be increased up to a higher level for the same loss and efficiency value of the design if the gate and output charges/parasitic are low.

Part Code	EPC2034	IRFB42N20DPbF	IRHMS6S7260	GS61004B	STD45N10F7	IRHMS6S7160	IGT60R190D1S	TK13A60D
Notes	EPC, enh-mode GaN transistor	Infineon, Power MOSFET	IRF, Rad-Hard Power MOSFET, TO254	GaN Systems, enh-mode GaN transistor	ST, Power MOSFET,	IRF, Rad-Hard Power MOSFET, TO254	Infineon, enh-mode GaN transistor	TOSHIBA Power MOSFET
Vds (V)	200	200	200	100	100	100	600	600
Ids (A)	45	44	45	45A	45A	45	12.5	13
Rds-on (mOhm)	10	55	29	15	14.5	11	190	330
Qgate (nC)	8.8	91	240	6.6	25	170	3.2 (VDS = 400 V)	40 (VDS = 400 V)
Qoss (nC)	75			11.5			16	
Coss (pF)	450 (Vds = 0 to 100)	530 (Vds = 25V) 5310 (Vds = 1V)	953 (Vds = 25V)	133 (Vds = 80V)	360 (Vds = 50 V)	1600 (Vds = 25V)	28 (Vds = 400 V)	250 (Vds = 25 V)
Ciss (pF)	950	2900	8045 (Vds = 25V)	328	1640	8877	157 (Vds = 400 V)	2300 (Vds = 25 V)
Tr (ns)		69	60		17	125		50
Tf (ns)		32	30		8	30		25

Figure 1.8 Benchmarking study for enhancement-mode GaN transistors, commercial Si-MOSFETs and radiation-hardened Si-MOSFETs

In Figure 1.8, some of the critical datasheet parameters for the commercial GaNFETs, commercial MOSFETs and radiation-hardened MOSFETs having the same V_{ds}-I_{ds} ratings can be observed. In the first group, 200V-44/45A devices could be compared. It can be interpreted that the GaNFET is superior to the commercial and the radiation-hardened Si-based MOSFETs in terms of switching performance parameters, noting that the conduction performance is better than others as well. It can be said that the input and output capacitance values of the GaNFET are also quite low compared to the others. For example, the gate charge of the 200V rad-hard MOSFET is 27 times larger than that of the GaNFET. It should be noted that the switching performance of the radiation-hardened MOSFET is also lower than the commercial

version with the same ratings. The second group is composed of 100V-45A devices. Similar conclusions can be made with the previous group. Among the second group, gate charge, input, and output capacitance values are reasonably low for the GaN device. Input capacitance of the rad-hard MOSFET is 27 times higher than that of GaNFET. Similarly, its gate charge is 25 times of the gate charge of the rad-hard MOSFET. It should also be noted that the switching characteristics of the commercial version of the MOSFET are better than the rad-hard version. The third comparison group has a higher voltage rating, 600V-12,5A/13A. There is no rad-hard version included for this group. Conclusions are the same for this group. Gate charge is 12.5 times, output capacitance is 9 times, input capacitance is 14 times, on-resistance is 1.7 times larger for commercial MOSFET compared to commercial GaNFET. Gate charge and output charge figure of merits for GaN-based and Si-based devices can be investigated in more detail in Figure 1.9.
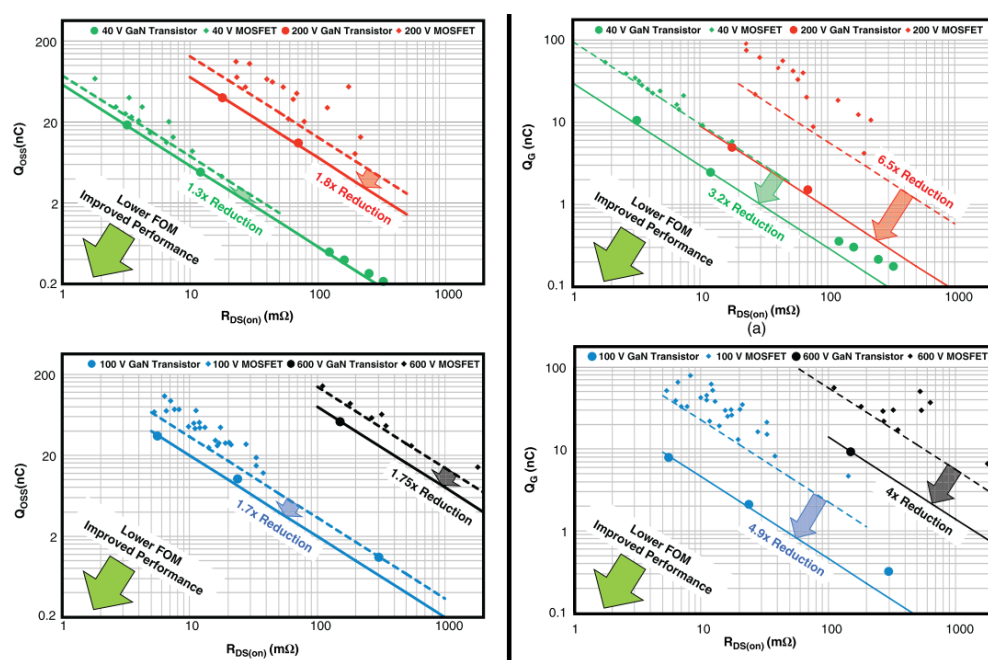
Figure 1.9 Output (left) and gate charge(right) figure of merit comparison for 40V, 100V, 200V and 600V GaN and Si transistors [12]

In [12], efficiency comparison of the GaNFET and MOSFET-based eighth-brick converter and half-brick PSE converters can be investigated for 36 V, 48 V, and 60 V

devices. For all comparisons, the GaNFET based ones are clearly superior to Si-based ones. Besides, efficiency and the power loss comparison can also be investigated for the synchronous buck converter. Similarly, the GaNFET based converters have lower loss and higher efficiencies. In [13], simulation results for the efficiency and loss comparison of the same rating GaNFET and MOSFET can be investigated for different frequencies from 25 kHz to 1 MHz for a 400 V boost converter application. In [14], efficiency comparison can be observed for the buck converter application for different frequencies. In [10], loss components are compared for GaN and Si devices for buck converter in detail. In short, all these references point to the superiority of the GaNFET over the MOSFET in terms of loss/efficiency performances.

1.4. Integration of the Normally-off Type GaNFETs Into the Space Power Designs

Unlike MOSFETs, GaNFETs can be regarded as recent technology because the first enhancement-mode GaNFET was introduced in 2009. It took for the MOSFET more than 30 years to reach its current technology/performance level. Even though the GaNFET is at the beginning of the road, it is clear that it is superior to mature Si-based MOSFETs. It is gradually replacing the MOSFET in industrial power designs. This change will surely be reflected in space power designs as time passes. In general, space designs resist change if there is already a proven system (a space heritage). The space designs are quite conservative, and many space companies have been continuing their old designs for years. As the GaNFETs don't have enough cumulative data for energy/power systems and especially for space power systems, their reliability is a big puzzlement today for the space industry. One of the main concerns in space designs is reliability. Thus, it takes some time for space power designers to integrate this new technology into their designs which are unwilling to change.

With the failure data obtained from the industry over the years, the electrical reliability of the GaN power transistors will already be revealed. Furthermore, the widespread

availability of space-compatible GaNFETs over the years will benefit the spread of its use in the spacecraft designs. Besides, other space electronic components serving the GaNFET operation -such as GaNFET driver- should be available in the space market.

For the GaNFET to be used in a space application having a long operational lifetime and harsh mission environment, radiation performances of the non-space-compatible parts for different radiation particles, such as the proton, heavy ions, gamma rays, etc., should be examined in detail and proved to be as positive. After the successful test results, sending it to space within the non-critical function to make it gain space heritage would be the next step. Once these steps have been accomplished, the use of GaNFETs in space power designs will become increasingly common.

1.5. Motivation and Research Objectives

Other than the electrical performance, the radiation performance of the GaNFET is a critical issue that needs to be addressed. If a designer is willing to use commercial GaNFET, she/he needs to be sure that the appointed GaNFET is resistant to the radiation environment in which it is supposed to operate in the mission. In [11], it is mentioned that the GaNFET has the ability to withstand the space radiation environment inherently. In [15], it is claimed that GaN semiconductor devices are inherently radiation-hard to total ionizing radiation dose. In [16], the intrinsic radiation robustness of the GANFET is mentioned.

To be used in the space, GaNFET must be proven to be resistant to the radiation environment they will be exposed to in the mission. This point is the main research topic of this thesis study. In this study, characteristics of commercial enhancement mode type GaNFETs under the radiation are observed experimentally by simulating the space radiation conditions by proton and gamma-ray irradiation tests.

Normally-on GaNFETs have been in use since the early 2000s, and their characteristics under the influence of the proton irradiation have been examined

16

several times [17]–[21]. Normally-off (enhancement mode) GaN transistors are relatively newer technology than the normally-on ones and continue to evolve. In Figure 1.10, the internal structure of the EPC's enhancement-mode (E-mode) GaN transistor is shown. Attracted high mobility electrons at the AlGaN and GaN interface form a two-dimensional electron gas (2DEG) layer in which carriers move across.
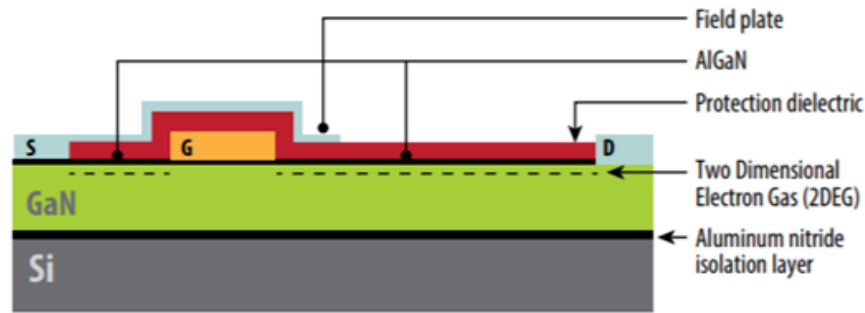
Figure 1.10 The inner structure of the EPC's enhancement-mode GaN power transistor

In [22], it is explained that this internal structure is naturally resistant to radiation. It is reported that if the electron is transferred from the 2DEG to the AlGaN layer by the radiation-induced effect, 2DEG tends to pull it back again. A similar mechanism applies to the opposite way. If the electrons are spread into the GaN layer, they are attracted back toward the 2DEG by the piezoelectric field.

What makes the commercial MOSFET susceptible to radiation is mainly the gate oxide layer in its internal structure. The charge accumulation in the oxide layer by the ionization causes the characteristics to be disturbed. Because the commercial power MOSFETs require thick gate oxides due to higher operating voltages, negative threshold voltage shifts take place by the radiation due to the trapped charges in the oxide layer. Unlike MOSFET, the GaNFETs do not contain oxide layers. Therefore, the GaNFETs are free of the trapped gate oxide positive charges by the ionizing radiation. Therefore, no performance degradation is expected by the TID for the GaNFETs.

To the best of author's knowledge, normally-off type power GaNFETs are not currently used in the power subsystems of today's in-orbit satellites with considerable operational life. Before implemented in real space applications, radiation effects must be accurately evaluated for the enhancement mode GaNFETs. Their proton and heavy-ion induced Single Event Effects (SEE) performance and Total Ionizing Dose (TID) effects performance should be evaluated according to [23] and [24]. There are no abounding radiation studies with enhancement-mode GaN transistors. In [25], no SEE is observed by Xe, Kr, and Au irradiation for 40V rated normally-off type devices for any voltage on the gate or drain. However, for 100V and 200V rated devices, SEE is reported as a drain current increase over 1 μA by xenon ion irradiation. Similarly, another study declares no SEE failure for 40V rated enhancement mode devices but destructive SEB as sudden drain leakage current increase for 100V and 200V devices by heavy ion irradiation [26]. Especially proton test studies with the normally-off GaNFETs are scarce in the literature. In [27], 40V devices were exposed to 800 MeV protons in both clocked and DC-biased conditions. No changes were observed during the monitored clocked condition.

This thesis is a pioneer in terms of the start of the studies which is conducted to integrate the GaNFETs to the spacecraft power subsystems. This is first conducted proton irradiation test on a component with real-time measurement and complying with the related standards in Turkey to the best of the author's knowledge. Besides, there are quite limited studies in the literature that made proton irradiation on the GaNFETs. Therefore, this study is one of the first examples of proton testing on GaNFETs. It is certain that the gamma-irradiation study of this thesis is one of the limited studies conducted in Turkey in compliance with the standards. As the planning, production, and testing phases are also explained in detail, this thesis is also important as a guide for future proton and TID tests.

1.6. Thesis Organization

In chapter 1, it is discussed how critical the power system is in terms of the total satellite mass and cost. In section 1.2.1 and 1.2.2, the mass and cost reduction methods for the power system of the satellite were discussed. They are namely, to increase the switching frequency by using a new technology/part instead of Si-based MOSFET and to use another low-cost technology instead of extraordinary costly radiation-hardened MOSFET. At this point, the GaNFETs emerge as a common solution for these two ideas. In section 1.3, the excellence of the GaNFET's performance over the performance of the MOSFET is discussed. In section 1.4, steps for GaNFET to be integrated into the space power designs are explained. In section 1.5, the research objective which is mainly to investigate the radiation performance of the GaNFET under the proton and gamma-ray irradiation is explained. Before the mentioned test details, in chapter 2, the space radiation environment is introduced for better understanding of the concept. After that, the possible effects of the radiation on the electronic components and the failure mechanisms are presented. In chapter 3, the proton irradiation testing on the commercial GaNFET which is done in the proton acceleration facility established in the Turkish Atomic Energy Agency is explained. In chapter 4, gamma-ray irradiation testing which is done in the Turkish Atomic Energy Agency (TAEA) - Gamma Irradiation Facility on two types of commercial GaNFETs to investigate cumulative effects of the space radiation is reported. In chapter 5, It is discussed what kinds of gains will be achieved if GaNFETs are integrated into power subsystem designs.

CHAPTER 2

SPACE RADIATION ENVIRONMENT AND ITS HAZARDOUS EFFECTS

This chapter begins with an explanation of the tough space radiation environment for space vehicles and electronic components. First, the space radiation sources and particles are summarized in detail. Next, dangerous radiation effects on the electronic components with the failure mechanisms behind them are explained. Finally, how to integrate the GaNFETs into the space power designs is discussed.

2.1. Space Radiation Environment

Over the years, with the gained experiences from the space missions, space radiation sources just as solar-based charged particles, galactic cosmic rays, and earth radiation belts are discovered and better understood. From the beginning of the space era to these days, many operational failures took place on satellite systems. As a result of detailed investigations of these failures, it is understood that the main reasons for these anomalies are space radiation environment, problems based on electronics, design mistakes, lack of quality and problems due to unknown reasons. In [28], it is declared that 20% of the spacecraft malfunctions with determined causes take place in consequence of space radiation. It should also be noted that about one-third of the reasons of satellite failures are still unknown.

The earth's radiation belts are one of the primary sources of space radiation particles. The Earth is one of the planets in our solar systems having a magnetic field. This magnetic field causes magnetic belts that trap charged particles because of the Lorentz Force and cause the charged particles to move almost periodically in specific zones. These belts are also called Van Allen Belts because radiation belts were first discovered by J. Van Allen at the beginning of the space era, late of the 1950s.

Radiation belts begin where the earth's atmosphere ends because the atmosphere eliminates trapped particles. According to [28], radiation belts are mainly composed of electrons and protons having the energy levels between 1keV-7 MeV and 1keV-300 MeV, respectively. There exist at least two radiation belts around the earth called inner and outer belts, noting that there were also more than two belts in the history. The outer is mainly consisting of electrons, and the inner includes both protons and electrons. Particles are particularly concentrated in some areas as shown in Figure 2.1.
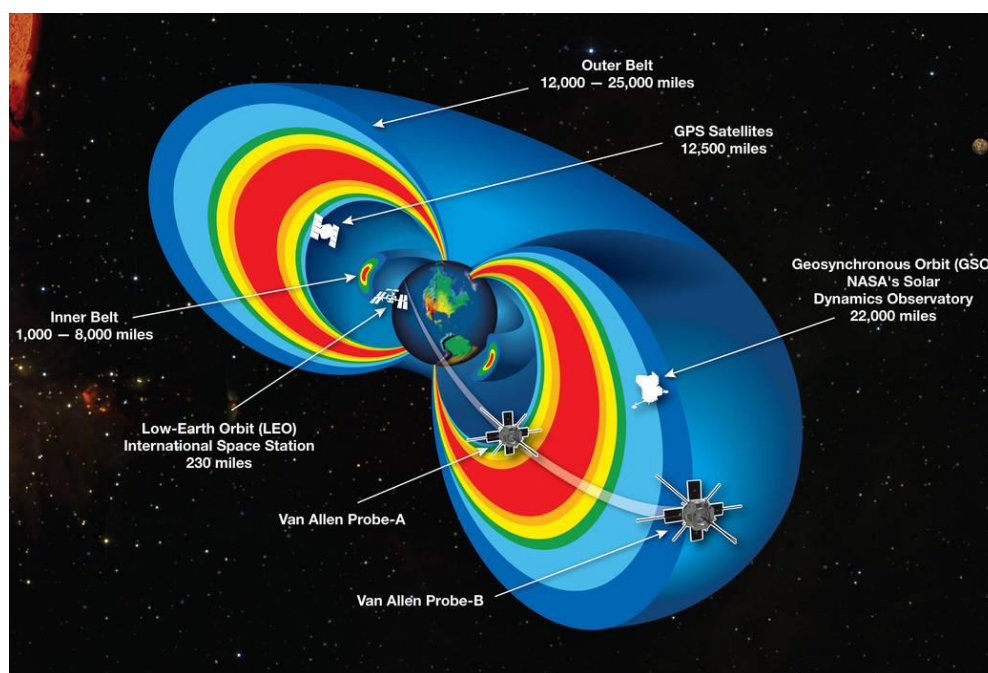
Figure 2.1 Figure showing the radiation belts [Credit: NASA]

The sun is another primary source of the charged radiation particles. Solar activities comprise of typically eleven years of periodical cycles. The eleven years of the solar period can be divided into two groups and named as solar maximum and solar minimum, respectively. Solar activities come off intensively in a solar maximum period, which lasts approximately seven years. In four years of the solar minimum period, solar activities are relatively low. On the other hand, in the solar minimum period, the trapped proton and galactic cosmic ray fluxes are at their maximum level.

The solar-based particles arise from two major categories, solar flares and coronal mass ejections (CME), respectively. While the former is prone to be rich in electrons, the latter is prone to be proton-intensive. In [28], It is reported that the hadrons originated from CME are composed of protons (96.4%), alphas (3.5%) and heavy ions (0.1%) with the energies up to 1 GeV, the fluence level up to 10^{10} cm^{-2} and the flux level up to 10^5 cm^{-2}s^{-1}. Total Ionizing Dose (TID) and Displacement Damage (DD) permanent damages could take place mainly due to protons arise from CME. Besides, all these particles -heavy ions, protons, and alphas- could lead to permanent or transient SEE.
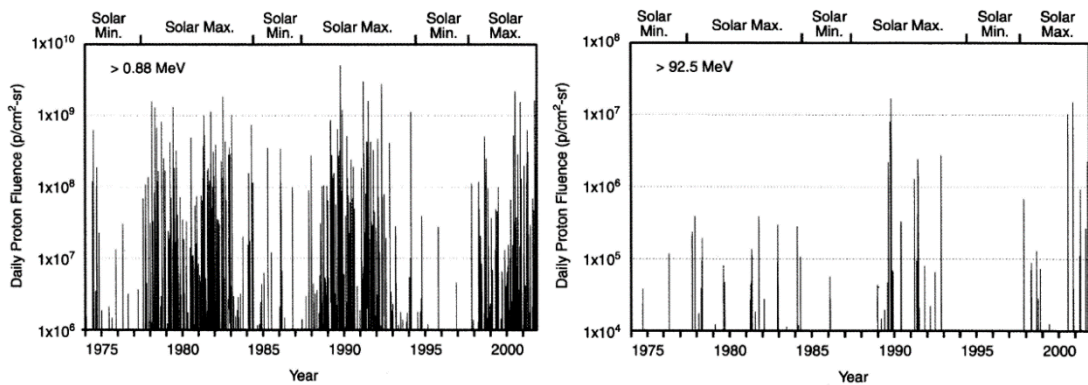
Figure 2.2 Solar events based daily fluences between 1974-2002 for >0.88 MeV and >92.5 MeV protons [28]

Figure 2.2 shows the daily fluence levels separately corresponding to >0.88 MeV and >92.5 MeV protons measured by GEO satellites and an interplanetary monitor platform in approximately 28 years. Solar maximum and solar minimum periods can be obviously observed from the figure. Based on these measurements, it is clear that the higher energetic protons are rarer compared to lower energetic ones. Solar wind consisting of weak protons and electrons is another sun-based radiation source, but it is generally ignored because it is dinky compared to solar flares and CMEs and hazardous with low probability only for components assembled outside of satellite.

The galactic cosmic rays (GCR) which are originated from the outside of the solar system, are yet another radiation source for satellite orbits. One remarkable estimation for the origin of cosmic rays is the supernovas. However, the exact cause is still

unknown. According to [28], the galactic cosmic rays are composed of protons (87%), alphas (12%) and heavy ions (1%) with the energy level up to 10^{11} GeV and flux levels from 1 to 10 $cm^{-2}s^{-1}$. It is also stated that the main effect resulting from the GCR is SEE.

Basically, space radiation effects can be divided into two main categories as cumulative and occasional effects. Cumulative effects appear as degradation of electronic components' performance in time. On the other hand, occasional effects can be defined as single event effects (SEE) on electronic components or circuits.

2.2. Radiation Effects on Electronic Components

The radiation environment for a spacecraft is quite mission dependent. For example, if the spacecraft is supposed to operate in Low Earth Orbit (LEO), the designers should take into consideration the trapped particles, solar particles, and GCR. However, if it is an interstellar mission, the designers could ignore the trapped particles. On the other hand, possible effects depend on the radiation environment which is dependent on orbit profile, technologies of the components used, and design details such as voltage level, frequency, duty cycle, temperature, redundancy philosophy, etc.

Figure 2.3 shows the basic diagram corresponding to radiation particles and their effects on the electronic parts.
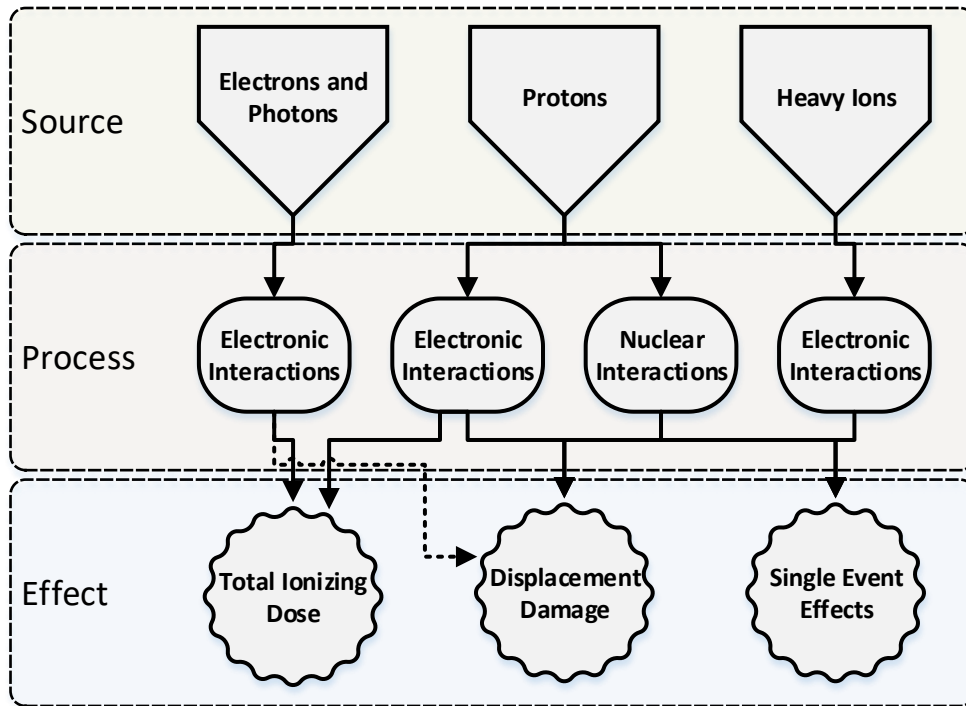
Figure 2.3 Diagram showing the radiation effects on the electronic components (this figure is drawn according to its original form given in [29] *)*

Sources of the radiation particles are mainly discussed previously in section 2.1. According to Figure 2.3, there are two main interaction types between the radiation particle and the device. According to [29], it is needed for the radiation source to interact with the atomic nucleus directly for the realization of nuclear interaction. The nuclear interaction with the nucleus is possible only for protons among the radiation particles in the diagram. The higher the energy transferred in nuclear interaction, the easier it will be to displace, break up to small parts, or explode the atom. The effects of nuclear interactions are more drastic compared to electronic interactions; however, the probability of nuclear reactions to take place is lower compared to the electronic ones. On the other hand, for the electronic interaction, the incident particle interacts with the electrons surrounding the atom. The energy of the radiation particle is transferred to the atom by this interaction. Excited electrons ionize within the higher energy level atom.

2.2.1. Total Ionizing Dose (TID)

Basically, when the radiation particle interacts with the electronic component, it imparts its energy and jumps the electrons inside the material's structure to the higher energy state, and positive charges are created in the remaining vacancies. Besides, the mobility of the electrons increases and conduction gets more comfortable even if it is in non-conductive material. For example, for a semiconductor device having a silicon (Si)/Silicon-Dioxide (SiO_2) interface, just as modern CMOS technology based electronic ICs, a positive charge created by ionization can be trapped at the Si/SiO_2 interface. Therefore, the conduction behavior of the device may change, and leakage currents may increase. The ionizing effect accumulates in time and higher the dose rate in time means more severe the effects.

Applying a shielding material to cover a component is a method to mitigate the TID effects. If the radiation particle loses a part of its energy while passing through the shielding, the ionization effect decreases down and even die out if all the particle energy is lost through the shielding. Shielding thickness and material selection are quite crucial because adding more and more weight for shielding makes the system heavy and heavy. Placing a massive system into space is also costly. Besides, the effectiveness of the shielding is not linear with the shielding thickness and expanding the thickness from a certain value is useless. Therefore, A tradeoff analysis for cost-reliability is needed for the optimization of the shielding design. In [30], it is stated that the penetration capability of the protons is higher than the electrons. Besides, depending on the orbital data from three LEO satellites, 8-14 mm thick shielding wears away the effects of the electrons, but it is not that much useful for diminishing the proton effects as shown in Figure 2.4.
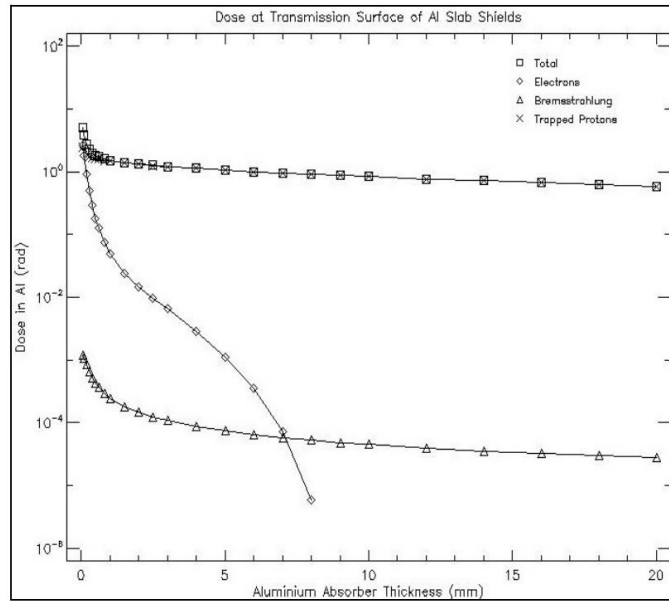
Figure 2.4 Shielding thickness vs. ionization dose data from Razaksat (666-689 km LEO) [30]

2.2.2. Displacement Dose (DD)

Another accumulating time-dependent effect is displacement damage. Unlike TID, nuclear interactions could also lead to displacement damage in addition to electronic interactions. The energy lost during the interaction causes atom to warm up by vibration. If this energy is higher than the interatomic bonding energy, it may cause the atom to change its original position within the crystal lattice structure. Consequently, when the atom is "displaced", the original atomic structure of the crystal lattice is disrupted and hence the principal operational behavior of the device may get worse. This can lead to a new conduction path, which is previously absent, causing leakage current or short circuit. The reverse is also possible if the atoms are displaced from the conduction planned paths. For example, amplification characteristics of the bipolar junction transistors (BJT) may degrade. Another example is given in [29] as follows. Solar cells are mainly based on p-n junction diodes of which the light illuminates to one side. With the radiation exposure in time, diodes lose their effectiveness resulting in an increase of leakage current, a decrease of the

internal electric field, a shorter lifetime of new electrons. Therefore, the solar cell's efficiency decreases during satellite operation.

2.2.3. Single Event Effects (SEE)

As the name indicates, Single Event Effect (SEE) is the effect caused by a single radiation particle that hits and passes through the electronic component. It refers to random failure modes. Both high energetic protons originated from radiation belts or sun and heavy ions rooted in galactic cosmic rays could be the cause of SEE. The last letter E, corresponding to the word "effect" includes many sub-effects, e.g., Latch-up (L), Transient (T), Gate Rupture (GR), Burnout (B), etc. Therefore the SEE acronym change as SEL, SET, SEGR, SEB, etc. according to corresponding sub-effects. These various effects can be classified under two main headings, namely nondestructive and destructive effects.

2.2.3.1. Destructive SEE

Destructive single event effects can be described as the effects which lead to permanent failure of the device's whole or specific functions. The device can no longer function properly if the destructive effects occur. According to [31], observable failure in data state or output takes place due to destructive SEE, and it is the main cause of fault or damage in the device's internal structure. Because the device is permanently destroyed as a result of destructive SEE, it is called "hard errors". Four primary destructive SEEs are described as below:

➢ Single Event Latch-up (SEL): It is a formation of a low impedance path which causes high current to pass through it as a result of triggered parasitic thyristor inside device structure by radiation ion[23]. It is a catastrophic and permanent mechanism, and once the device is latched, excessive current flows between power and ground until the power is turned off.

➢ Single Event Gate Rupture or Single Event Dielectric Rupture (SEGR or SEDR): It is a breakdown of a layer inside the device structure or gate oxide, and it results from the strike of radiation ion[23]. The result is high leakage current with applied

28

bias, and the SEGR is mainly specific to power MOSFETs. [32] (MIL-ST-750 Method 1080) defines the SEGR as a rapid leakage current rise on the gate when the drain and/or gate is biased under irradiation. The failure occurs at a voltage which is lower than the rated voltage of the MOSFET in general. Therefore, it is one of the reasons why a designer needs to use the MOSFET by derating the maximum voltage rating written in the datasheet.

➢ Single Event Burn-out (SEB): When the single radiation ion hits the MOSFET device, electron-hole pairs are created through its path. Forward bias resulted from these pairs turns on inherent parasitic BJT and makes it conduct current unintentionally. As a result of high current and thermal anomaly, MOSFETs are destructed permanently[33].

2.2.3.2. Non-Destructive SEE

As its name indicates, non-destructive SEEs do not annihilate or damage the electronic component itself. The effect generally appears as transient or temporal and disappears after a while. Therefore, the circuit can return its original operational mode again in a short period when the excess charges are removed from critical junctions of the device's internal structure. In the non-destructive SEE scenario, only the output of component or circuit changes for analog circuits. Besides, the data state of the affected node can change for digital circuits. In both cases, radiation does not damage the components, and merely the output or data are disrupted. Therefore, non-destructive SEEs are generally mentioned as soft errors [31].

➢ Single Event Upset (SEU): It is erroneously changing of a logic node from zero to one or vice versa. An SEU is not persistent, and the corrupted logic node can be reset or rewritten [23]. SEU forms a permanent data failure; however, the component itself is not damaged internally. After the faulty data overwritten with the necessary, correct data, the circuit continues to function correctly [31].

➢ Single Event Functional Interrupt (SEFI): It is a soft failure which causes malfunction of a device such as a reset, lock-up, etc. [23].

➢ Single Event Transient (SET): It is a temporary voltage spike due to the impact of an energetic particle at a particular node in a linear or logic integrated circuit [23]. They are mainly referred as an analog pulse at the output that reaches to correct voltage value eventually.

According to [29], two main factors determining how severe the effects are energy and Linear Energy Transfer (LET) which are valid for protons and heavy ions correspondingly. LET is the unit that shows the energy lost by the radiation particle while passing through the material. Because the energy of a particle could diminish along the path it moves in the particle, direction and path depth is effective on the LET. Therefore, the unit of LET is mega electron-volt per centimeter (MeV/cm) and includes the effect of the path length. Directional or path depth dependency is not valid for proton nuclear interaction, and hence the energy of the particle is used for proton.

Different than the TID and DD, shielding has almost no effect on the mitigation of SEE if the device is not excessively susceptible to low energy protons or low LET ions. Other mitigation techniques, mainly based upon circuit designs, are generally applied to mitigate the effects of single events. One SEE mitigation technique is quite common in power subsystems of the satellites. The main aim of this technique is to create the majority voting for critical signals. A critical signal is sent from three different paths, and it is assumed to have only one error occurs in these paths at the same time. As a result, at least two of the sent signals will be correct, and one of the majorities (one of two correct signals or one of three correct signals) is transferred.

Lastly, it would be useful to report commercial MOSFET's radiation performances. Various radiation test results for commercial power MOSFETs are reported in the literature. For instance, in the [34], Single Event Effect (SEE) test results are given for three different power MOSFETs as follows:

- For IRHLF87Y20 (International Rectifier, 20V, N-channel, radiation-hardened logic level power MOSFET), destructive effects (SEGR and SEB) are observed by 1039-MeV Ag (LET=48 MeV•cm^2/mg) irradiation at $V_{ds} = 20V - V_{gs} = 0V$, $V_{ds} = 18V - V_{gs} = -2V$ and $V_{ds} = 16V - V_{gs} = -3V$.

- For Si7414DN (Vishay, 60V, N-channel power MOSFET), failures are declared at 33V V_{ds} by Ar (548 MeV & 400 MeV and LET=14&9.7 MeV•cm^2/mg) irradiation and 45V V_{ds} by Ne (283 MeV, LET=2.7 MeV•cm^2/mg) irradiation.

- Besides, it is declared that gate degradation is observed at 375 V by Ar (466 MeV, LET$_{SiC}$ = 9.3 MeV•cm^2/mg) and gate-drain degradation is observed at 200 V by Cu (566 MeV, LET$_{SiC}$ = 24 MeV•cm^2/mg) for the Silicon Carbide (SiC) power mosfet CPM2-1200-0025B (CREE, 1200V-98A, N-channel)

- In [35], 250 MeV proton irradiation results are reported for MOSFET with unknown part code. According to results, the drain leakage current of the MOSFET is increased from 1.68 µA to 2.89 µA, and the gate threshold voltage is decreased down to 0.8V from 1.3V.

- In [36], the TID irradiation test results were reported for both biased and unbiased conditions for two p-channel power MOSFETs form ST (-60V, -3A) and Infineon (-100V, -4A). According to results, for a biased state, the gate threshold voltage change is more severe for both MOSFETs and static drain on-resistance (R_{ds-on}) change is more notable for Infineon's MOSFET. While the inverse diode voltage drop change is more critical for a biased condition for ST's mosfet, Infineon's mosfet is more susceptible for the unbiased condition

2.3. Summary of the Chapter

This chapter was intended for a better understanding of the space radiation environment and its effects on the electronic parts. First, the radiation sources namely, sun, galactic cosmic rays, and radiation belts were introduced. Then, the radiation particles such as electrons, protons, photons, and heavy ions were mentioned together

with their sources. It should especially be noted that almost all radiation sources are rich in protons. Secondly, the interactions with the radiation particles and material and their effects on the components were discussed. It is important that the protons are the only particles among the all which have the nuclear interaction capability with the material. Besides, all the electronic components in the space designs are exposed to total ionizing dose in time depending on the mission operational lifetime. Therefore, the proton irradiation testing and the TID testing with the commercial GaNFETs in this thesis are of great importance for the realistic simulation of the space radiation environment.

CHAPTER 3

PROTON IRRADIATION TESTING ON NORMALLY-OFF TYPE GANFETS

In this chapter, proton irradiation on an enhancement type GaNFET is investigated. EPC2034 GaNFETs from EPC [37] were irradiated with 30 MeV protons up to a fluence level of 1.476×10^{13} protons/cm^2 which is 147 times higher concentration than 10^{11} protons/cm^2 appointed in ESCC 25100 standard. In this way, space radiation environments, especially cosmic ray, trapped particle, and solar flare particle environments which comprise protons are simulated. SEE is divided into non-destructive (e.g., single event upsets, transients, functional interrupts, etc.) and destructive (e.g., single event latch-ups, burnouts, gate ruptures, snapbacks, etc.) effects. The destructive effects involve permanent damage to the affected part [38]. In this proton irradiation experiment, the aim was to observe if there would be any damaging effects resulting in the device's irreversible operational failure. It was observed that devices sustained their switching operation during and after the proton exposure.

3.1. Proton Irradiation Testing Overview

The primary Single Event Effects testing standard that gives direction to the present chapter of this thesis study is namely ESCC Basic Specification No.25100 – Single Event Effects Test Method and Guidance [23]. Test procedures and necessary productions were mainly prepared by considering the instructions written in this standard. It is useful to give basic definitions of the subject before referring to the direction written in the ESCC spec. No.25100.

33

- ➢ **Flux:** It refers to the total radiation ion number in a unit time that passes through the perpendicular unit area to the beam. Flux unit: Ions/cm^2/sec (Protons/cm^2/sec for proton). [23]

- ➢ **Fluence:** It is the integration of the flux over the irradiation time interval. Fluence unit: Ions/cm^2. (Protons/cm^2 for proton). [23]

- ➢ **Energy:** Conveyed energy from accelerator to the radiation ion. Generally preferred energy unit is MeV. For SEE irradiation with high energetic protons, the energy can be regarded as a reference unit. Threshold energy corresponds to the minimum energy needed for SEE to take place.

- ➢ **Linear Energy Transfer (LET):** It corresponds to total energy lost by the radiation ion while passing through the exposed material and striking the electrons of the atoms. It is represented with the energy per unit length. LET unit: MeV/cm or MeV/mg/cm^2 or. For SEE irradiation with heavy ions, the LET can be regarded as a reference unit.

Because the basic definitions are explained, before introducing test preparation steps, it would be useful to mention instructions given in the ESCC spec. No.25100.

According to [23], the field of radiation needs to be distributed uniformly, and the maximum allowed deviation from the fluence or energy uniformity on the target area is 10 % as maximum. In [23], it is also declared that the high energetic proton facility shall be able to supply protons having the energy range of 20-200 MeV with adjustable flux level from 10^5 p/cm^2/s to the minimum of 10^8 p/cm^2/s to the DUTs. If the irradiation is performed with high energy protons, the device under test can be irradiated in the air with its package, and there is no need to open the device package[23]. The radiation beam is generally applied normal to the device.

According to [23], it should be given importance for test infrastructure, including test boards and necessary cabling to be noise-free. Cable length needs to be kept as short as possible to inhibit interference[32]. Besides, the test setup should be capable of sensing and recording of the single event transients if it is planned to be monitored.

To detect single event functional interrupts, the part shall be tested under its possible working conditions if it is possible. To allow for destructive single event burnout to occur, high drain resistance overly limiting the drain current should be avoided. Proper gate stress (typically, more than half of the datasheet rated gate voltage value) should be applied for destructive single event burnout to be able to take place. Low temperature or room temperature is suggested as a worst-case condition for SEB and SEGR.

On the other hand, according to [23], for the non-destructive effects' characterization, the minimum sample size should be two at least, and three samples are recommended as general. For the destructive event characterization, the minimum sample size should be 3. Statistically, it is more convenient to have a larger number of test samples to specify the failures in a more detailed way. Samples should be identical to each other in terms of technology and production methods [23]. The real-time data handling, measurement, display, and storage capabilities of the test system makes it more practical and functional.

In [23], the typical test duration is declared as between 1 to 20 minutes. Considering this irradiation period, the flux value should be chosen such that the valuable or remarkable number of single events can build up. Accordingly, recommended target fluence level for heavy ions is 10^7 ions/cm^2 [23], [32] while for the protons it is given as 10^{11} protons/cm^2 [23].

3.2. Test Preparation

Two test PCBs having two GaNFETs on each were planned to be produced. The block diagram of the circuit schematic for each test PCB is shown in Figure 3.1. Frequency/duty adjustable square wave was designed to be generated from the timer IC. Driver ICs drive GaNFETs, and the drain currents are controlled by the external load resistors. Drain currents were to be sensed by current sense ICs and with sense resistors through drain current paths. LM555 timer IC from Texas Instruments (TI)

for switching frequency and duty adjustment, UCC27611 low side GaN driver IC from Texas Instruments (TI) to drive transistors, AD8212 current sense IC from Analog Devices (AD) to measure drain current were chosen for the irradiation test PCBs. The output of AD8212 was named as $I_{ds-sensed}$. 47-Ω external load resistor was determined to be connected through the drain current path to adjust the I_{ds} current around 1 A. V_{gs} voltage was decided to be sensed by the resistor divider, and divider output was named as $V_{gs-sensed}$. Sensed I_{ds} and V_{gs} signals were planned to be connected to the headers for external cable connection for real-time measurements before, during, and after irradiation.
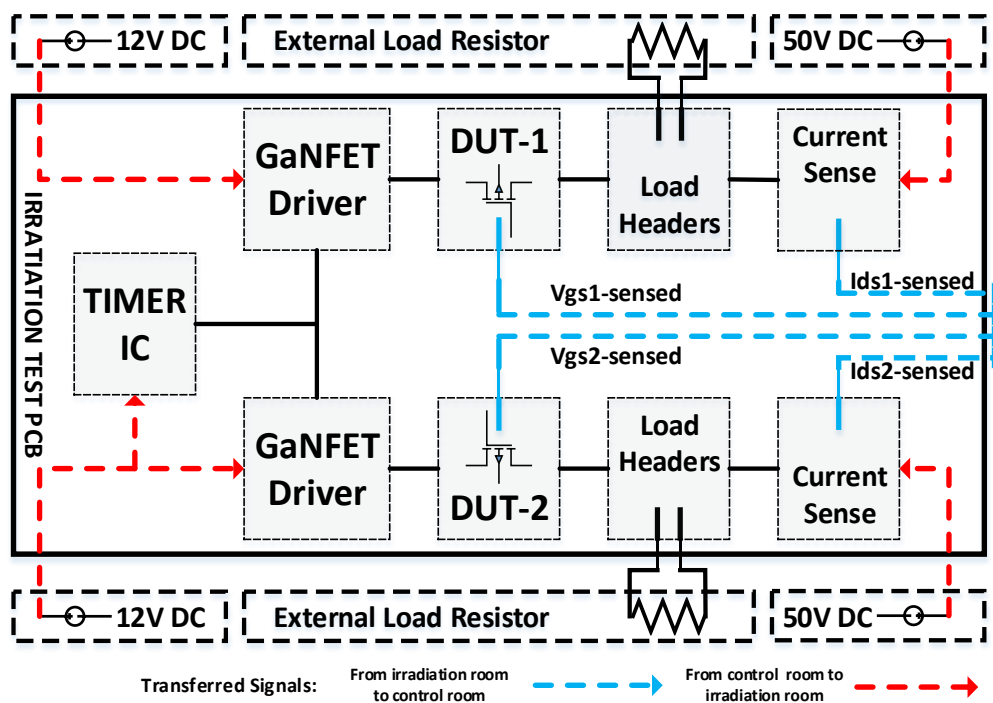
Figure 3.1 Block diagram of the schematic configuration of the individual test PCB

3.2.1. Fabrication of Test PCBs

Because of the reasonably long half-life of the copper, it was understood that the radiation remains for a long time on the PCB proportional to the amount of copper on it. Therefore, it was decided to minimize the amount of the copper on printed circuit

boards to reduce the take-back time of the boards from the irradiation room after the tests. Thus, the test boards were planned and designed as a single top layer without the bottom layer. The take-back time of the test PCBs from the irradiation room was calculated as 4-5 days by considering the copper area and thickness of the single-layer PCBs.

3.2.1.1. PCB Production, Assembling and Visual Inspection with X-RAY

Empty PCBs were produced as one layer by scraping of copper plates. EPC2034 has 200V-48A ratings and has a dimension of 2.6 mm x 4.6 mm. Device Under Test (DUT) is a BGA package, and the bottom view of the device is shown in Figure 3.2. After assembling the parts, PCBs were controlled for soldering defects under BGA packages by using the X-RAY machine as shown in Figure 3.3.
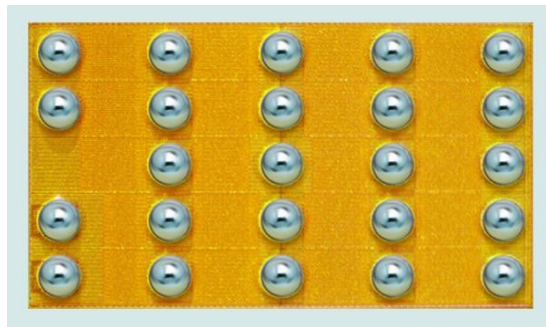
Figure 3.2 Bottom view of the BGA package DUT (EPC2034)
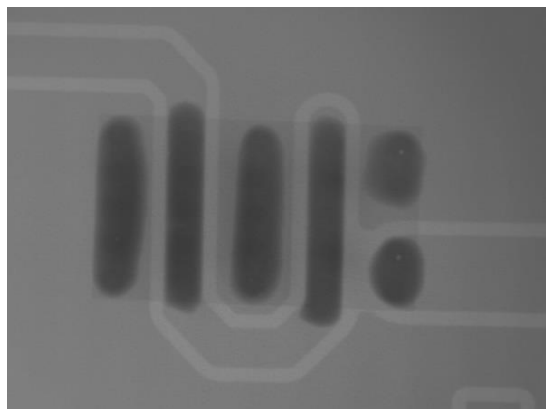
Figure 3.3 X-RAY image of soldered DUT

The DUTs were located in the center of the board and radiation-sensitive commercial components which are LM555, UCC27611 and AD8212 were positioned to the bottom and up side of the PCB top layer in a way that they were as far as away from irradiation area in which the DUTs were positioned. Test PCBs and components' positioning can be seen in Figure 3.4.
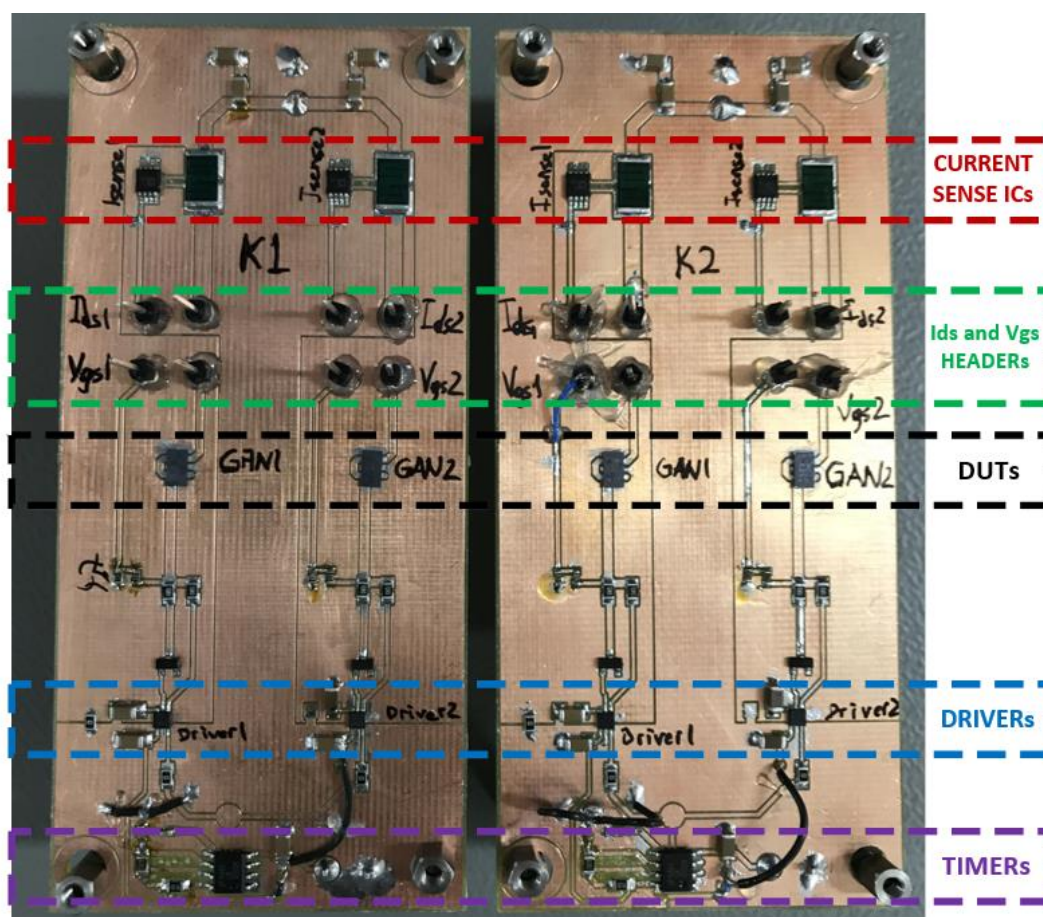
Figure 3.4 Top view of two irradiation test PCBs

3.3. Pre-Testing

Before the irradiation test setup installation in proton accelerator facility, preliminary electrical test studies were done in The Scientific and Technological Research Council of Turkey - Space Technologies Research Institute (TUBITAK-Space) test facilities.

From the laboratory tests in TUBITAK-Space, one of the oscilloscope screen view corresponding to V_{gs}-I_{ds} measurements of the DUT1 on test PCB1 is shown in Figure 3.5. Drain current was adjusted to 1A (exact value: 1.05A) for the ON condition of GaNFETs. Rise time and fall time for V_{gs} are 118 ns and 72 ns, respectively. Drain voltage was determined as 50 V, and the duty cycle was adjusted to 53.4 %. These two values simulate a possible open circuit voltage of solar panel of the LEO earth observation satellite and possible operational duty cycle for buck converter-based battery charge regulators. Frequency is set to 1 kHz (exact value: 1.07 kHz). In section 3.4, is it explained why the 1 kHz switching frequency was chosen instead of commonly-held switching frequencies of converter circuits used in spacecraft power subsystems.
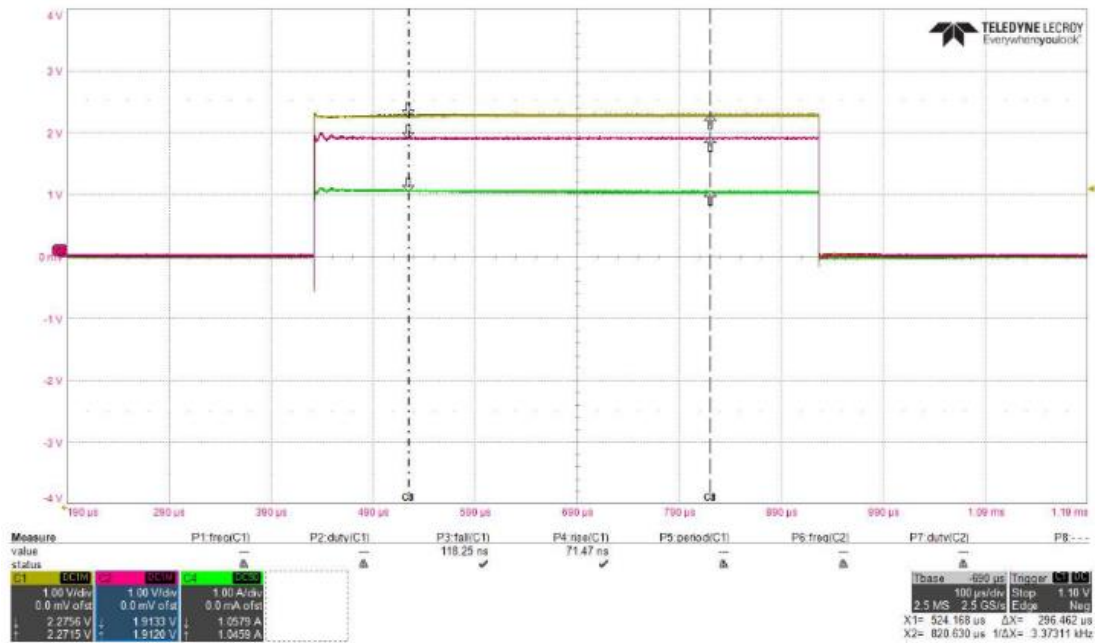
Figure 3.5 Scope screenshot while DUT1 was switching, Yellow: Sensed-V_{gs}, Pink: Sensed-I_{ds}, Green: Ids measured with the current probe.

3.4. Irradiation Test Setup

Applied radiation test took place in the preliminary setup of the Middle East Technical University Defocusing Beamline (METU-DBL) constructed in the Turkish Atomic Energy Agency (TAEA) – Proton Accelerator Facility (PAF) [39]. Two rooms were used in the test facility, irradiation room, and control room, respectively, as shown in the proton irradiation test setup block diagram in Figure 3.6. In the irradiation room, METU-DBL preliminary irradiation setup was constructed.
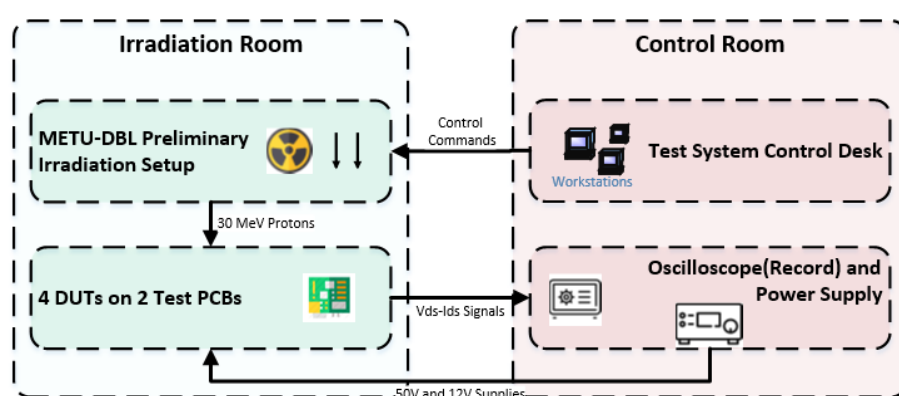
Figure 3.6 Proton irradiation test setup

Because all the components on the test PCBs were commercial and sensitive to radiation, shielding was needed for sensitive components apart from GaNFETs. An application-specific radiation protection shield was designed by METU-DBL considering component positions on PCBs. Thus, a 10mm x 60mm window only enclosing the GaNFETs, which are at the center of the board was created, as shown in Figure 3.7. In this way, sensitive components apart from DUTs were protected from radiation dose. Therefore, it was assured that any possible failures would originate from the GaNFETs instead of commercial radiation-sensitive parts.

Figure 3.7 Protection shield and radiation window

A custom-designed board holder as shown in Figure 3.8 was produced by the METU DBL team and used for controlling the position of boards on the X-Y axis to coincide the DUTs with irradiation test window.
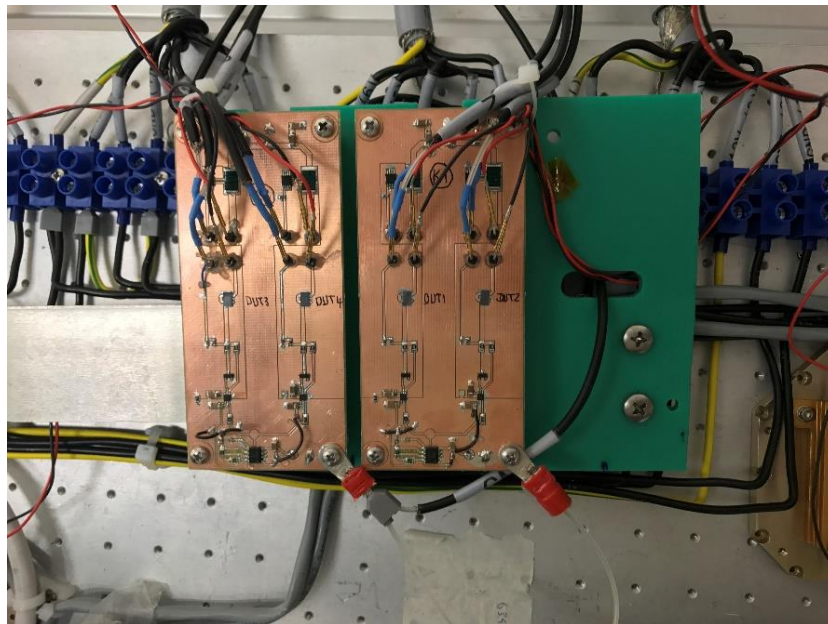
Figure 3.8 Board holder(green)
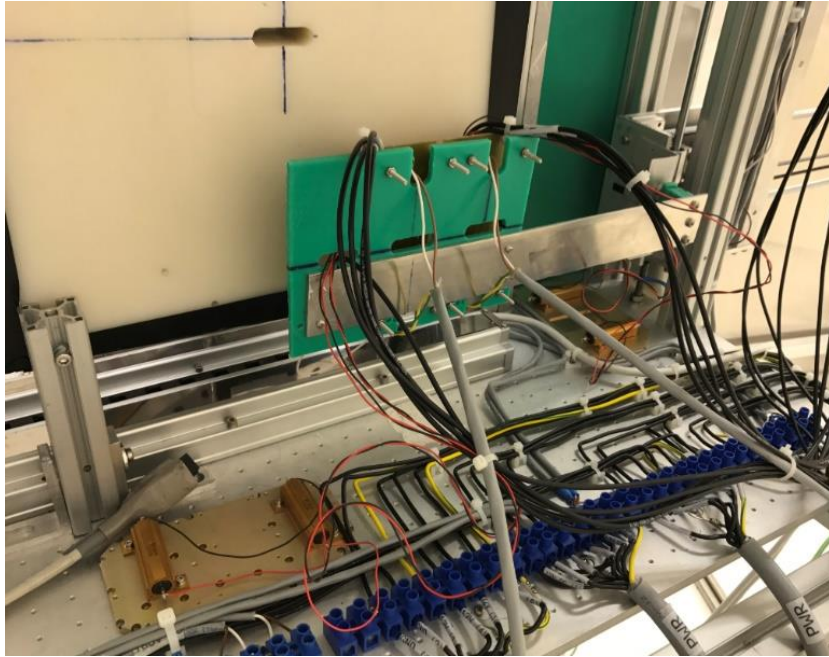
Figure 3.9 Test mechanism showing shield, radiation window, PCB holder and load resistors

Two load resistors, one for each switching GaNFET channel on test PCB, were mounted on two aluminum heat sinks, as shown in Figure 3.9. All the test configurations such as flux adjustment, beam stopper, and board positioning were controlled from the control desk in the control room by the METU-DBL team. Amrel SPD120-3 DC dual power supply is used for 12 V and 50 V supply needs of the test board. Keysight MSO58 series scope is used to record signals transferred from irradiation room to control room with a sampling rate of 1Msample/second.

The distance between the test fixture in the radiation room and the control desk in the control room was measured about 30 meters in the first facility visit. Therefore, signal transferring through the 30 meters of twisted cables was tested in the TUBITAK-Space laboratory successfully before the construction of the irradiation test system in the TAEA. It was investigated that the rise and fall times were increased up to several microseconds because of the RC time constant created by the resistors on the sensing points and cable capacitances. Therefore, it was needed to have an

adequate period for transferred signals to be a square wave. This is the main reason why the switching frequency was limited to 1 kHz instead of the general operating frequency range of satellite converters, which is around 100-150 kHz. Likewise, in the test infrastructure in the TAEA, 30 m of shielded-twisted AWG cables were used to transfer sensed I_{ds} and V_{gs} signals from irradiation room to control room and source voltages from irradiation room to control room. However, after installing the test system, the electromagnetic interference problem was encountered during signal transfer. Because of the high noise about 2 V peak-to-peak on transferred signals, the test for the first trial is canceled.

For the next trial of two weeks later, cables were replaced with coax cables by reconstruction. Electromagnetic interference was decreased down to a 50mV peak-to-peak, and this was an acceptable level for the transferred signals, which were around 1.6 V for I_{ds} signals and 2.3 V for V_{gs} signals, as shown in Figure 3.10. Rise and fall times for transferred signals were increased up to 13 us for I_{ds} signals and 45 µs for V_{gs} signals.

Figure 3.10 Signals transferred from irradiation room to control room before irradiation: Yellow: Sensed-Ids1, Blue: Sensed-Vgs1, Red: Sensed-Ids2, Green: Sensed-Vgs2

3.5. Irradiation Test Procedures

Applied irradiation test parameters in the test site are shown in Table 3.1. Flux value was 8.2 x 10^9 protons/cm^2/s, and it was needed to irradiate the DUTs for 12.5 seconds to reach the ultimate fluence level of 10^{11} protons/cm^2 for proton testing as declared in the ESCC standard.

Table 3.1 Proton irradiation test properties

Proton Energy	30 MeV
Flux	8.2 x 10^9 p/cm^2/s
Homogeneity	X:1 %, Y: 1%
The time needed to reach fluence level on ESCC standard	12.5 second
Total Secondary Particle Dose	Gamma: 0.2 ± 0.02 mSv Neutron: 1.7 ± 0.17 mSv
Temperature	Room temperature
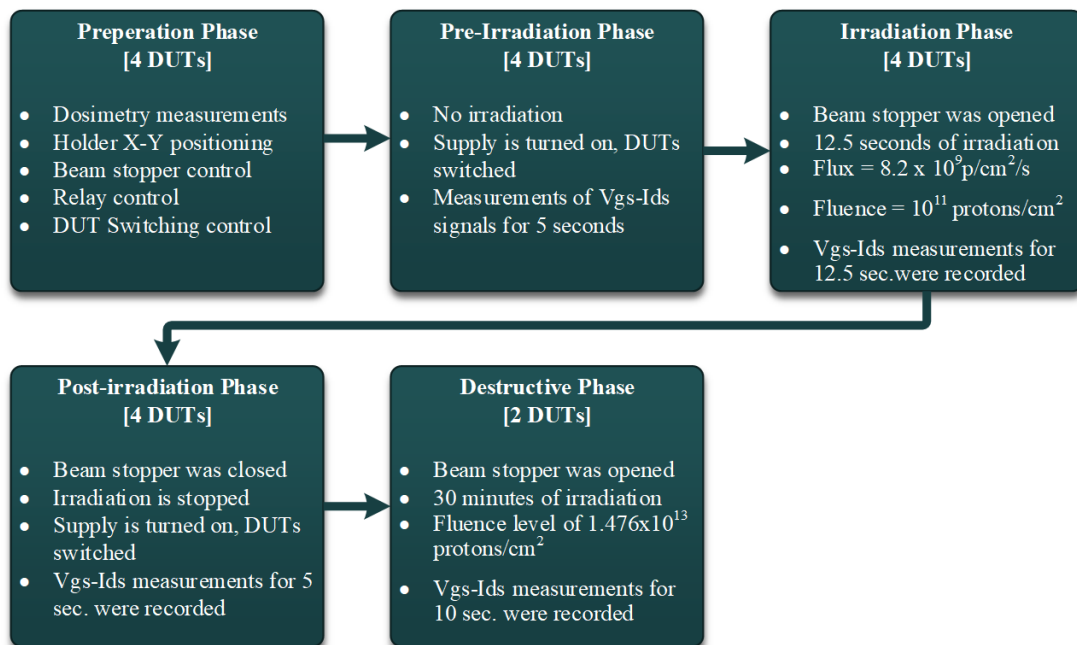
Figure 3.11 Proton irradiation test procedures block diagram

The proton irradiation test procedures can be divided into subcategories. These categories are outlined in Figure 3.11. Basic points can be examined from the block diagram. On the other hand, the detailed test procedures can be investigated in the APPENDICES section.

3.6. Irradiation Test Results

Recorded point-to-point (time vs. magnitude) data are transferred into graphs and converted to meaningful switching signals. Waveforms are created for different switching phases named as pre-irradiation, irradiation, post-irradiation, and destructive phases. Pre-irradiation graphs correspond to the device's original switching characteristics before irradiation was performed. Therefore, all other waveforms can be compared with the pre-irradiation waveforms to see if there is a failure on devices or degradation of performance. All signals in the graphs are created from 3000 recorded consecutive points and comprised three switching cycles of 1 ms. As shown in the switching waveforms, including pre-irradiation waveforms, signals contain small ripples. In fact, these noises were caused by the long cabling between the radiation room and the control room. One can check the created waveforms from records of the pre-irradiation stage given in Figure 3.12 Obviously, minor noises on the device's original waveforms can be ignored from the main form of the signal.

It is known that it is not possible to observe a single event transient occurrence because of large cable capacitance that filters out the transient waveform. However, one can observe if irreversible and destructive failures (open circuit, short circuit, burnout, characteristics change, etc.) take place or device operation stops because of the radiation dose.
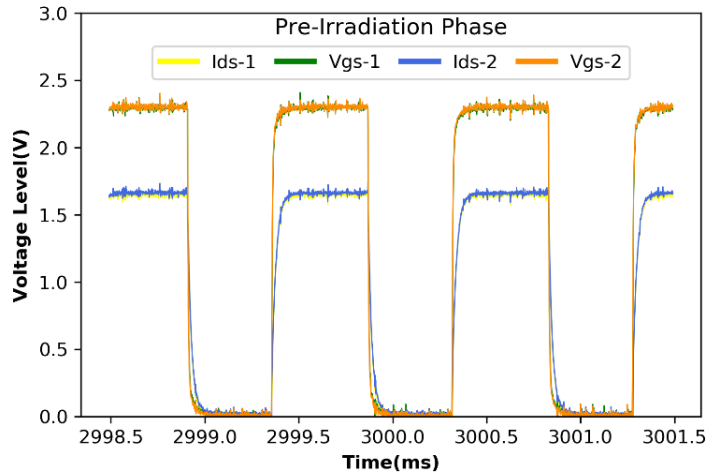
Figure 3.12 Pre-Irradiation Phase, sensed I_{ds} and V_{gs} waveforms of DUT1 and DUT2 on test PCB1

Each switching figure is generated for two DUTs on each test PCB. Therefore, each consists of four measured signals I_{ds-1}, V_{gs-1}, I_{ds-2}, and V_{gs-2}, respectively. Waveforms indicating the devices' original switching characteristics are shown in Figure 3.12. They correspond to data three seconds after the Pre-Irradiation phase records started. Sensed V_{gs} signal is half of the actual V_{gs} signal on PCB because of resistor divider on GaNFET's gate. In Figure 3.12, the average value of the V_{gs} signal is 2.3 V when GaNFET is turned on, and it corresponds to 4.6 V actual V_{gs} voltage on the board. Similarly, a 1.65 V average value of sensed I_{ds} signal when GaNFET is conducting current corresponds to 1 A actual I_{ds} current.

Three different graphs are created for the irradiation phase to observe if there would be any characteristics change during irradiation. Figure 3.13(a) stands for the beginning of the irradiation phase and corresponds to one second after irradiation starts. Similarly, Figure 3.13(b) and Figure 3.13(c) represent the switching waveforms from the middle and end of the irradiation phase, respectively. It seems that there is no failure in terms of the device's functional continuity. Besides, no switching characteristic variation is observed not only among irradiation phase graphs but also between pre-irradiation and irradiation graphs.
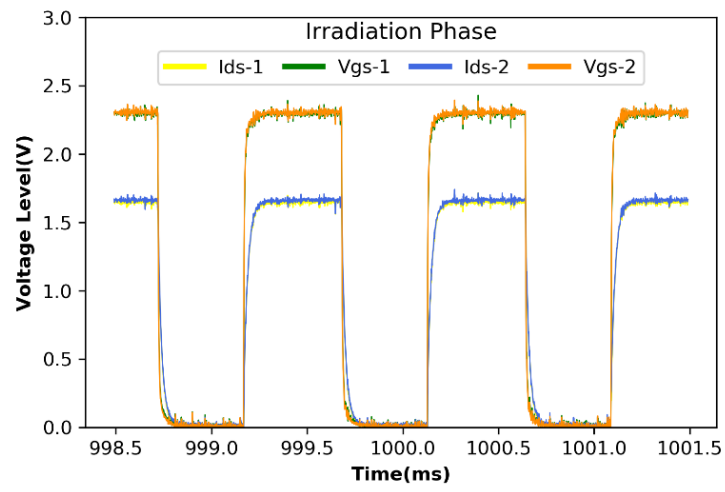
(a)
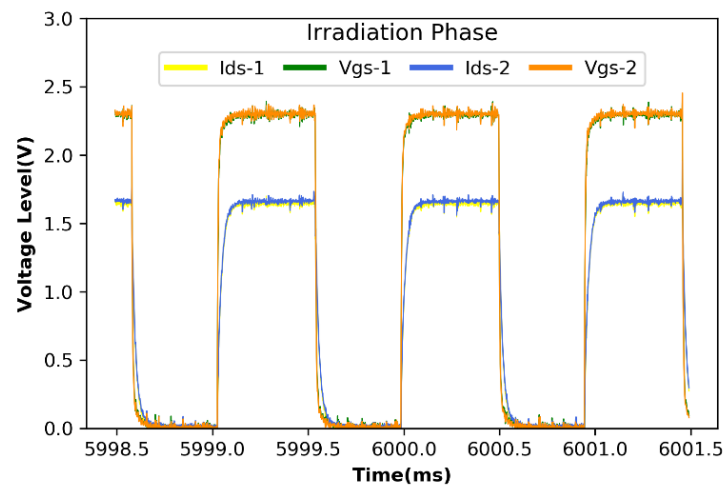
(b)
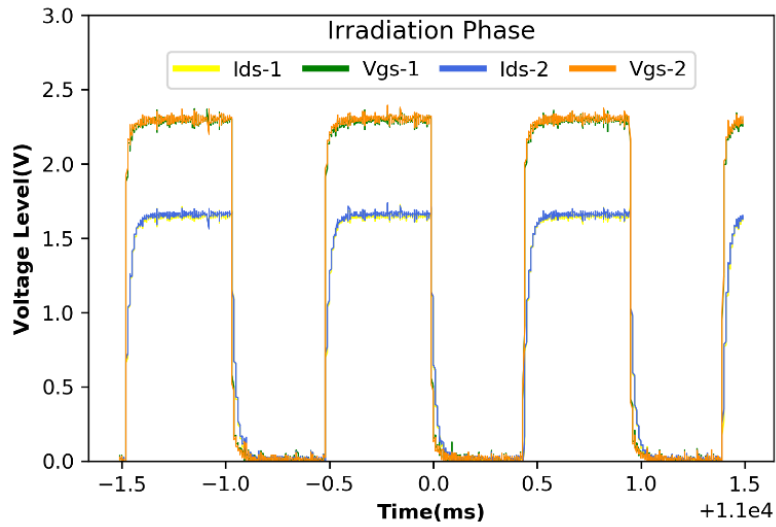
(c)

Figure 3.13 Sensed I$_{ds}$ and V$_{gs}$ waveforms of DUT1 and DUT2 on Test PCB1 (a) beginning (b) middle (c) end of the Irradiation Phase

In Figure 3.14, three switching cycles of the post-irradiation recordings are shown. Again, no failure or characteristic change was observed in terms of devices' operation. Other than the shared figures which are created to represent switching characteristics of the DUTs for different phases, different waveforms were created as well, but they are not shared here to avoid recurrence. By the detailed investigation of the given waveforms and ungiven waveforms in this thesis work, it can be said that there is no significant difference among the switching waveforms of the DUT1 and DUT2 on PCB1 for all phases.
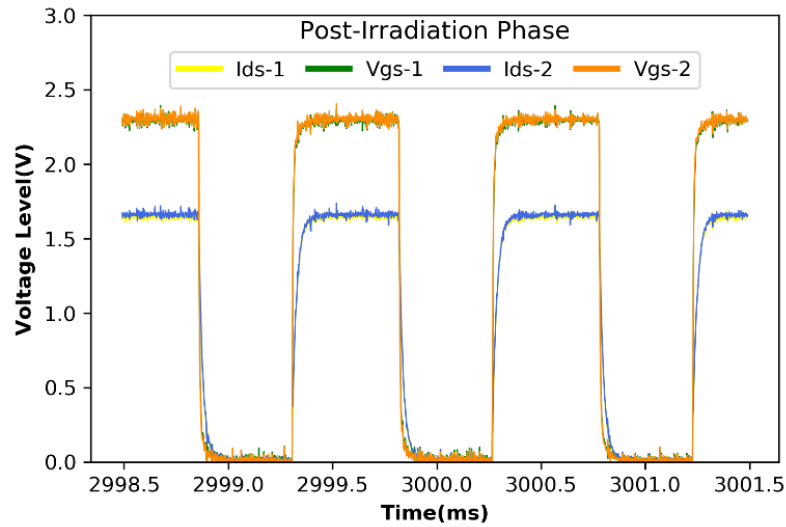
Figure 3.14 Post-Irradiation Phase, sensed Ids and Vgs waveforms of DUT1 and DUT2 on Test PCB1

The same switching waveforms with the ones created so far for the DUTs on test PCB1 were also created for DUTs on the test PCB2. Switching characteristics of the DUTs on test PCB2 for all phases of irradiation tests were analyzed as well. Waveforms are quite similar to each other, and the waveforms of PCB1 and no meaningful difference was observed between waveforms of DUTs on test PCB1 and test PCB2. Pre-Irradiation, Irradiation, and Post-Irradiation waveforms can be seen in Figure 3.15, Figure 3.16, and Figure 3.17, respectively.

49
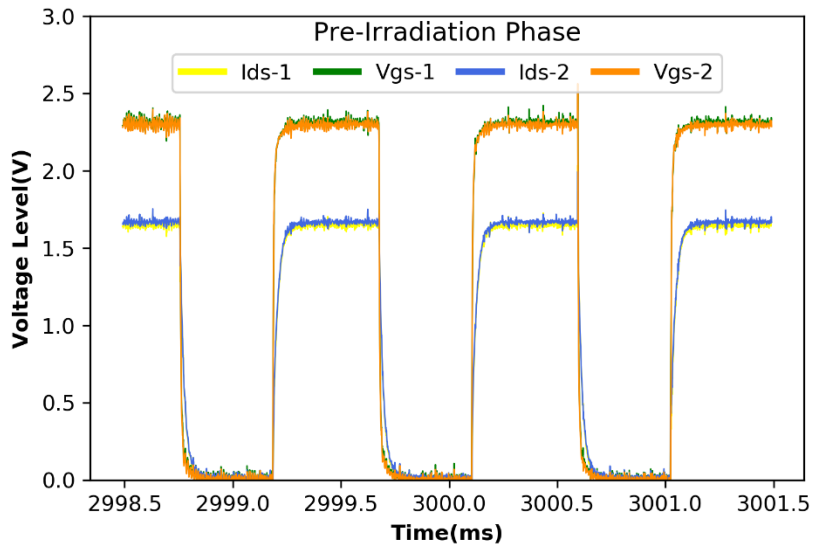
Figure 3.15 Pre-Irradiation Phase, sensed I_{ds} and V_{gs} waveforms of DUT1 and DUT2 on test PCB2
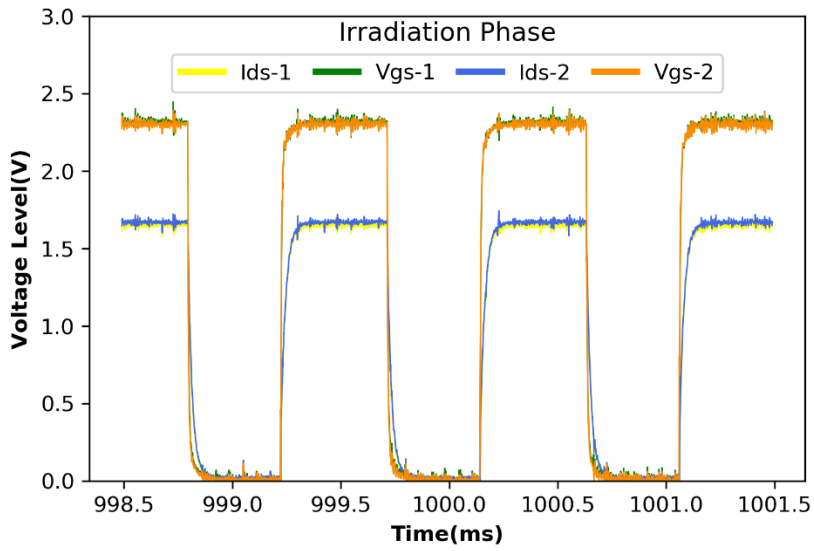
(a)
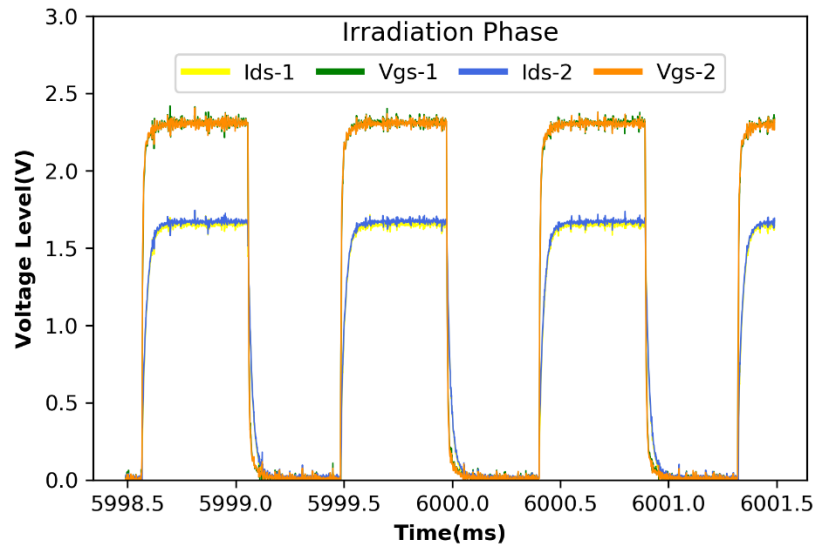
(b)
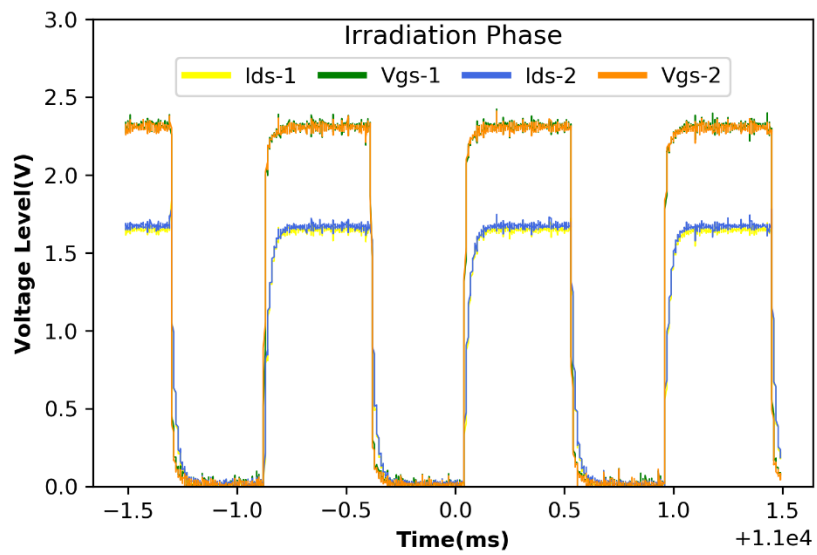
(c)

Figure 3.16 Sensed I_{ds} and V_{gs} waveforms of DUT1 and DUT2 on Test PCB2 (a) beginning (b) middle (c) end of the Irradiation Phase

51
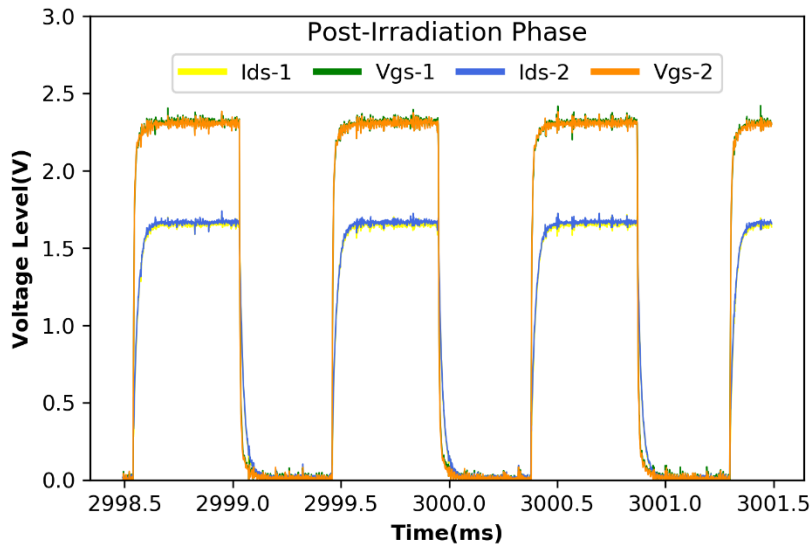
Figure 3.17 Post-Irradiation Phase, sensed Ids and Vgs waveforms of DUT1 and DUT2 on Test PCB2

As shown in the test procedures, after the post-irradiation phase is finished for the PCB2, PCB1 was carried in front of the irradiation window for destructive proton irradiation. The last 10 seconds of 30 minutes destructive irradiation phase has been recorded, and Figure 3.18 represents the switching characteristics of GaNFETs at the end of this record. Despite that considerably high radiation dose was reached $(1.476 \times 10^{13}$ protons/cm$^2)$ which is 147 times more than the value proposed in ESCC standard, GaNFETs continued to operate and remained fully functional during and after the destructive test.
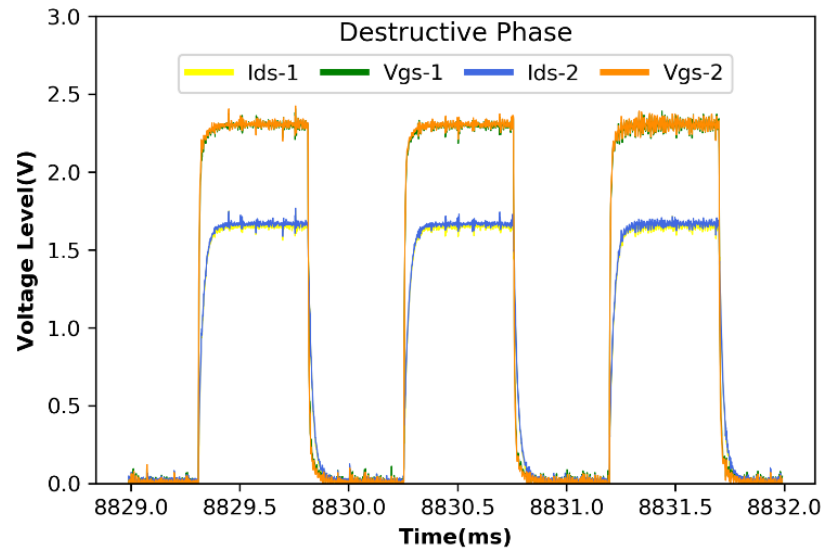
Figure 3.18 Destructive Irradiation Phase, sensed Ids and Vgs waveforms of DUT1 and DUT2 on Test PCB1

3.7. Summary of the Chapter

Proton irradiation effects on commercial normally-off type GaN transistors were experimentally observed. The test summary can basically be observed from Table 3.2. Switching characteristics are compared for distinct phases of the test. It was not encountered any destructive failure during any phase of this experiment, and devices continued to operate as they did in their unirradiated form. Results reveal that irradiated GaNFET in this experiment has radiation tolerance under proton testing in terms of the sustainability of device operation. It is needed to be specified that with constructed test infrastructure, it was not possible to catch the single event transients. However, from a power engineering viewpoint, we can sometimes ignore temporary transients. For example, if a transient occurs for one cycle and GaNFET does not switch, the control circuit recovers the converter operation from the next cycle, and converter could continue to operate appropriately. On the other hand, leakage current change after irradiation could not be investigated with the test infrastructure. Again, an engineer could ignore the leakage current in some situations considering the operational requirements.

53

Table 3.2 Proton irradiation test summary

Device Under Test	Proton Energy (MeV)	Flux (p/cm^2/s)	Irradiation Duration	Fluence	Results
EPC 2034 #1	30	8.2 x 10^9 p/cm^2/s	12.5 seconds	1 x 10^{11} protons/cm^2	• No destructive effect • Stayed functional • No characteristic change
EPC 2034 #2	30	8.2 x 10^9 p/cm^2/s	12.5 seconds	1 x 10^{11} protons/cm^2	• No destructive effect • Stayed functional • No characteristic change
EPC 2034 #3	30	8.2 x 10^9 p/cm^2/s	30 minutes	1.476 x 10^{13} protons/cm^2	• No destructive effect • Stayed functional • No characteristic change
EPC 2034 #4	30	8.2 x 10^9 p/cm^2/s	30 minutes	1.476 x 10^{13} protons/cm^2	• No destructive effect • Stayed functional • No characteristic change

One should carefully consider strong and weak points of this proton irradiation experiment and then decide whether to use the tested device on space designs. It would be useful to remind the fact that the integration of GaN transistors to spacecraft power subsystems could lead to radical changes in future designs in terms of space-saving, efficiency increase, and cost reduction. Irradiated GaNFET, with its proton irradiation performance, has revealed that it is a significant and critical candidate for being one of the future power switching elements in space. The first steps of the revolution for space power equipment will be initiated as similar studies evidencing the radiation tolerance of enhancement mode GaN transistors are carried out.

CHAPTER 4

GAMMA-RAY IRRADIATION TESTING ON NORMALLY-OFF TYPE GANFETS

In this chapter, the experimental results of the gamma-ray irradiation testing (or TID testing) on the commercial enhancement-mode GaNFETs are presented. First, the TID testing is introduced with the guidance of the related test standards. Secondly, the preparation and production stages of the TID test are introduced. Then, the irradiation test setup and the applied test procedures were explained in detail. Finally, the results of the irradiation experiment are discussed.

4.1. TID Testing Overview

Before the electronic component is used in the space application, its characteristics under the appropriate radiation environment should be known. For a better understanding of the device's behavior, it is needed to check the device's vulnerability to the radiation environment, which it will be exposed to in operation. Therefore, the component needs to be subjected to radiation stress in the laboratory to determine if it is suitable to implement this component to space designs. For sure, it is not possible to duplicate the same radiation profile under which the device is supposed to operate in orbit. There is no chance to create the same irradiation profile with all its different sources and various energy spectrum. However, the cumulative effect can be imitated by using a proper radiation source with known energy and dose. Total Ionizing Dose effect is time-dependent and cumulative, as explained in section 2.2.1. TID corresponds to changes in the device's original electrical characteristics/parameters due to extra charges induced by radiation.

There are two main TID testing standards that gave direction to the present chapter of this thesis study, namely ESCC Basic Specification No.22900 - Total Dose Steady State Irradiation Test Method[18] and MIL-STD-883K – Department of Defense Test

Method Standards Microcircuits[40]. Test procedures and necessary productions were mainly prepared by considering the instructions written in these standards.

There are two primary sources of ionizing damage, namely Cobalt 60 (^{60}Co) Gamma-ray source and accelerator beam of the electron [24]. Today, the generally applied method for the ionizing dose test is to use Cobalt 60 (^{60}Co) Gamma-ray source. ^{60}Co source is described as a stable and steady-state dose in [41]. Before mentioning the test requirements in more detail, it would be useful to introduce some important terms for better understanding of the requirements

- ➢ **Total Dose Ionizing Radiation:** Absorbed radiation amount of irradiated device, mainly expressed as RAD(Si) or GRAY(Si) [41].
- ➢ **ERG:** The ERG is an energy unit, and it is equal to 10^{-7} Joules (100nJ) [41].
- ➢ **RAD:** 1 RAD radiation dose corresponds to 100 ERG of ionizing energy per unit gram of irradiated material; 1 RAD(Si) = 100 ERG/g(Si) [41].
- ➢ **Dose Rate:** In RAD(material)/second [41].
- ➢ **Dose Level:** In RAD(material) [41].

According to ESCC specification no.22900 (Total Dose Steady State Irradiation Test Method) [24], dose rates can be divided into two basic categories namely "standard dose rate" and "low dose rate." Prior corresponds to the dose rate range between 0.36 to 180 krad(Si)/hour, and the latter corresponds to 36 to 360 rad(Si)/hour. A low dose rate is generally applied to investigate the suspected time-dependent or specific dose rate effects. In [24], it is also declared that the dose rate measurement resolution should be 10% at most, and the maximum nonuniformity of the radiation field should be 10%. Besides, irradiation temperature should be kept around the ambient temperature of +20 ±10°C and should not change more than 3°C during irradiation[24]. In[40], this temperature range is declared as +24 ±6°C. DUTs shall be exposed to the radiation up to the specified dose levels in the test plan with a 10% percent difference as maximum. If the more than one irradiation phase is planned for target dose level, post-irradiation electrical measurements need to be done after each irradiation phase[40]. If the devices

under test need to be transported to another room between two consecutive exposure for electrical measurement, the maximum allowed temperature rise comparing to irradiation temperature is 10°C [24], [40].

All the components -other than the evaluated one- which are used to apply bias or real-time measurements, and which are supposed to be exposed to radiation should be non-sensitive to aimed accumulated radiation dose. If they are susceptible to targeted radiation, their characteristics would change, or they may fail. Consequently, this would change the original test conditions (bias, isolation, voltage levels, etc.) and affect the actual test results. On the other hand, PCB design should be convenient for radiation to be distributed uniformly on the different DUTs on it[24].

Depending on the measurement method, the radiation test can be classified as "in-situ testing" and "remote testing". The electrical parameters of the DUTs are measured when they are under irradiation exposure for the in-situ testing case. As its name indicates, in remote testing cases, measurements of the electrical parameters are done when the irradiation stops and DUTs are taken out of the radiation room. Prior to irradiation, necessary electrical measurements written in the test plan need to be done for both cases. In-situ testing is more advantageous than the remote one if time-dependent variations occur in post-irradiation. However, in-situ testing generally requires more complex arrangements considering long cabling, appropriate connections, noise, leakage, etc. Additionally, it is easier for the one to make a more detailed test in the remote-testing case. In [11] and [13], it is also suggested that terminals of the irradiated DUT should be connected/shorted to each other while transferring from the radiation chamber to test side to diminish the time-dependent effects in the post-irradiation. Functional tests and measurements to be taken shall be clearly defined in the test plan. To check the test/measurement equipment's stability, one control sample shall be tested in each measurement phase before and after irradiations and the validity of the measurements should be proven in this way [24], [40]. All the electrical measurements shall be done by the same measurement infrastructure and with the same sequence. The electrical measurement time intervals

between two adjacent irradiation shall be limited, and it is also declared in [24]. The maximum time between the end of the exposure and the beginning of the electrical measurement shall be 60 minutes as maximum. Besides, the time between two consecutive irradiations should be no more than 2 hours[24].

Bias conditions (voltage levels, biased terminals, duty cycles, etc.) shall be clearly identified prior to the test. During the test, they should be kept as a maximum of 10% deviated from specified conditions[24]. In order to obtain more reliable results, worst-case biases -if they are known- should be chosen to create the most hazardous case in terms of part's radiation-induced failure. Except for the time breaks for electrical measurements of intermediate dose levels, for all the irradiation phase, the bias conditions should be kept constant. In [40], it is also suggested that the device's terminals should not be left as floating during the exposure. Instead, they should be short-circuited with each other.

4.2. Test Preparation

A test plan was made concerning the items mentioned and unmentioned in chapter 4.1 from related standards [24], [40]. Two GaNFET device types from two different manufacturers are chosen as test samples, namely EPC2034 from EPC and GS61004B [42] GaN Systems. The first device is the same device that was evaluated with the proton irradiation testing in chapter 3. Observing the performance of the device under both proton and gamma-ray irradiations would be worthy in terms of complete radiation characterization and determination of the device's reliability level. EPC2034 is normally-off type GaNFET having the 200V-48A ratings. It is a candidate device for use in space power designs having high voltage (100V) regulated bus, medium voltage(50V) bus or low voltage (28V) unregulated bus of power subsystem. It is decided to investigate the radiation performance of another GaNFET with different technology from another brand. The GaN Systems, having different enhancement type GaNFETs, was chosen. GaN System's products are divided into two classes according

to their Vds voltage ratings of 100V and 650V. Devices with a 650V voltage rating could be considered as overrated for space power systems with a bus voltage of 100V, 50V or 28V. Therefore, GS61004B was chosen, and it has the ratings of 100V-45A. Considering the 80% voltage derating rule for FETs [43], it is not possible to use it in a 100V bus of power subsystems, but it could be used in medium and low voltages buses. The physical views of the selected parts can be seen in Figure 4.1.
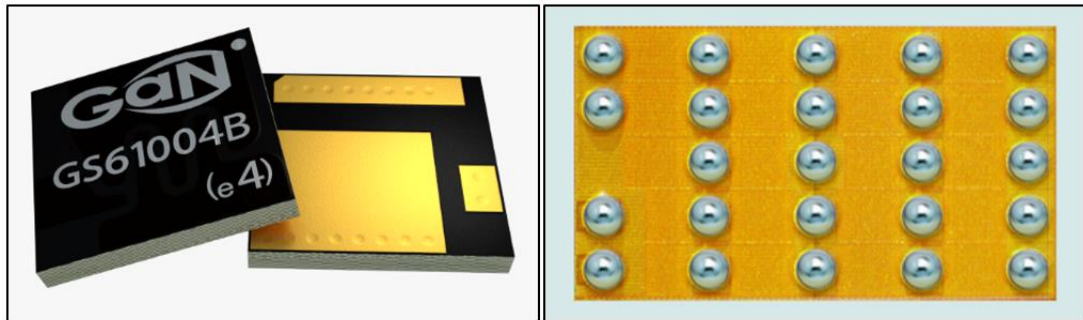
Figure 4.1 GaNFET GS61004B (left hand side) [42]*, GaNFET EPC2034 (right hand side)* [37]

Experiences gained from proton irradiation testing showed that setup of the real-time measurement system through the long cabling is a quite complicated and tedious issue. It is witnessed that long cabling is a source of critical problems. Because the transferred signals were mainly square waves, transferred signals were affected by the big capacitance and inductance of cables. Likewise, noise and electromagnetic interference are other difficulties of in-situ measurement through long cables. These problems were solved using coax cables instead of regular AWG cables and substantial time was lost due to reconstruction in the test site. On the other hand, depending on the literature written about TID testing experiences [44], the remote testing method is a widely used and typically preferred method for TID irradiation. In light of these information, it was decided to apply the remote testing method instead of in-situ testing.

There are various examples of TID testing with both unbiased and biased conditions. In [36], TID tests are reported for the commercial of the shelf (COTs) p-channel power MOSFET, which are irradiated in both biased and unbiased. In unbiased conditions, all the mosfet legs are connected to ground potential. In a biased case, the drain terminal is held at 50V and the gate is kept at -20V while the source terminal is at ground potential. It is also reported that the radiation effects are more significant for the biased case. In [44], TID testing results for three different commercial trench type MOSFETs with 30, 40, and 70 V ratings are reported. Various bias conditions are applied for both V_{gs} and V_{ds} (including negative bias for V_{gs}). It is stated that when the gate is biased, the drain is grounded. It is declared that the maximum gate threshold voltage decrease took place for all device types when the maximum gate bias (16V) is applied. Besides, drain bias has almost no effect on the V_{th} shift. It is also reported that the gate leakage current increases with the increasing gate bias voltage both negative and positive. In short, various effects (including drain breakdown voltage change, drain leakage current increase, R_{dson} shift) are observed together with the different bias conditions.

4.2.1. Production Plan

A production plan is prepared for remote TID testing by predicting possible needs. The production plan block diagram can be investigated in Figure 4.2. According to the block diagram, it was planned to produce seven main parts, namely test card, irradiation room cards 1 and 2, reference cards 1 and 2, loads and cabling. The main purpose of the TID test is to examine the switching characteristics of the devices at intermediate and final dose levels. The test card was designed to drive GaNFETs with predetermined frequency and duty cycle. To that end, it includes a square wave generator to adjust the switching frequency and duty cycle, GaNFET drivers to drive GaNFETs properly and necessary supply voltages for these ICs and switching off the GaNFETs. Because the test card is planned to stay in the test side for electrical measurements and it is not supposed to be exposed to radiation, it is free to use radiation-sensitive industrial components on it. It is also planned to mount three

female headers to the drivers' outputs for male headers - connected to gate-source-drain of the DUTs - to be placed in. Two male headers are put to the drain path of the GaNFETs to attach the external load by female headers connected to it.
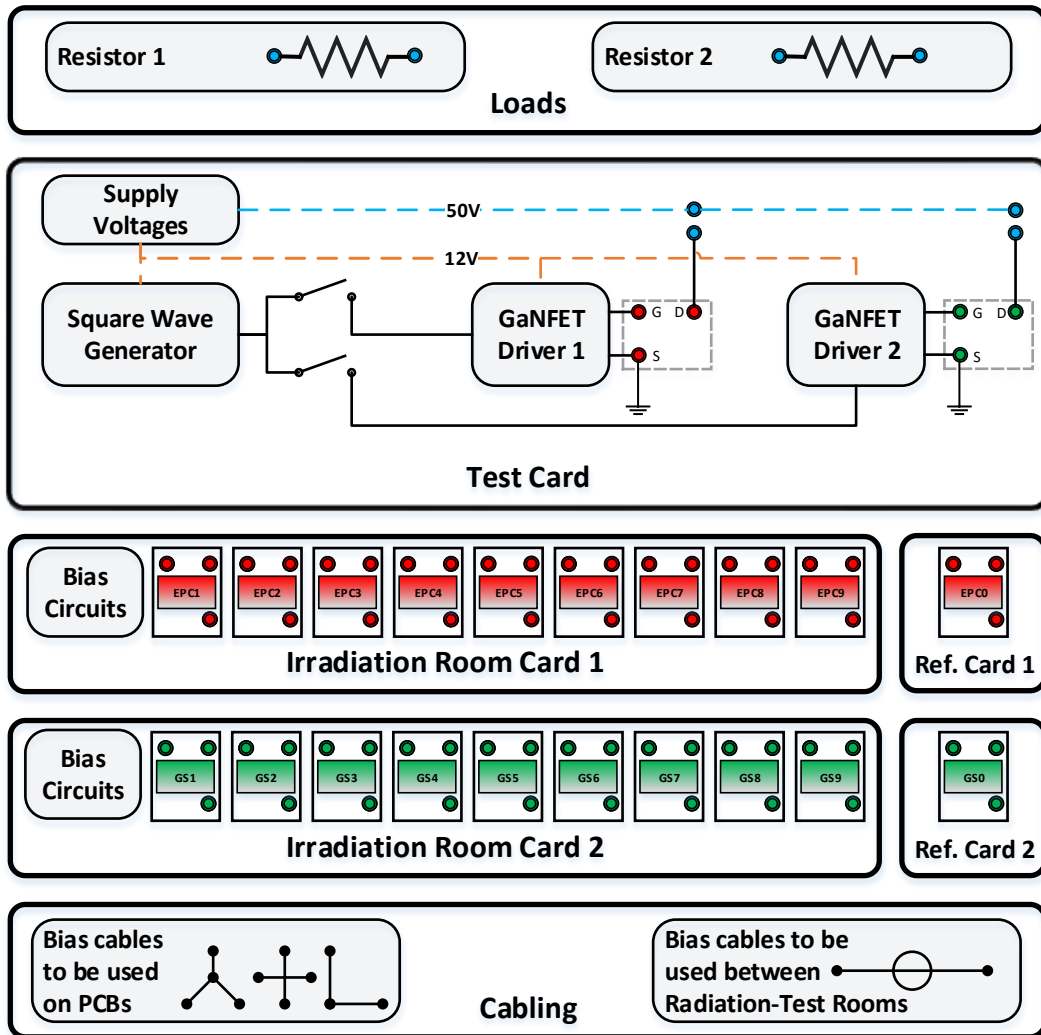
Figure 4.2 Production plan for remote TID testing

Irradiation room cards are designed for DUTs to be mounted on it and undergo the gamma-ray irradiation. Because these cards are planned to be exposed to radiation, all the components on it other than DUTs are supposed to be insusceptible to radiation. It

is decided to put male headers connected to all the gate-source-drain pins of the DUTs, and they are designed to be placed in the female headers at the output of the drivers on the test card. 9 DUTs from one manufacturer are positioned to each room card. Three of the DUTs are to be biased from gate-to-source with drain, and source terminals are shorted together while the 3 of them are to be biased from drain-to-source with gate to source terminals are connected. Remaining 3 DUTs are to be unbiased with all the terminals are shorted to each other. Therefore, two bias circuits are positioned to each irradiation room card for the gate-to-source and drain-to-source biases. Reference cards are for reference/control samples to be assembled on them, and they are supposed to stay in the electrical test side only. Reference cards are for confirmation of the validity and stability of the test/measurement system, as explained in section 4.1. It is also needed to produce external resistors with appropriate heat sinks to adjust the drain current of the switching DUTs. On the other hand, proper cabling is also required to connect the biases to DUTs on the irradiation room card and to transfer bias voltages from the test room to the irradiation room.

4.2.2. Design Considerations

It was planned to design a single test card for both irradiation room cards. Because the test card is not supposed to be irradiated, it is free to use commercial radiation sensitive devices in this card. With the previously gained experiences through this thesis study, UCC27611 5-V, 4-A to 6-A Low Side GaN Driver [45] was chosen to drive GaNFETs, and LM555 Timer IC from Texas Instruments [46] was selected to produce input duty signals of the drivers. A switch was put between drivers and timer IC for on-off control of the duty signal. In this way, it is possible for the one to start the switching of the DUTs by switch-on the driver input using switches. A common supply voltage was chosen as 12V for both driver IC and timer IC to prevent additional supply need in the test setup. It was put to 3 female headers representing the device's gate, source and drain terminals at the place of GaNFETs instead of putting real

devices. GaNFET's source terminal headers were connected to ground potential for low side driving and not to allow complexity in driving. As it is understood, the driver's outputs were connected to GaNFET's gate terminal header through the gate resistor. 2 male headers were placed at the drain current paths of each device to attach external load resistors. One of these male headers was connected to supply voltage (drain current source) while the other was connected to GaNFET's drain terminal header.

Irradiation room cards 1 and 2 were designed for appropriate placement of the EPC2034s and GS61004Bs respectively. Each irradiation card has 9 DUTs on it. It is aimed that the three of the devices will be biased from gate to source while the other three from the drain to source and remaining three stays as unbiased. Therefore, each room card has 2 bias circuits, one of which is for the gate to source and the other for the drain to source of GaNFETs.

Irradiation room cards were designed to allow proper plug in-out operation. Therefore, male headers are attached to each DUTs on the irradiation room cards to insert them to the gate-source-drain female headers at the test card. Care was taken not to use radiation-sensitive parts in the room cards. Therefore, only resistors and capacitors, which are not susceptible to radiation by nature, were used for the bias circuit. It was placed male headers to the suitable points in bias circuits to make required connections with the gate-source-drain male headers on the same card when the card is under irradiation. For the bias cablings to be short, bias headers were positioned to around the center of the 3 DUTs group which is supposed to be biased with this voltage.

4.2.3. Fabrication of the Necessary Items

After the preliminary test plan was done, as explained in section 4.2, the next step was the realization of the designs. First, the schematic design was completed for the mentioned functions of each PCBs. Details started to be clarified along with the schematic design. Necessary components and supply voltages to be used on the PCBs

were determined. Secondly, PCB layout designs were made considering the smooth plug in-out of the DUTs on the radiation room cards to appropriate headers on the test card. Then, PCBs were produced by these layouts. Proper cablings were designed and produced to provide the necessary bias conditions on the irradiation room cards. In the end, components were assembled to the PCBs, and the DUTs were visually controlled with X-rays.

Empty PCBs were produced by the method of scraping of two-sided copper plates. Irradiation room cards were produced as a one PCB, and then they were separated from each other by cutting with a guillotine. Test card and reference cards 1 and 2 were built as one PCB as well. Reference cards were cut out from the test card by using a dremel tool. Assembled PCBs can be investigated in Figure 4.4. EPC2034s (BGA package DUTs) and GS61004Bs were assembled to empty PCBs by using special assembling machines which enable to show the bottom of the package by X-ray for exact matching of solder balls, device's footprints and PCB pads. Proper cables with female headers were produced to enable the bias connection configuration which is shown in the block diagram in Figure 4.3. Produced cabling can be seen as detailed in Figure 4.12.
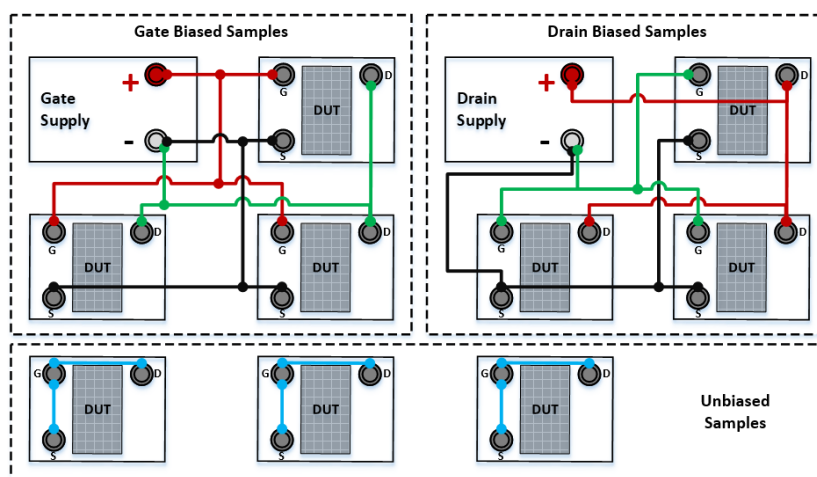
Figure 4.3 Block diagram showing the bias configuration on a single irradiation room card and bias cabling.
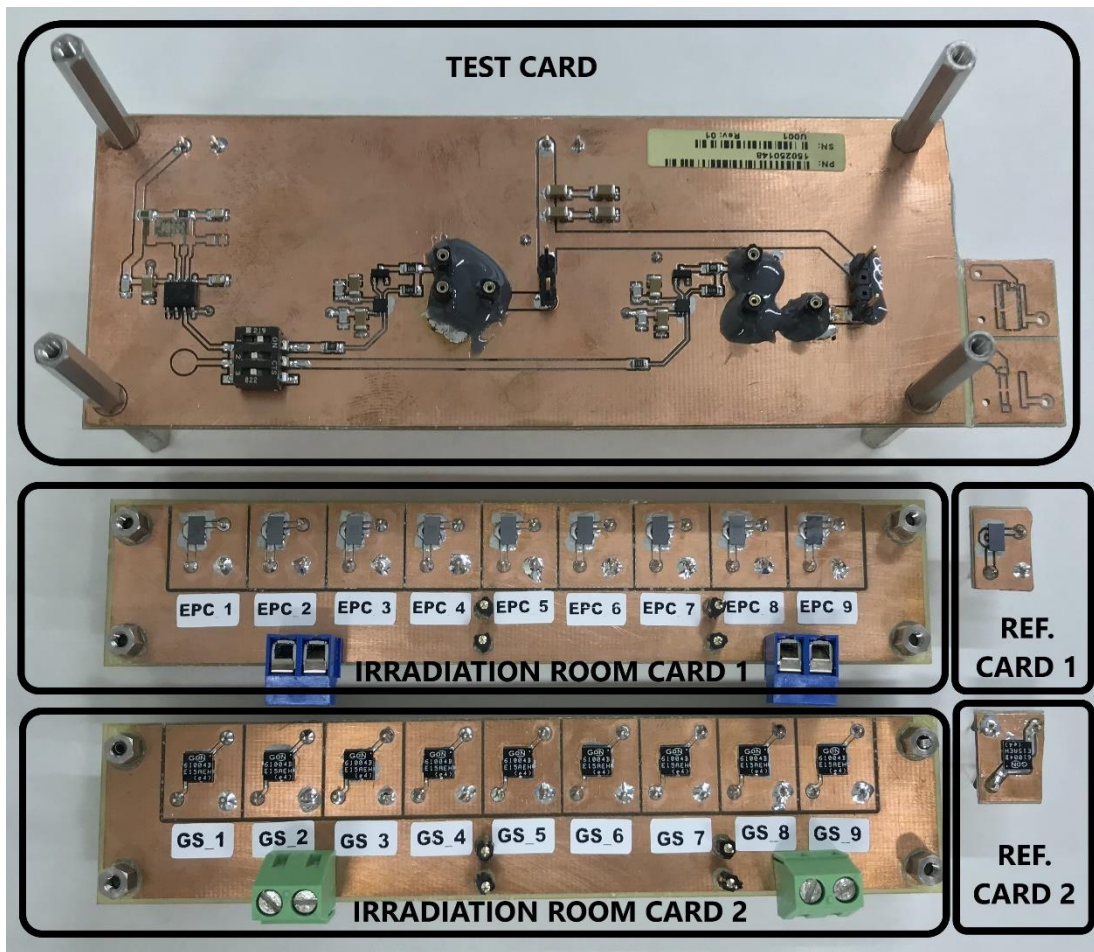
Figure 4.4 Produced PCBs for TID testing

4.3. Pre-Testing

Each device's characteristics, including DUTs and reference samples, were investigated in the laboratory by making them switch one by one. The drain resistor is chosen as 47 ohms to make the drain current around 1 A at 50 V supply voltage. Each device is attached to the female sockets one by one as shown in Figure 4.5. The test setup is shown in Figure 4.6.
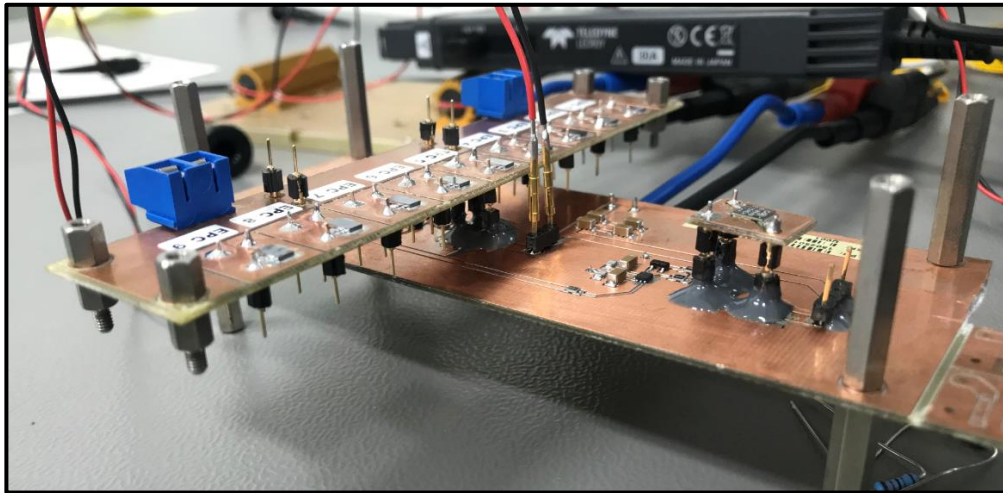
Figure 4.5 Irradiation card and reference card attached to test card
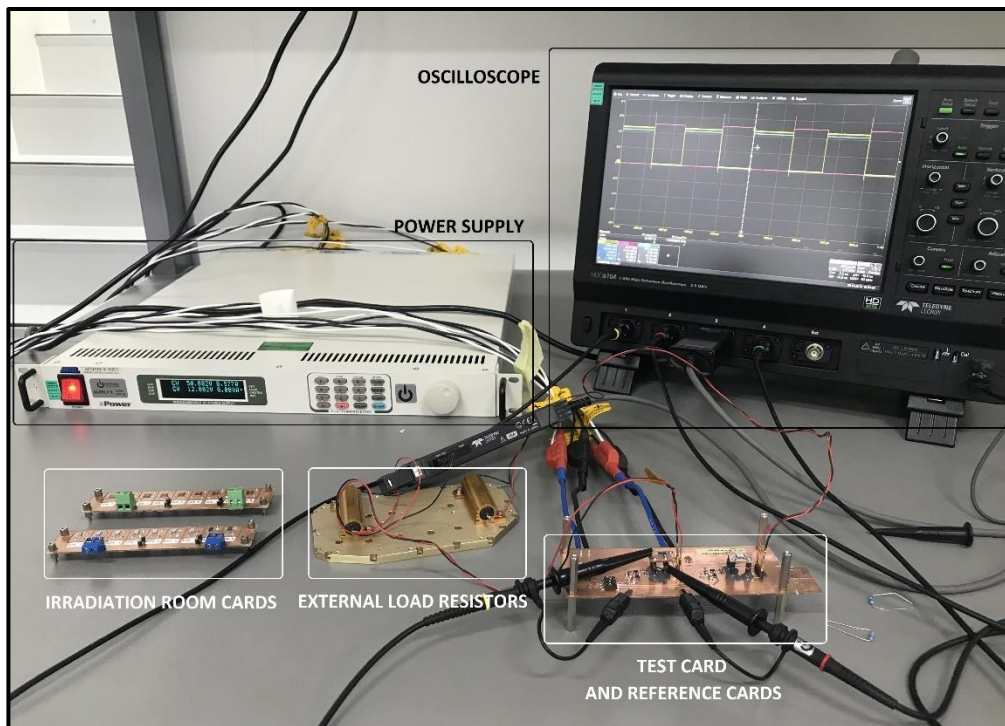
Figure 4.6 Pre-Test setup

I_{ds}, V_{gs} and V_{ds} waveforms of the turn-on timeframe of each device were recorded in the LabNotebook file format of Lecroy oscilloscope with 2.5 Gs/s sampling rate as shown in Figure 4.7. Waveforms are analyzed with the WaveStudio scope interface

66

program specialized to Lecroy oscilloscopes. In Figure 4.7, turn-on waveforms of the GaNSystems's control sample can be viewed.
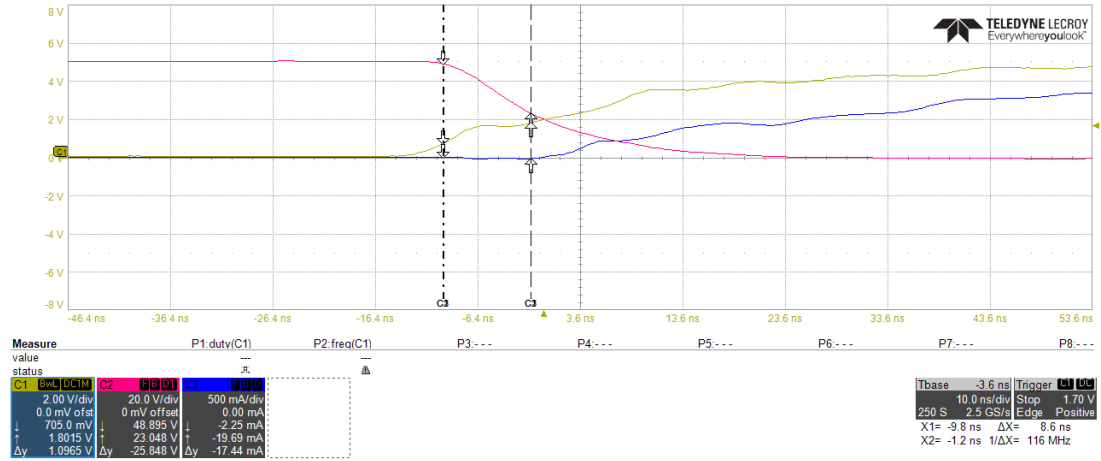
Figure 4.7 GaNSystems control sample's turn-on waveforms, Red: V_{ds}, Yellow: V_{gs}, Blue: I_{ds}

The details of the turn-on waveforms of the EPC control sample can be investigated in Figure 4.8. Unlike Figure 4.7, waveforms in Figure 4.8 are separated from each other for detailed examination with cursors due to the method the WaveStudio works. At this point, it would be useful to make two definitions specific to this TID test:

➢ **V_{gs-th}**: It corresponds to a V_{gs} voltage of the GaNFET when the drain to source voltage drops down to a 49 ± 0.075 V during the device turn-on.

➢ **$V_{gs-plateau}$**: It corresponds to a V_{gs} voltage of the GaNFET when the drain current reaches to 5 ± 0.5 mA during the device turn-on.

As can be seen from the red V_{ds} waveform in Figure 4.8, the cursor is at -5.4 nsecond in the time axis when the V_{ds} voltage drops down to 49.010 V. Besides, the cursor is at 5.3 nsecond in the time axis when the I_{ds} current increases to 5.31 mA as in blue waveform. As a result, from the black V_{gs} waveform, the V_{gs-th} of the EPC control sample can be found as 951 mV (cursor X1 is at -5.4 nsec.) and the $V_{gs-plateau}$ of the EPC control sample can be found as 2.1917 V (cursor X2 is at 5.3 nsec.). With the

same strategy, the V_{gs-th} and $V_{gs-plateau}$ voltages of the remaining 19 devices are found by manually checking the waveforms by cursor positioning. According to tests done in the laboratory, EPC and GS devices' original characteristics showing the V_{gs-th} and $V_{gs-plateau}$ voltages can be investigated from Table 4.1 and Table 4.2.
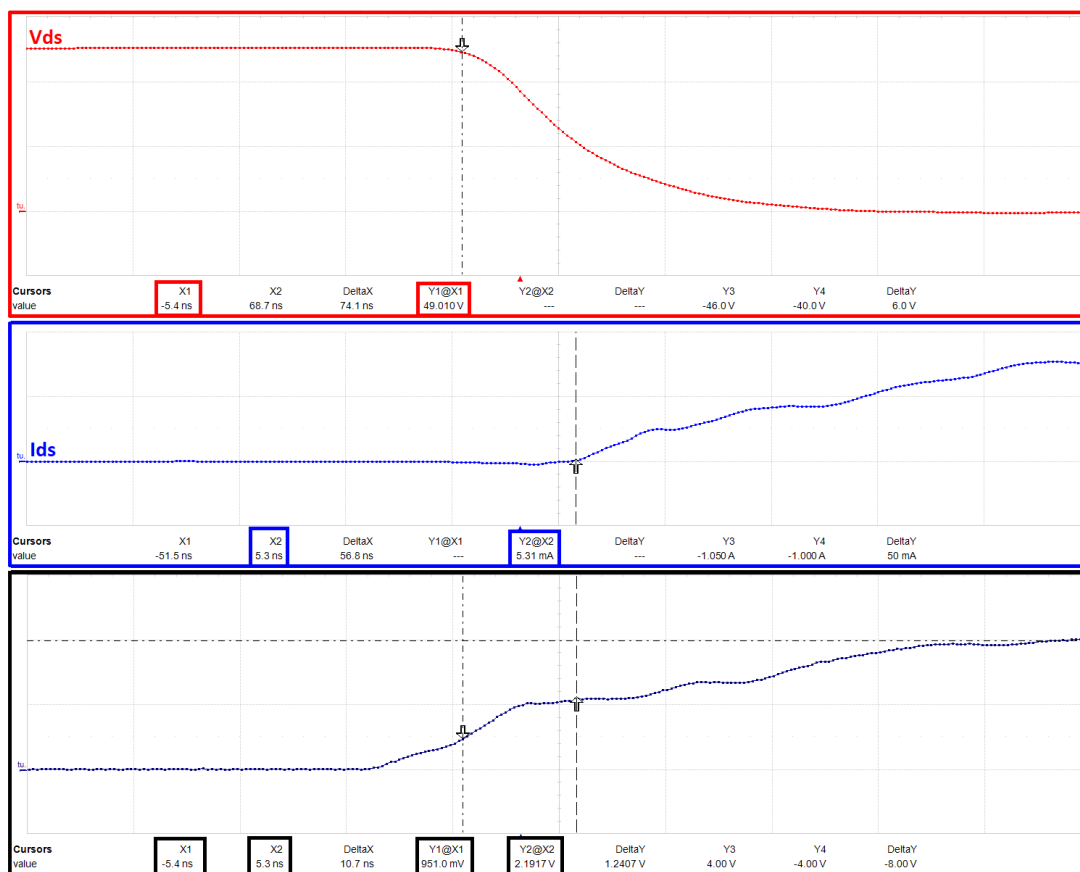
Figure 4.8 EPC control sample turn-on details, Red: V_{ds}, Blue: I_{ds}, Black: V_{gs}

Table 4.1 The original characteristics of the EPC devices

Device Number	V_{ds} (V)	Cursor-V_{ds} (ns)	I_{ds} (mA)	Cursor-I_{ds} (ns)	$V_{gs\text{-}th}$ (mV)	$V_{gs\text{-}plateau}$ (V)
Control EPC	49.010	-5.4	5,31	5.3	951	2.1917
EPC1	49.020	-26	5,5	-17.3	834	1.960
EPC2	48.933	-24	4,81	-14.1	864	2.0575
EPC3	48.950	-23.6	5,06	-13.8	879	2.0368
EPC4	48.958	-23.1	5,5	-12.9	882	2.1027
EPC5	49.013	-24.1	4,94	-14.3	878	2.0575
EPC6	48.950	-21.5	5,5	-12.1	917	2.0722
EPC7	48.973	-23.4	5,19	-13.1	927	2.0602
EPC8	49.020	-21.8	5,12	-11.1	921	2.1147
EPC9	48.977	-21.9	5,25	-11.2	918	2.1412

Table 4.2 The original characteristics of the GS devices

Device Number	V_{ds} (V)	Cursor-V_{ds} (ns)	I_{ds} (mA)	Cursor-I_{ds} (ns)	$V_{gs\text{-}th}$ (mV)	$V_{gs\text{-}plateau}$ (V)
Control GS	49.010	-9.9	5.19	0.119	678	1.9647
GS1	48.970	-14.7	5.19	-5.2	726	2.0278
GS2	48.965	-19	5.75	-8.8	778	1.8000
GS3	49.015	-18.7	5.5	-8.3	807	1.8400
GS4	48.947	-19.7	6.13	-9.4	797	1.756
GS5	49.035	-15.3	6.13	-4.3	692	2.1915
GS6	48.985	-16.3	5.13	-5.9	729	2.1903
GS7	49.032	-9.9	6.13	0.200	678	1.9818
GS8	49.028	-4.1	5.06	6.4	634	1.9845
GS9	48.938	-12.9	5.94	-2.3	765	1.8248

4.4. TID Irradiation Test Setup

Applied TID radiation test took place in the Turkish Atomic Energy Agency (TAEA) - Gama Irradiation Facility. Two rooms were used in the test facility,

irradiation room, and test room, respectively, as shown in the test setup block diagram in Figure 4.9. Cobalt^{60} gamma-ray source is positioned in the irradiation room. There are tons of water at the bottom of one side of this room for shielding purposes. Before the personnel entering the room, the radiation source is taken under the tons of water by means of a mechanism which is controlled by the operator from the test room. In this way, the stuff is protected from the catastrophic effects of the radiation on human health. After the stuff leaves the room, the radiation source repositioned above the water for the irradiation to start.
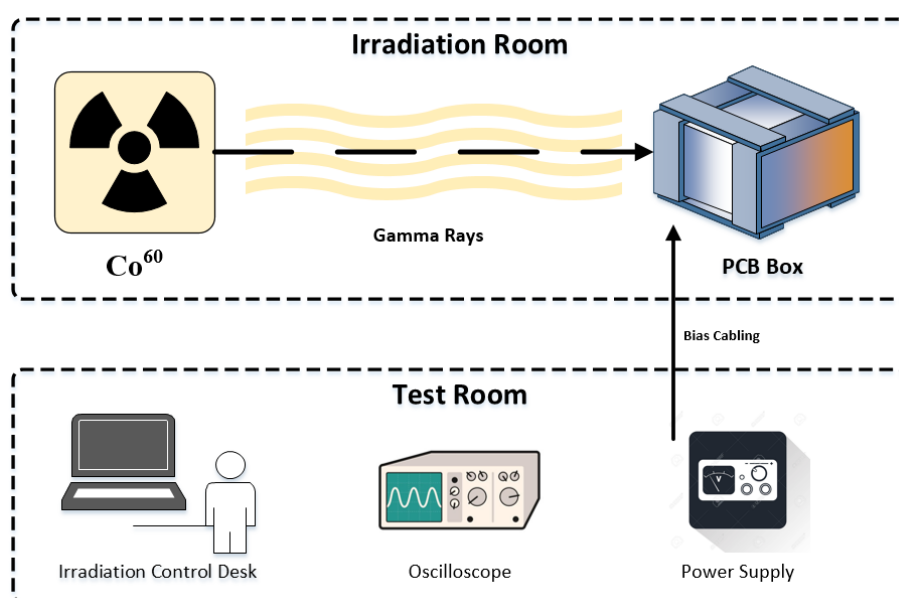
Figure 4.9 TID irradiation test setup block diagram

Cherenkov radiation [47], which is resulted by the gamma rays while passing through the water with the speed which is greater than the speed of light in the water, can be seen in Figure 4.10.

Figure 4.10 Cherenkov radiation when the Co^{60} source is under the water
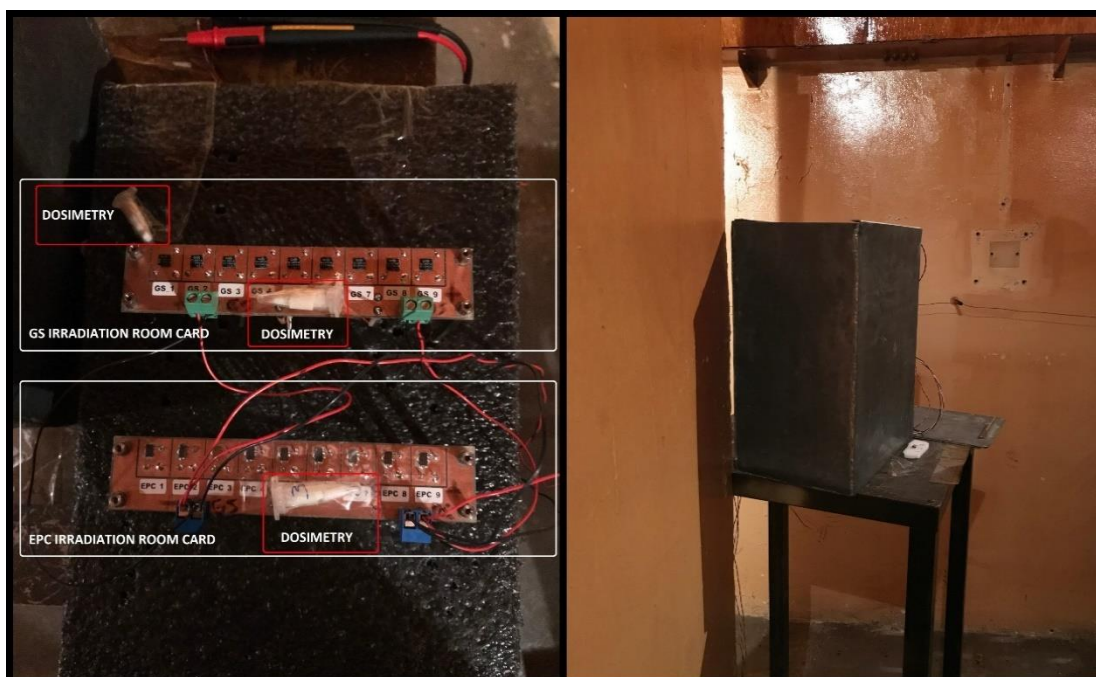
Figure 4.11 Left: dosimetries and irradiation room cards on the styrofoam, Right: PCB box (irradiation room)

Irradiation room PCBs having DUTs were placed onto a piece of styrofoam. This styrofoam stayed in the PCB box during the irradiation. Before the irradiation begins for the DUTs, pre-dose-measurements were done to adjust the dose rate inside the empty PCB box. Moreover, to correlate the dose measurements before and after the irradiation, dosimeters were attached to each irradiation room cards and Styrofoam. They stayed on the PCBs and styrofoam during the whole radiation phases. Attached dosimeters are alanine type [48] which is an internationally accepted dose measurement method with its 1 % accuracy. Mentioned details can be investigated in Figure 4.11.

25 meters of twisted AWG cables were used to transfer the V_{ds} and V_{gs} bias voltages from the power supply which is in the test room to the PCB box which is the irradiation room. Bias voltages were chosen as 50 V and 4.7 V, respectively. Before each irradiation stage was started, it was controlled with a multimeter that if the bias voltages were transferred to PCBs appropriately. Bias voltages were distributed to drain-biased (DUTs 7-8-9) and gate-biased (DUTs 4-5-6) samples by bias cabling and male headers at the bottom of the PCBs in a way shown in Figure 4.12. Gate, drain, and source terminals of the unbiased samples shorted to each other as seen.
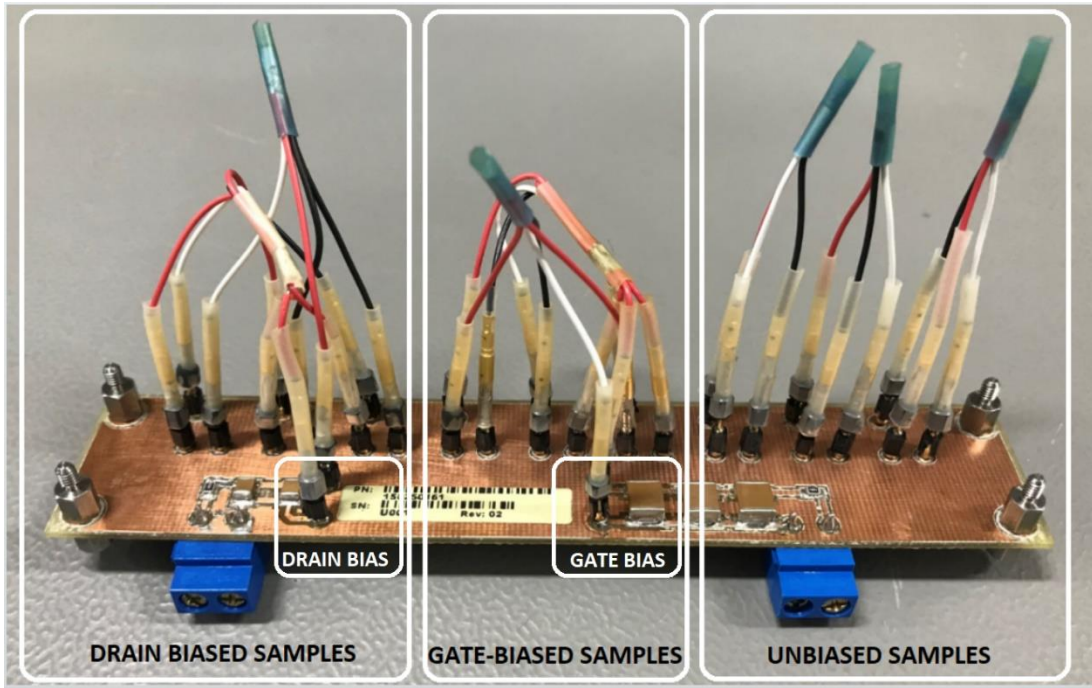
Figure 4.12 Bias distribution on the PCB by bias cabling and male headers
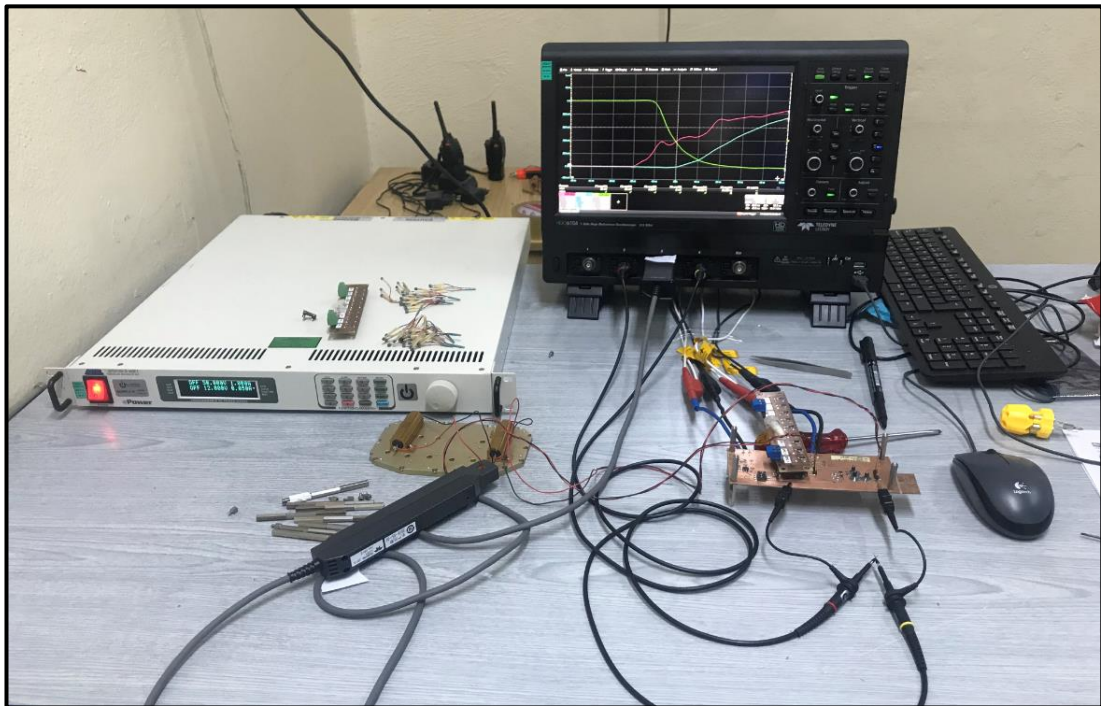
Figure 4.13 Test desk in the test room

A test desk was arranged in the test room to make preliminary, intermediate-doses, and post-irradiation tests. It can be seen in Figure 4.13. Test card, reference cards, and external load resistors stayed in the test desk. Start and end commands of the irradiation were controlled by the facility operator from the control computer which was resided in the test room as well.

4.5. Irradiation Test Procedures

TID irradiation test procedures can be divided into subcategories. These categories are outlined in Figure 4.14. Basic points can be examined from the block diagram. On the other hand, the detailed test procedures can be investigated in the APPENDICES section.
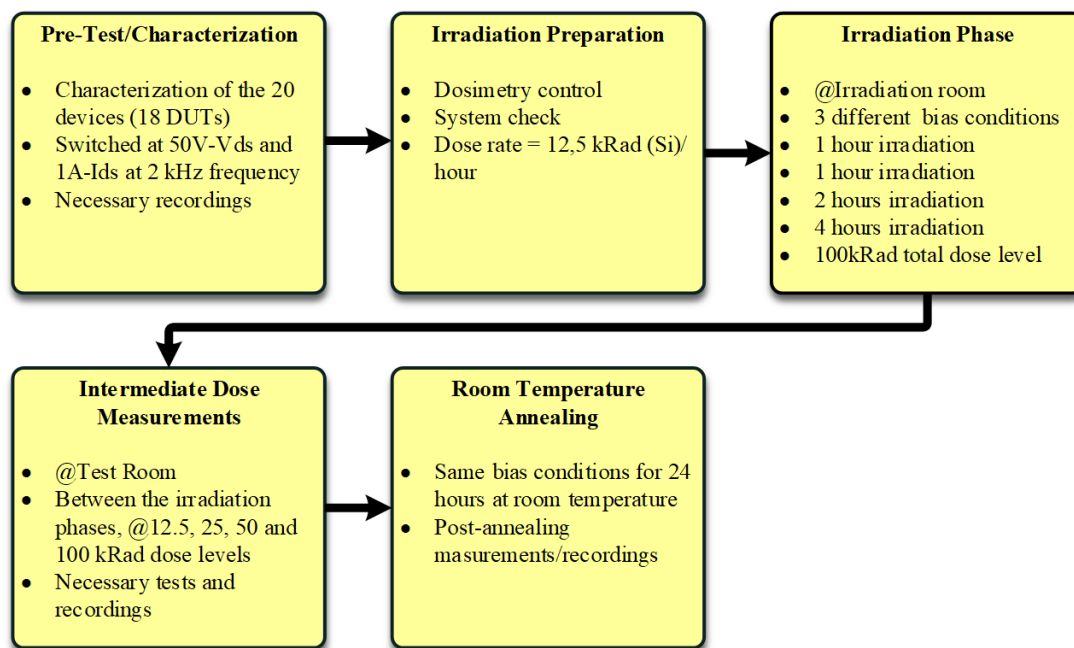
Figure 4.14 Gamma-ray irradiation test procedures block diagram

4.6. Irradiation Test Results

For all the test stages -from the pre-irradiation tests in the TID irradiation facility to the tests after the room temperature annealing in the laboratory- including the intermediate-dose test, turn-on waveforms of all devices (I_{ds}, V_{gs}, and V_{ds}) were recorded with 2,5 Gs/s sampling rate for 100 nseconds. Therefore, 250 samples were recorded for each channel in the turn-on waveforms. On the other hand, 2 mseconds of switching waveforms including 4 consecutive periods were recorded with the same sampling rate and file format for the pre-irradiation test, intermediate/final dose rate tests, and the test after the annealing. Therefore, 5.000.000 points were recorded per each channel for each stage. One of the recorded switching waveforms in the LabNotebook file format for the EPC5 gate-biased sample after the 100kRad total dose rate can be investigated in Figure 4.15.

The test results are categorized into three subcategories. In the first one, $V_{gs,th}$ and $V_{gs,plateau}$ voltages of all devices from the two brands are examined. To have a remainder again, $V_{gs,th,}$ and $V_{gs,plateau}$ voltages correspond to the V_{gs} voltage when the drain voltage is decreased to a 49 ± 0.075 V and the V_{gs} voltage when the drain current increases up to a 5 ± 0.5 mA, respectively. They were found manually one by one, and by the method explained in section 4.3.
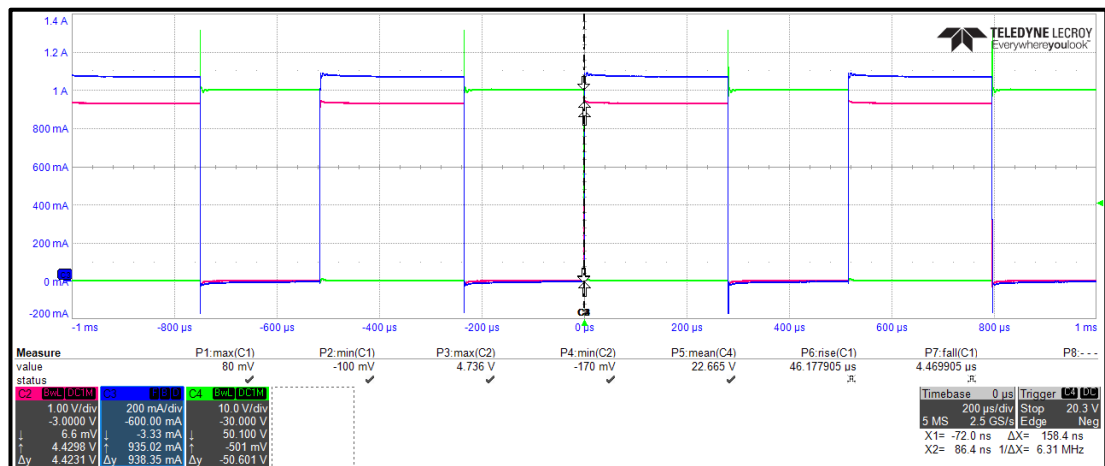
Figure 4.15 Switching waveforms of the gate-biased sample -EPC5- after the 100 kRad total dose level.

[Red: V_{gs}, Blue:I_{ds} and Green: V_{ds}]

In the second category, the gate turn-on and turn-off characteristics of all devices are examined for all stages of the TID irradiation test, including pre-irradiation and post-annealing test. Therefore, rise times and fall times (10% to 90% and 90% to 10%) of the V_{gs} waveforms for all the parts were found. WaveStudio program was used to attain these values. In Figure 4.16, an example of the single V_{gs} waveform for the device EPC5 can be seen with the rise and fall time measurements.

Measurements	Amplitude	Max	Mean	Min	Area	Base	Top	Rms	Pk-Pk	Overshoot+	Overshoot-
value	4.6433 V	4.736 V	2.5507 V	-170 mV	5.10135023 mWb	8.7 mV	4.6520 V	3.4439 V	4.906 V	3.8 %	1.8 %
Measurements	Delay	Duty	Fall 90-10	Fall 80-20	Rise 10-90	Rise 20-80	Period	Frequency	Width+	Width-	
value	-748.708184 µs	54.651 %	21.886 ns	14.139 ns	65.404 ns	38.292 ns	515.115297 µs	1.94131296 kHz	281.513423 µs	233.602267 µs	
Cursors	X1	X2	DeltaX	Y1@X1	Y2@X2	DeltaY	Y3	Y4	DeltaY		
value	-308.9920 µs	200.0000 µs	508.9920 µs	4.6460 V	4.6516 V	5.6 mV	5.00 V	1.00 V	-4.00 V		

Figure 4.16 V_{gs} waveform and rise and fall time measurements for the EPC5 gate-biased sample after the 100 kRad total dose level

Measurements	Amplitude	Max	Mean	Min	Area	Base	Top	Rms	Pk-Pk	Overshoot+	Overshoot-
value	50.043 V	65.58 V	22.665 V	-600 mV	45.3303023 mWb	40 mV	50.083 V	33.670 V	66.18 V	1.3 %	31.0 %
Measurements	Delay	Duty	Fall 90-10	Fall 80-20	Rise 10-90	Rise 20-80	Period	Frequency	Width+	Width-	
value	-748.673723 µs	45.340 %	19.799 ns	13.029 ns	43.924 ns	29.487 ns	515.115682 µs	1.94131151 kHz	233.555224 µs	281.560458 µs	
Cursors	X1	X2	DeltaX	Y1@X1	Y2@X2	DeltaY	Y3	Y4	DeltaY		
value	-123.7056 µs	200.0000 µs	323.7056 µs	50.060 V	59 mV	-50.001 V	50.0 V	10.0 V	-40.0 V		

Figure 4.17 V_{ds} waveform and rise and fall time measurements for the EPC5 gate-biased sample after the 100 kRad total dose level

In the third category, the drain turn-on and turn-off characteristics of all devices are examined for all stages of the TID irradiation test, including pre-irradiation and post-

annealing tests. Therefore, rise times and fall times (10% to 90% and 90% to 10%) of the V_{ds} waveforms for all the parts were found by using WaveStudio likewise to the previous. EPC5 gate-biased device's post-100kRad V_{ds} waveform and measurement details can be seen in Figure 4.17 as an example.

Discrete graphics were created for the control sample, unbiased samples, gate-biased samples, and drain-biased samples. Therefore, the bias effects on the device's radiation performance can be observed. Which bias-group the graph belongs to is indicated in the graph's top header. Each graph shows the test stages and measured/calculated values on the X-axis. Besides that, the focused property of the part is written in the Y-axis header. It would be valuable to remind the fact that the control/reference samples were used to investigate the variations caused by the test system or the device's original characteristics. It is normal that there would be slight variations on some readings even for the reference sample, such as $V_{gs,th}$ voltage. It shouldn't be forgotten that negligible shifts could take place between two different switching cycle recordings even without irradiation. This may be due to the instantaneous behavior of the component or the effect of the measurement device (note: the scope worked 18 hours nonstop in the facility). Before examining the results of devices under radiation, it is useful to evaluate the results of the reference sample that is not exposed to radiation. If the results of the irradiated parts are significantly different from those of the reference sample, it can be interpreted that a radiation-dependent character change has occurred on a DUT. Especially, if there is a regular and continuous change in the specific behavior of a device in a single manner, it will be possible to say that this has occurred due to radiation. Overall, it can be easily said that no catastrophic or permanent failure was observed in any of the devices. No irreversible effect damaging the device's functionality comes about due to gamma-ray irradiation. All the devices remained fully functional after the irradiation. The effects of the total dose irradiation on the behavior of the components will be examined in detail in the following sections, namely 4.6.1, 4.6.2, and 4.6.3.

4.6.1. Test Results for the V_{gs-th} and $V_{gs-plateau}$ Characteristics

V_{gs-th} is one of the critical parameters related to the turn-on of both MOSFET and GaNFET. It represents the threshold voltage that the MOSFET/GaNFET starts to turn-on [49], [50]. In [49], it is defined as the gate voltage when the drain current reaches a 250 µA, and in [40], it is defined as when the drain current increases up to 1 mA noting that the drain and gate are shorted together. Since in the experiment of this thesis devices were biased with 50V from drain terminals instead of drain and the gate are shorted during switching, it was not possible to extract V_{gs-th} with the referred method. Furthermore, in [51], various detailed V_{gs-th} voltage extraction methods are explained for MOSFETs. Since the mentioned methods are not possible to apply with recorded data types and equipment infrastructures in this experiment, a new definition of a V_{gs-th} was originally produced for this thesis study considering the recorded data type. Other than this, another definition -$V_{gs-plateau}$- was created to achieve a more reliable test result by increasing the number of turn-on characteristic check.

In Figure 4.18 and Figure 4.20, the V_{gs-th} and $V_{gs-plateau}$ values of the EPC samples can be observed for different test stages. Normally, the main effect seen on MOSFETs after total dose irradiation is the decrease in V_{gs-th}. From the figures, it can be said that no diminution is observed in the V_{gs-th} voltage of both types and the V_{gs-th} level maintained pretty much constant. Insignificant variations can be ignored considering the test results of the control samples. Further, no bias effect is observed on the V_{gs-th} performance of the devices. There is no systematic change in V_{gs-th} for any of the EPC or GS devices.

Similarly, Figure 4.19 and Figure 4.21 corresponds to the $V_{gs-plateau}$ voltages of the EPC and GaNSystems samples, respectively. There is a quasi-increase in the $V_{gs-plateau}$ along with the progressive test steps. However, It would not be right to say that it is a meaningful increase since the $V_{gs-plateau}$ voltages of both reference samples rise at close rate. Further, no bias dependent effect was noticed.
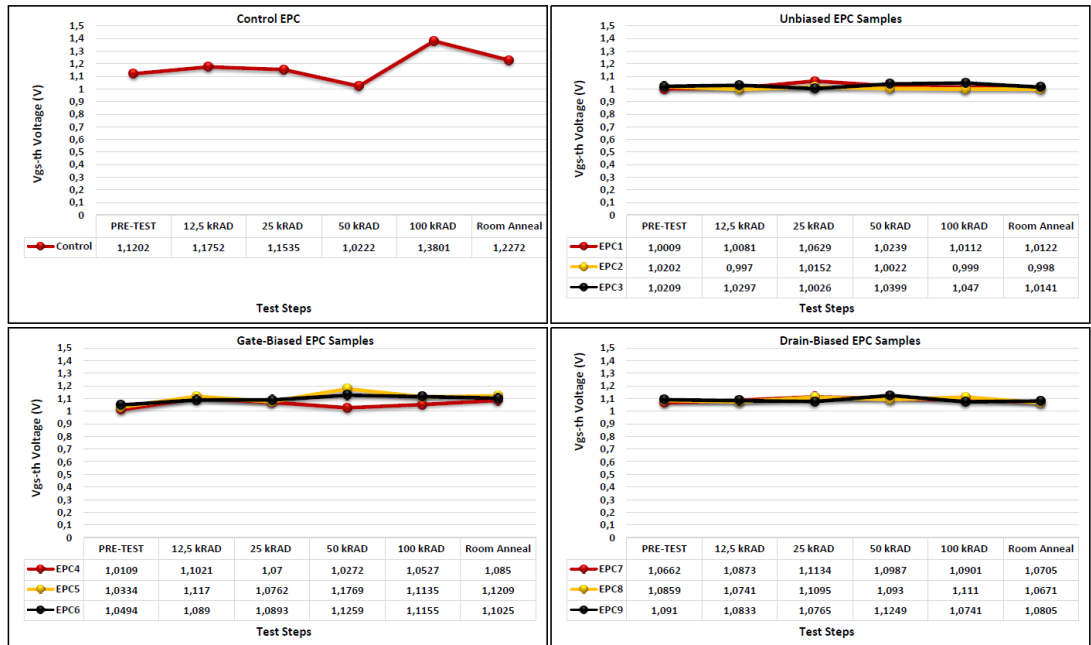
Figure 4.18 V$_{gs\text{-}th}$ characteristics for unbiased, gate-based, and drain biased EPC samples at different test stages
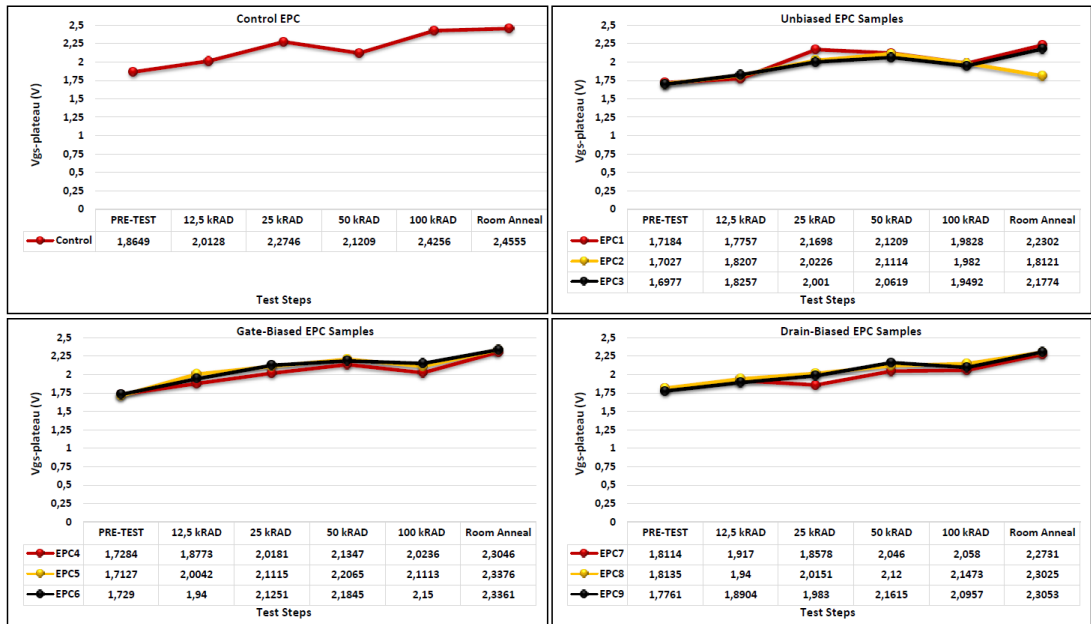
Figure 4.19 V$_{gs\text{-}plateau}$ characteristics for unbiased, gate-based, and drain biased EPC samples at different test stages

79

Control GS

	PRE-TEST	12,5 kRAD	25 kRAD	50 kRAD	100 kRAD	Room Anneal
Control	1,0035	1,0059	1,0155	1,0132	1,0076	1,0054

Unbiased GS Samples

	PRE-TEST	12,5 kRAD	25 kRAD	50 kRAD	100 kRAD	Room Anneal
EPC1	1,0289	1,0299	1,0141	1,0507	1,0284	1,0474
EPC2	0,984	0,929	0,961	0,94	0,985	0,951
EPC3	0,987	0,98	0,982	0,992	0,967	0,958

Gate-Biased GS Samples

	PRE-TEST	12,5 kRAD	25 kRAD	50 kRAD	100 kRAD	Room Anneal
EPC4	0,961	0,996	1,011	0,987	0,984	0,966
EPC5	1,0519	1,1385	1,0734	1,0742	1,0649	1,0437
EPC6	1,0749	1,0556	1,1119	1,0549	1,0938	1,0517

Drain-Biased GS Samples

	PRE-TEST	12,5 kRAD	25 kRAD	50 kRAD	100 kRAD	Room Anneal
EPC7	0,95	1,0104	1,0294	1,0355	1,0555	1,0324
EPC8	1,057	1,067	1,0371	1,0341	1,0745	1,0393
EPC9	1,005	0,944	0,986	0,977	0,98	0,939

Figure 4.20 $V_{gs\text{-}th}$ characteristics for unbiased, gate-based, and drain biased GaNSystems samples at different test stages

Control GS

	PRE-TEST	12,5 kRAD	25 kRAD	50 kRAD	100 kRAD	Room Anneal
Control	2,2076	2,175	2,127	2,1883	2,279	2,2809

Unbiased GS Samples

	PRE-TEST	12,5 kRAD	25 kRAD	50 kRAD	100 kRAD	Room Anneal
EPC1	2,293	2,2514	2,2168	2,3384	2,279	2,4815
EPC2	1,86	2,0746	1,9469	1,9424	1,9506	1,9392
EPC3	1,8767	1,9554	1,9364	1,9966	1,9252	1,9163

Gate-Biased GS Samples

	PRE-TEST	12,5 kRAD	25 kRAD	50 kRAD	100 kRAD	Room Anneal
EPC4	1,8486	1,971	1,9764	1,9637	2	1,8949
EPC5	2,3302	1,8829	2,328	2,413	2,375	2,4359
EPC6	1,935	2,24	2,2265	2,2854	2,3326	2,37

Drain-Biased GS Samples

	PRE-TEST	12,5 kRAD	25 kRAD	50 kRAD	100 kRAD	Room Anneal
EPC7	1,9066	2,0817	2,132	2,1951	2,2456	2,3
EPC8	2,1515	2,303	2,235	2,318	2,3653	2,405
EPC9	1,8225	1,9329	1,9921	2,0661	1,9695	1,9561

Figure 4.21 $V_{gs\text{-}plateau}$ characteristics for unbiased, gate-based, and drain biased GaNSystems samples at different test stages

80

4.6.2. Test Results for the Gate-to-Source Rise and Fall Characteristics

Ideally, gate-to-source rise and fall times of a device depend on the gate voltage, gate resistor, device's gate charge, and gate capacitances. Since the outside effects were maintained constant, possible characteristics change on the devices' rise/fall times are expected to be resulted from the change in the device's internal structure due to the radiation. V_{gs} rise and fall time characteristics of EPC samples for different test stages can be investigated in Figure 4.22 and Figure 4.23, respectively. It can easily be said that there is no change in the V_{gs} fall time in any of the EPC devices during any test steps. Slight changes exist in the V_{gs} rise times of the EPC parts however, they can be ignored considering the fact that they are not regular or linear in one direction and similar change exists in the control sample.

In a similar fashion, the V_{gs} rise and fall times of the GaN Systems samples for different dose rates and test steps can be examined in Figure 4.24 and Figure 4.25. No major change was recognized among the graphs. Changes in the rise and fall time values of the tested samples are not significantly different from the change in the reference sample. Besides, no dose-dependency or bias-dependancy on the results was observed for both sample types.

From the graphs, it may also be useful to give as general information that while the V_{gs} rise and fall times are approximately equal among the EPC samples, they may vary among the different GaNSystems samples.

Control EPC

	PRE-TEST	12,5 kRAD	25 kRAD	50 kRAD	100 kRAD	Room Anneal
Control	61,906	60,526	67,016	63,831	61,82	58,725

Unbiased EPC Samples

	PRE-TEST	12,5 kRAD	25 kRAD	50 kRAD	100 kRAD	Room Anneal
EPC1	63,362	57,643	65,493	63,335	65,073	58,569
EPC2	63,767	58,567	66,147	62,104	62,17	58,221
EPC3	64,906	67,011	66,312	63,905	65,015	61,058

Gate-Biased EPC Samples

	PRE-TEST	12,5 kRAD	25 kRAD	50 kRAD	100 kRAD	Room Anneal
EPC4	65,151	60,68	67,296	61,825	65,302	61
EPC5	64,751	58,235	66,957	66,676	65,404	59,521
EPC6	64,652	58,529	66,244	63,019	64,111	58,575

Drain-Biased EPC Samples

	PRE-TEST	12,5 kRAD	25 kRAD	50 kRAD	100 kRAD	Room Anneal
EPC7	65,647	58,111	66,003	63,368	65,247	61,581
EPC8	67,722	58,624	67,174	63,518	62,109	58,327
EPC9	67,826	60,163	66,944	62,824	62,595	61,23

Figure 4.22 V$_{gs}$ 10-90 % rise times for unbiased, gate-based, and drain biased EPC samples at different test stages

Control EPC

	PRE-TEST	12,5 kRAD	25 kRAD	50 kRAD	100 kRAD	Room Anneal
Control	22,579	22,585	22,623	22,573	22,066	22,3

Unbiased EPC Samples

	PRE-TEST	12,5 kRAD	25 kRAD	50 kRAD	100 kRAD	Room Anneal
EPC1	21,634	21,8	21,903	21,88	22,069	21,878
EPC2	21,451	22,496	22,025	22,125	21,941	21,845
EPC3	21,786	22,082	21,988	22,071	22,106	21,86

Gate-Biased EPC Samples

	PRE-TEST	12,5 kRAD	25 kRAD	50 kRAD	100 kRAD	Room Anneal
EPC4	21,955	23,522	22,128	22,143	22,143	22,061
EPC5	21,93	21,799	21,956	21,877	21,886	22,564
EPC6	21,833	21,684	21,393	21,59	21,911	21,54

Drain-Biased EPC Samples

	PRE-TEST	12,5 kRAD	25 kRAD	50 kRAD	100 kRAD	Room Anneal
EPC7	21,953	21,533	21,851	21,759	21,797	21,683
EPC8	21,759	21,709	21,964	21,656	21,7	21,615
EPC9	23,774	21,881	21,762	21,827	22,05	21,715

Figure 4.23 V$_{gs}$ 90-10 % fall times for unbiased, gate-based, and drain biased EPC samples at different test stages

82

Control GS

	PRE-TEST	12,5 kRAD	25 kRAD	50 kRAD	100 kRAD	Room Anneal
Control	36,485	31,107	38,017	30,828	31,398	38,606

Unbiased GS Samples

	PRE-TEST	12,5 kRAD	25 kRAD	50 kRAD	100 kRAD	Room Anneal
GS1	31,384	29,809	29,185	29,878	31,019	38,071
GS2	49,678	41,171	41,986	42,426	41,461	43,261
GS3	49,608	40,643	42,423	42,392	43,102	42,498

Gate-Biased GS Samples

	PRE-TEST	12,5 kRAD	25 kRAD	50 kRAD	100 kRAD	Room Anneal
GS4	50,211	50,442	48,461	49,189	50,438	49,979
GS5	34,045	30,723	29,88	30,969	30,143	38,139
GS6	30,747	38,032	30,523	30,954	30,8	38,566

Drain-Biased GS Samples

	PRE-TEST	12,5 kRAD	25 kRAD	50 kRAD	100 kRAD	Room Anneal
GS7	31,451	30,79	30,428	32,02	31,951	38,792
GS8	30,522	30,377	29,784	31,031	30,911	38,402
GS9	36,658	39,791	40,133	40,802	39,424	40,918

Figure 4.24 V_{gs} 10-90 % rise times for unbiased, gate-based, and drain biased GaNSystems samples at different test stages

Control GS

	PRE-TEST	12,5 kRAD	25 kRAD	50 kRAD	100 kRAD	Room Anneal
Control	12,645	13,41	12,835	13,59	13,225	12,199

Unbiased GS Samples

	PRE-TEST	12,5 kRAD	25 kRAD	50 kRAD	100 kRAD	Room Anneal
GS1	13,417	13,065	13,099	12,618	13,063	12,362
GS2	22,32	24,017	25,184	24,438	24,228	22,897
GS3	22,383	24,168	23,795	25,014	24,785	22,592

Gate-Biased GS Samples

	PRE-TEST	12,5 kRAD	25 kRAD	50 kRAD	100 kRAD	Room Anneal
GS4	23,504	25,877	26,603	25,612	26,803	24,726
GS5	13,873	12,557	12,41	12,577	12,569	12,412
GS6	14,233	12,711	12,89	12,995	12,674	12,838

Drain-Biased GS Samples

	PRE-TEST	12,5 kRAD	25 kRAD	50 kRAD	100 kRAD	Room Anneal
GS7	13,526	13,156	13,235	13,218	13,076	12,994
GS8	13,448	12,7	12,851	15,423	12,811	12,869
GS9	21,539	22,715	21,653	23,062	23,56	20,276

Figure 4.25 V_{gs} 90-10 % fall times for unbiased, gate-based, and drain biased GaNSystems samples at different test stages

83

4.6.3. Test Results for the Drain-to-Source Rise and Fall Characteristics

Theoretically, drain-to-source rise and fall times of a device depend on the drain voltage, the impedance of the drain path, the device's output capacitance (C_{oss}). Since the outside effects were maintained constant, possible characteristics change on the devices' drain-to-source rise/fall times are expected to be resulted from the change in the device's internal structure due to the radiation. V_{ds} rise and fall time characteristics of EPC samples for different test stages can be investigated in Figure 4.26 and Figure 4.27, respectively. It can obviously be said that the changes in the rise and fall times of drain-to-source voltage are very small compared to the changes in the gate-to-source rise and fall time values. One can observe that the values remain quite constant for different total dose rates and different bias conditions. It seems that the radiation has no effect on the device's output turn-on and turn-off characteristics.

The results for the GaNSystems samples are quite similar to those of the EPC samples. Rise and fall times of the GS samples can be viewed from Figure 4.28 and Figure 4.29, respectively. The radiation has no effect on the rise and fall times of the GS samples for all bias conditions. While the V_{ds} rise and fall times are matched among the EPC samples, there are small variations among the values of GaNSystems samples.

Control EPC

	PRE-TEST	12,5 kRAD	25 kRAD	50 kRAD	100 kRAD	Room Anneal
Control	44,359	43,596	42,883	42,898	42,59	42,709

Unbiased EPC Samples

	PRE-TEST	12,5 kRAD	25 kRAD	50 kRAD	100 kRAD	Room Anneal
EPC1	42,211	44,378	43,799	44,14	44,421	44,222
EPC2	43,177	44,746	43,977	43,64	44,189	44,425
EPC3	43,94	44,196	43,508	43,9	44,46	43,73

Gate-Biased EPC Samples

	PRE-TEST	12,5 kRAD	25 kRAD	50 kRAD	100 kRAD	Room Anneal
EPC4	44,658	43,886	44,126	43,23	43,585	44,117
EPC5	44,442	43,691	43,474	44,039	43,924	43,704
EPC6	44,603	44,679	43,809	43,408	43,957	44,016

Drain-Biased EPC Samples

	PRE-TEST	12,5 kRAD	25 kRAD	50 kRAD	100 kRAD	Room Anneal
EPC7	44,68	43,355	42,41	42,669	43,13	42,431
EPC8	43,863	43,477	42,965	42,171	42,67	42,699
EPC9	44,256	43,381	42,826	42,257	43,31	42,395

Figure 4.26 V_{ds} 10-90 % rise times for unbiased, gate-based, and drain biased EPC samples at different test stages

Control EPC

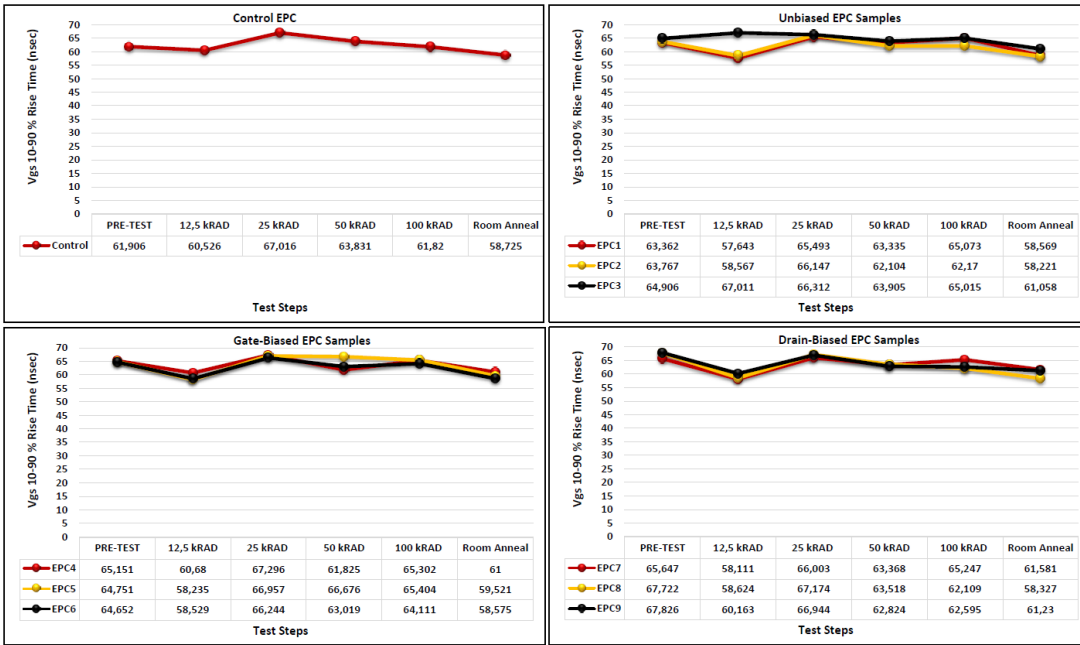|	PRE-TEST	12,5 kRAD	25 kRAD	50 kRAD	100 kRAD	Room Anneal
Control	20,292	19,817	19,822	19,72	20,343	19,466

Unbiased EPC Samples

	PRE-TEST	12,5 kRAD	25 kRAD	50 kRAD	100 kRAD	Room Anneal
EPC1	20,266	19,717	19,608	19,557	19,559	19,274
EPC2	20,219	19,752	19,678	19,575	19,497	19,346
EPC3	20,347	19,736	19,581	19,64	19,528	19,358

Gate-Biased EPC Samples

	PRE-TEST	12,5 kRAD	25 kRAD	50 kRAD	100 kRAD	Room Anneal
EPC4	20,345	19,92	19,97	19,699	19,516	19,836
EPC5	20,286	19,921	19,76	19,875	19,799	19,881
EPC6	20,394	20,054	19,963	19,918	19,792	19,931

Drain-Biased EPC Samples

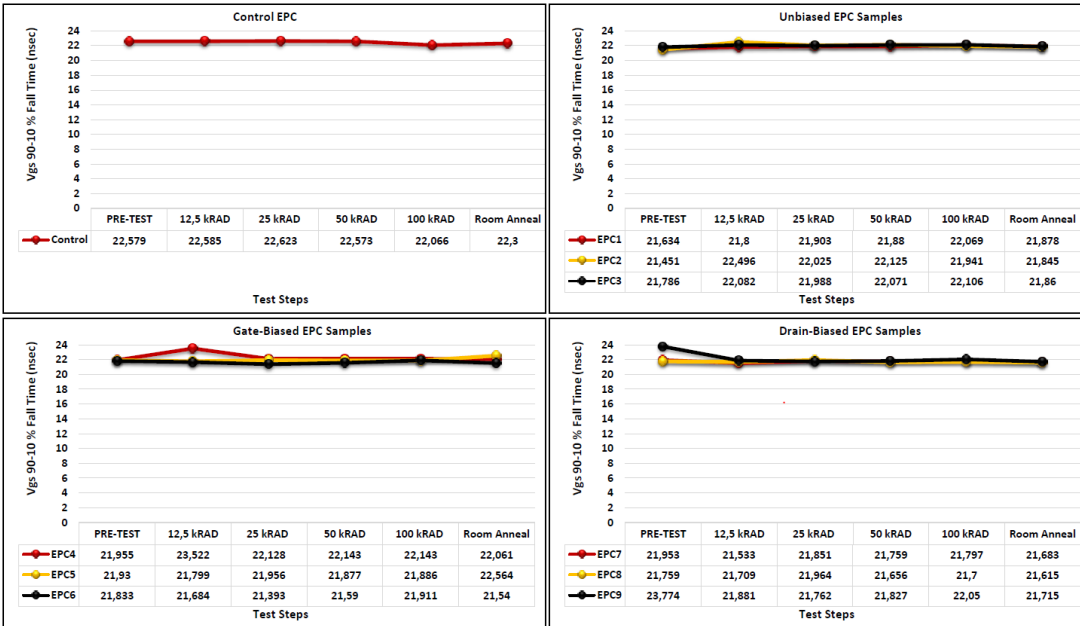|	PRE-TEST	12,5 kRAD	25 kRAD	50 kRAD	100 kRAD	Room Anneal
EPC7	20,383	19,768	19,346	19,441	19,385	19,307
EPC8	20,123	19,673	19,496	19,444	19,528	19,254
EPC9	20,223	19,713	19,416	19,511	19,58	19,278

Figure 4.27 V_{ds} 90-10 % fall times for unbiased, gate-based, and drain biased EPC samples at different test stages

85

Control GS

	PRE-TEST	12,5 kRAD	25 kRAD	50 kRAD	100 kRAD	Room Anneal
Control	12,35	12,297	12,283	12,317	12,365	12,304

Vds 10-90 % Rise Time (nsec) / Test Steps

Unbiased GS Samples

	PRE-TEST	12,5 kRAD	25 kRAD	50 kRAD	100 kRAD	Room Anneal
GS1	12,072	12,203	12,162	12,256	12,13	12,116
GS2	11,955	12,146	12,177	12,128	12,187	12,142
GS3	11,953	12,086	12,059	12,124	12,176	12,019

Vds 10-90 % Rise Time (nsec) / Test Steps

Gate-Biased GS Samples

	PRE-TEST	12,5 kRAD	25 kRAD	50 kRAD	100 kRAD	Room Anneal
GS4	12,046	12,208	12,183	12,109	12,209	12,162
GS5	12,457	12,531	12,451	12,671	12,632	12,523
GS6	12,214	12,348	12,303	12,29	12,467	12,462

Vds 10-90 % Rise Time (nsec) / Test Steps

Drain-Biased GS Samples

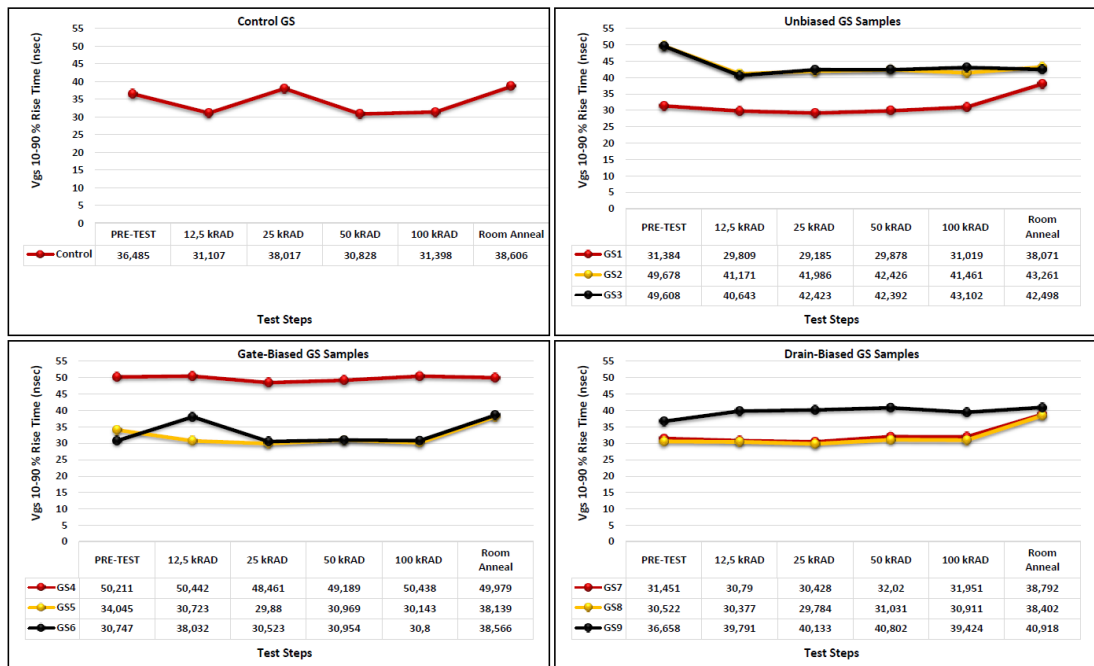|	PRE-TEST	12,5 kRAD	25 kRAD	50 kRAD	100 kRAD	Room Anneal
GS7	12,442	12,607	12,708	12,749	12,989	12,86
GS8	12,482	12,615	12,611	12,735	12,994	12,837
GS9	12,024	12,174	12,106	12,153	12,362	12,24

Vds 10-90 % Rise Time (nsec) / Test Steps

Figure 4.28 V_{ds} 10-90 % rise times for unbiased, gate-based, and drain biased GaNSystems samples at different test stages
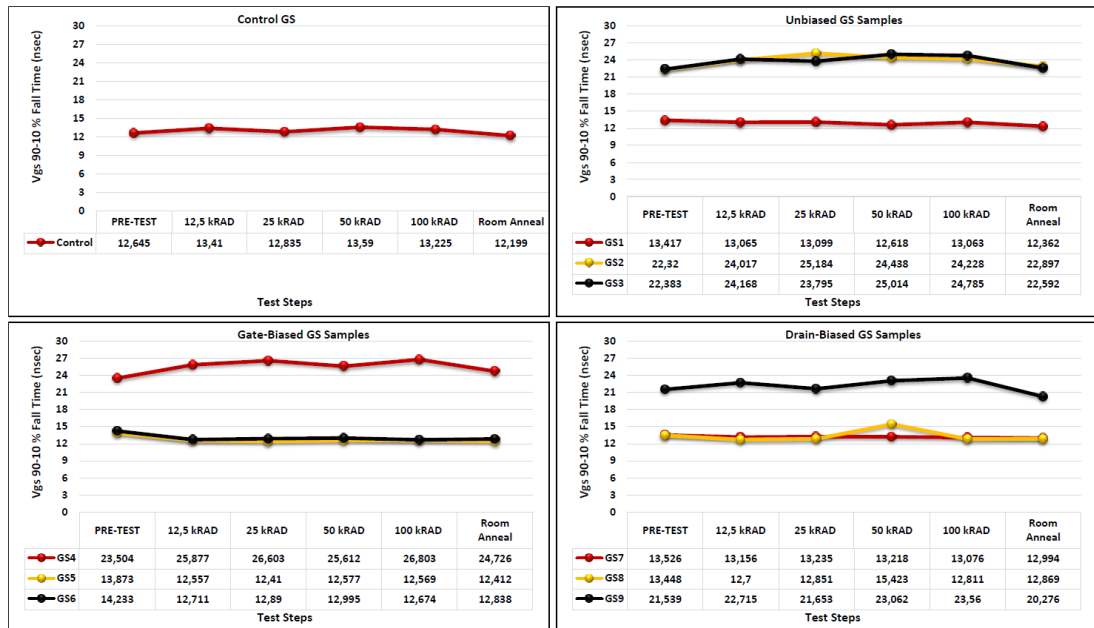
Control GS

	PRE-TEST	12,5 kRAD	25 kRAD	50 kRAD	100 kRAD	Room Anneal
Control	18,742	18,767	18,362	18,525	18,491	17,916

Vds 90-10 % Fall Time (nsec) / Test Steps

Unbiased GS Samples

	PRE-TEST	12,5 kRAD	25 kRAD	50 kRAD	100 kRAD	Room Anneal
GS1	18,983	18,839	18,672	18,591	18,56	18,316
GS2	25,809	24,507	24,238	24,641	24,223	24,849
GS3	25,271	24,142	24,136	23,896	24,206	24,178

Vds 90-10 % Fall Time (nsec) / Test Steps

Gate-Biased GS Samples

	PRE-TEST	12,5 kRAD	25 kRAD	50 kRAD	100 kRAD	Room Anneal
GS4	27,086	26,171	26,327	27,29	27,745	27,429
GS5	19,05	18,688	18,822	18,807	18,694	18,359
GS6	19,026	18,509	18,557	18,579	18,493	18,129

Vds 90-10 % Fall Time (nsec) / Test Steps

Drain-Biased GS Samples

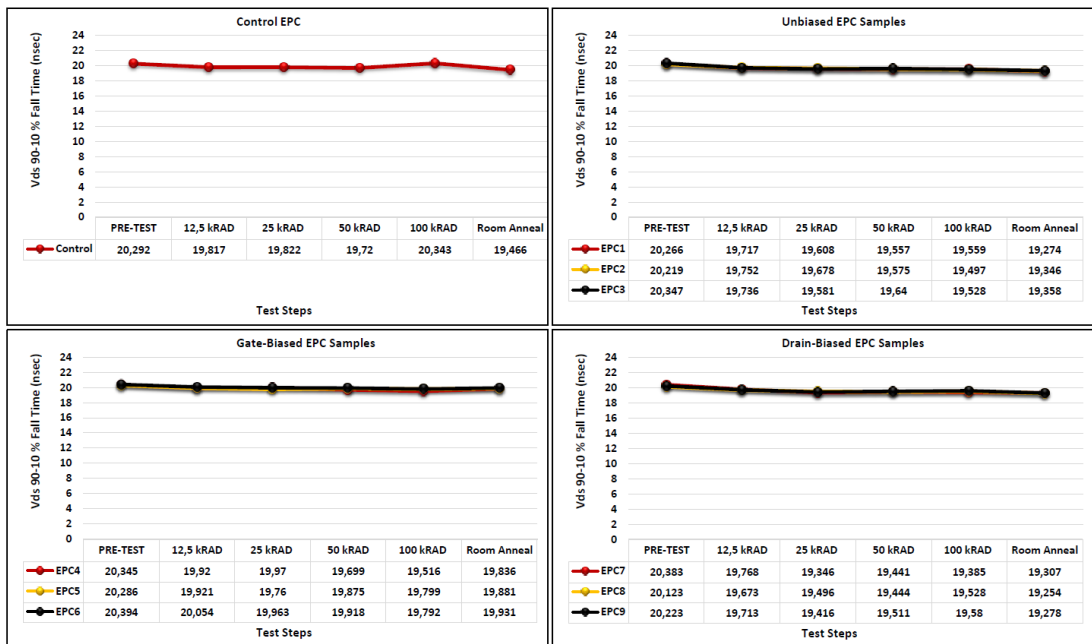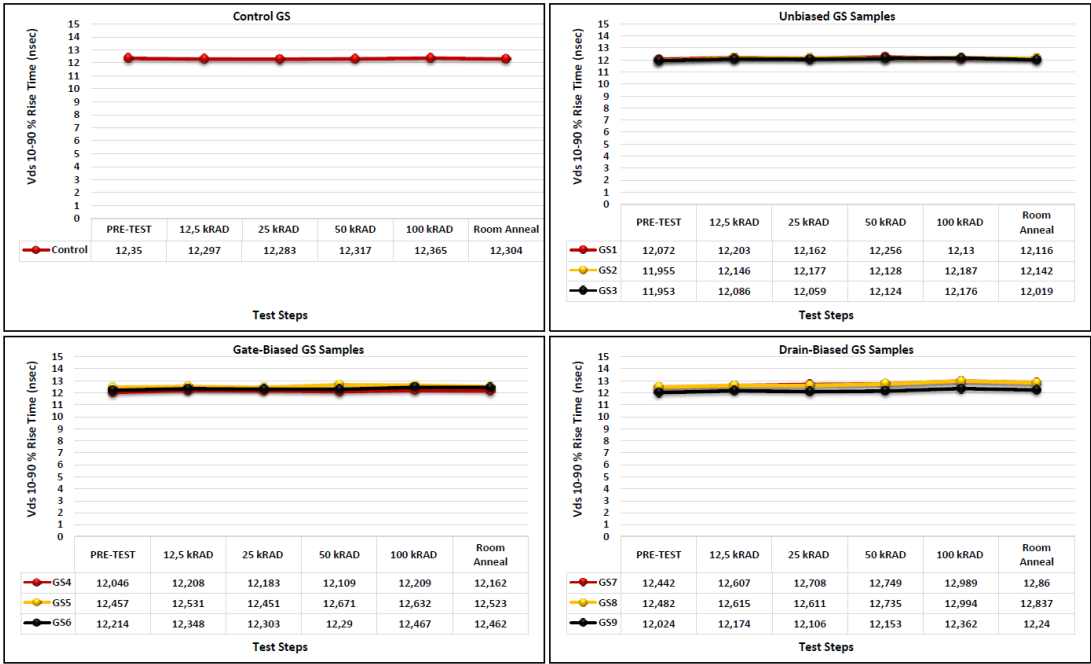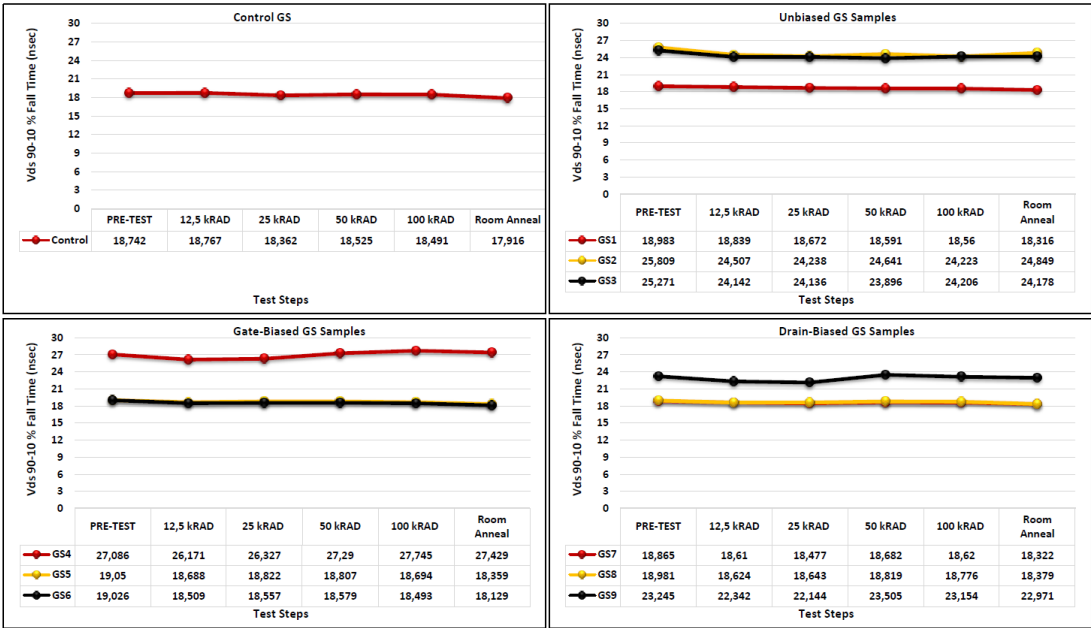|	PRE-TEST	12,5 kRAD	25 kRAD	50 kRAD	100 kRAD	Room Anneal
GS7	18,865	18,61	18,477	18,682	18,62	18,322
GS8	18,981	18,624	18,643	18,819	18,776	18,379
GS9	23,245	22,342	22,144	23,505	23,154	22,971

Vds 90-10 % Fall Time (nsec) / Test Steps

Figure 4.29 V_{ds} 90-10 % fall times for unbiased, gate-based, and drain biased GaNSystems samples at different test stages

86

4.7. Summary of The Chapter

In this chapter, the cumulative total ionizing radiation dose effects on commercial normally-off type GaNFETs were experimentally observed. The gamma irradiation test on two types of enhancement mode commercial GaNFETs is done. Nine EPC2034 samples and nine GS610004B samples were irradiated with a high dose rate of 12.5 kRad/hour. Measurements were taken by remote testing before the test, at the 12.5, 25, 50 and 100 kRad total dose values and after the 24 hours of room temperature annealing. V_{gs-th}, $V_{gs-plateau}$, V_{gs} rise and fall times, V_{ds} rise and fall times characteristics were investigated in detail. Switching characteristics are compared for distinct phases of this experiment for different bias conditions. The aim was to observe if the characteristics change, degradation on the device's performance or the permanent failures take place. It can easily be said that all test samples have been successfully maintained their health, even at the 100krad dose level regardless of the bias condition. No meaningful change in the device characteristics or degradation of the device's function was observed. Results revealed that the irradiated GaNFETs has the radiation tolerance under the 100 kRad maximum dose level of this test. As general, the 100 kRad radiation tolerance is well enough even for most of the geostationary orbit mission having a long operational lifetime such as 15-20 years. The irradiated GaNFETs showed that they are very strong candidate to become the switching element of the future space power designs.

CHAPTER 5

CONCLUSION

In this thesis, mass, volume and cost reduction methods for the space power designs were proposed. Two strategies were suggested. While the first one is to use commercial reliable switching components instead of radiation-hardened MOSFET, the second one is to increase the switching frequency of the converter boards. Both methods showed the use of GaNFET as a common idea. Since the enhancement mode GaNFETs are new parts, they do not yet have adequate space heritage. Before the integration of the GaNFETs to the space power designs, their performance under radiation must first be proven.

This thesis reports two of the earliest radiation irradiation studies for the commercial enhancement-mode GaNFETs. Two different radiation tests are reported in this thesis, namely proton and gamma-ray irradiation tests. In the proton irradiation test, GaNFETs were irradiated up to radiation fluence level of 1.476×10^{13} protons/cm^2 which is quite a higher level than that of appointed in the ESCC standard. Even after this excessive fluence level, GaNFETs have revealed positive results. They were able to stay healthy and continue to function. No irreversible and destructive effects took place after the irradiation. On the other hand, the GaNFETs passed the TID test successfully as well. 18 GaNFETs from 2 brands were irradiated with gamma-rays and all maintained their operation. No characteristics change or performance degradation was observed. No permanent failure took place, and all stayed fully functional.

Obtained results encourage the designer to use the GaNFETs in the satellite power systems of future designs. After the accomplished positive results of this thesis work,

in this chapter what kind of benefits can be achieved by using the GaNFETs will be discussed.

5.1. Design Example and the Benefits to be Obtained

In this section, two designs having GaNFET and MOSFET as a switching element will be compared for PCU battery charge regulator example with buck converter topology. The design is assigned for the example GEO satellite having a regulated bus. Considering the 80% derating rule pointed in the ECSS derating standard for the FET family group, 200V rated semiconductors are decided. IRHMS6S7260 (200V-45A) rad-hard MOSFET from IRF and EPC 2034 (200V-45A) commercial GaNFET from EPC are chosen for the loss comparison at different frequencies. Calculations are made according to the following design assumptions given in Table 5.1.

Table 5.1 Design assumptions

Bus Voltage	100V
Average Battery Voltage	75V
Duty	75%
Load Current	10A
GaNFET's Total Switching Time	20 nsec
MOSFET's Total Switching Time	145 nsec
GaNFET's Gate Voltage	5 V
MOSFET's Gate Voltage	12 V

Datasheet parameters were used as well when needed during calculations. Loss formulas written in Table 5.2 are used for the calculations. Then the loss values of two switching elements at different frequencies are found as in Table 5.2. The losses can also be compared from the graph given in Figure 5.1.

Table 5.2 Loss comparison of the GaNFET and MOSFET for the battery charge regulator example

| Frequency	@75 kHz		@100kHz		@125kHz		@150kHz	
Formula	EPC2034	IRHMS6S 7260	EPC2034	IRHMS6S 7260	EPC2034	IRHMS6S 7260	EPC2034	IRHMS6S 7260
1. Conduction Loss (W) Io^2 * Rdson * Duty	0,75	2,175	0,75	2,175	0,75	2,175	0,75	2,175
2. Gate Charge Loss (W) Qgate * Vgate * fsw	0,033	0,216	0,0044	0,288	0,0055	0,36	0,0066	0,432
3. Switching Loss (W) 1/2 * Vds * Ids* (tr + tf) * fsw	0,75	5,4375	1	7,25	1,25	9,0625	1,5	10,875
4. Output Capacitance Loss (W) 1/2 * Coss * Vds^2 * fsw	0,675	1,4295	0,9	1,906	1,125	2,3825	1,35	2,859
Total Loss (W)	2,21	9,26	2,65	11,62	3,13	13,98	3,61	16,34
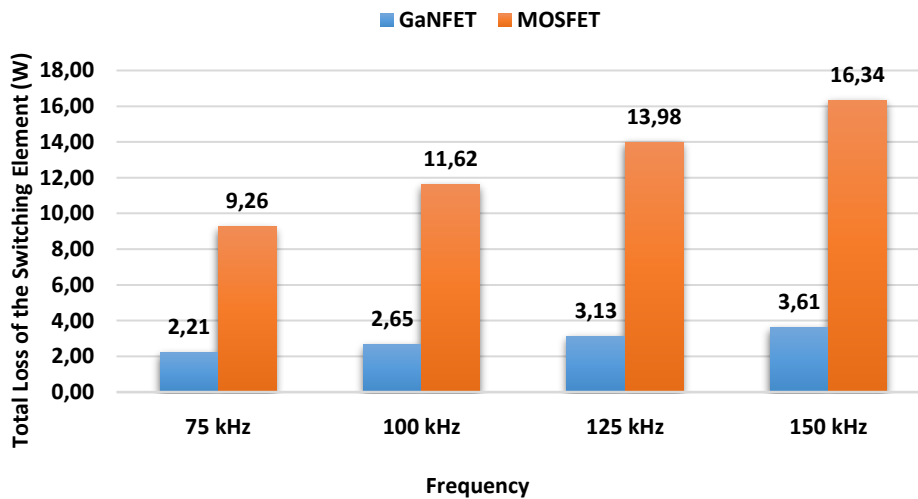
Figure 5.1 Loss comparison graph for the battery charge regulator example

It is obvious that using the GaNFET instead of the space-qualified MOSFET is absolutely advantageous in terms of efficiency. To the best of author's knowledge, the currently preferred switching frequency range is between 75kHz and 150 kHz for charge and discharge boards of PCU in general. Increasing the frequency further after a certain level leads to a limitation of the qualification temperature range of the PCU

due to heating problems of the switch. Therefore, the space power regulator designs are mature enough and shrinking the filter components significantly is not that much easy with current space MOSFET technologies.

According to calculations, the loss value of the MOSFET at a 100 kHz frequency (11.6 W) is equal to the loss of the GaNFET at 570 kHz. It must be accepted that increasing the frequency to 570 kHz wouldn't be practical considering today's GaNFET packages and heating of the GaNFETs as well. However, increasing it to around 250 kHz where the loss value is 5.5 W would be reasonable for now for the following analyzes. Now, it will be assumed that the commercial or space-qualified GaNFET is used instead of MOSFET in the battery charge and discharge converter boards and the switching frequency is increased up to 250 kHz from 100 kHz. Then, depending on this assumption, what kind of benefits will be obtained can be examined in detail in Figure 5.2. Before the discussion of the figure, it would be useful to sort the assumptions which are dependent on the author's experiences as follows:

- 7-9 kW load power is assumed
- 40-50 kg PCU weight is assumed
- 2 spacecraft models as Engineering Qualification and Flight Models are assumed to be produced.
- 6 Solar Array Regulator boards having 4 MOSFET each is assumed
- 6 Battery Discharge Regulator boards having 6 MOSFET each is assumed
- 2 Battery Charge Regulator boards having 2 MOSFET each is assumed
- Commercial GaNFET=$ 5, Engineering Model (EM) GaNFET = $ 155, Flight Model (FM) GaNFET=$ 285, EM MOSFET=$ 875, and FM MOSFET= $ 1250
- 68 μH metalized polyester film capacitor: EM = $ 280, FM = $405
  39 μH metalized polyester film capacitor: EM = $72, FM = $210
- BDR has 500 gr filter inductor/transformer
- BCR has 150 gr filter inductor and 100 gr filter capacitor
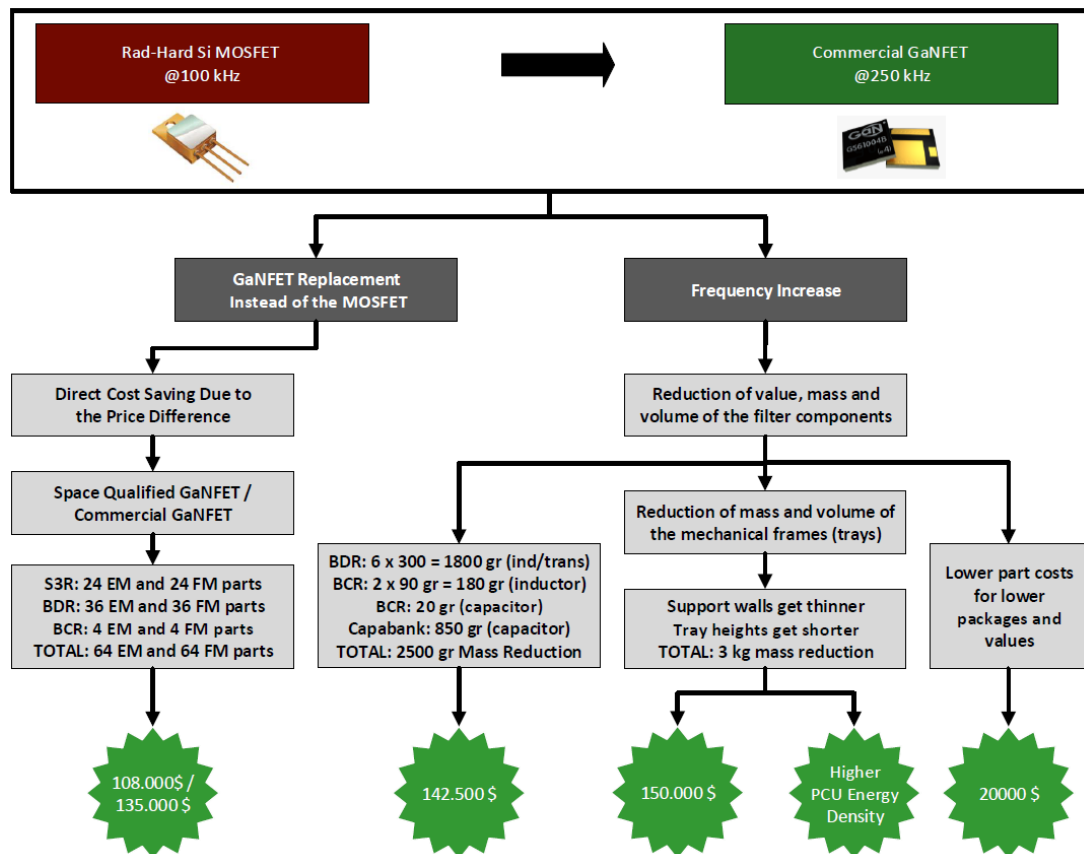- $ 50.000 launching cost per kilogram [2]

92

Figure 5.2 Benefits to be acquired by the GaNFET integration to the PCU

To understand the benefits gained by the GaNFET integration to the PCU equipment, a 7-9 kW power system example will be investigated. The usage of GaNFET instead of the space-qualified MOSFET will result in direct cost reduction owing to the cost difference of the parts. Because even the space-qualified GaNFETs are low-cost compared to space-qualified MOSFETs, either the commercial GaNFETs or the space-qualified GaNFETs usage instead of the space MOSFET will be making a significant difference in the component cost. Firstly, two spacecraft models, namely Engineering Qualification Model (EQM) and Flight Model (FM), are assumed to be produced. Secondly, Based on the author's experience, 6 Solar Array Regulator boards, 6 Battery Discharge Regulator boards and 2 Battery Charge Regulator boards are assumed to take part in the PCU. Besides, these boards contain 4, 6 and 2

MOSFETs each, respectively. It is also assumed that the engineering model (EM) components will be used for the EQM satellite, and the flight model (FM) components will be used for the FM satellite. Together with these assumptions, 64 EM MOSFETs and the 64 FM MOSFETs are supposed to be replaced by the GaNFET. Then the total cost saving becomes $ 108.000 for the space-qualified GaNFET replacement or $ 135.000 for the commercial-grade GaNFET replacement. It will also be valuable to note that the two spacecraft models assumption for a mission is an optimistic approach. Therefore, the cost-saving will be more for the programs having more than two spacecraft models.

The second and the main achievement by the GaNFET integration is the ability of the frequency increase as explained in section 1.2.1. By the frequency increase, the filter inductors and the capacitors will be shrunk. Increasing the frequency from 100 kHz to 250 kHz causes the capacitor and inductor values to fall to two-fifths. Then, the following are assumed: the inductor weight decreases 300 gr for each BDR boards, 90 gr for each BCR boards and BCR filter capacitors decrease 20gr for each board. In the capacitor bank boards, the mainly used capacitor type is self-healing metalized polyester film capacitors [52]. From the datasheet [52], 50 PM907 type 68 µF-200V capacitors (having 54.2 gr weight and 32 mm height) are supposed to be used in the capacitor bank boards. Then, they were assumed to be replaced by the same type of 39 µF-200V (37.3 gr and 22 mm) capacitors. Therefore, the capacitor bank mass drops up to 850 gr. All these factors correspond to a total of 2850 gr mass drop of filter components. It corresponds to a $ 142.500 cost reduction in the launch phase.

Depending on the technology level, 40-50 kg of PCU weight is appropriate for this power level. It would be a fair assumption that 30 % of the total 50 kg PCU is consists of the mechanical parts (trays, lids, busbars, etc.). By the downsizing of the heavy filter components, the support walls can be thinner. Besides, the main components which determine the tray height are filter components in general especially for the converter boards and the capacitor bank. Then, with the shrinkage of the filter components, the tray height could also decrease and the total PCU length and volume

shorten. Then, the 20 % mass decrease (3kg) is assumed for the mechanical parts which makes a $ 150.000 difference in the launch cost.

The cost of a capacitor is directly related to the capacitance value. It is assumed to replace the 68 µF PM907 capacitors with 39 µF PM907 capacitors in the capabanks. For the 50 EM parts and 50 FM parts, it corresponds to a $ 20000 of the price difference.

All these changes allow to PCU to shrink as well. With the above assumptions, the mass of the PCU decreases between 10-15 %. The volume of the PCU also lessens owing to the shortening of the tray heights. Therefore, the energy density of the PCU in terms of the mass or volume increases notably. High energy density means flexibility in the positioning of the equipment in the satellite. Besides, it means the lower total spacecraft mass. These advantages make it preferable in the market if the manufacturer has a plan to sell or export the equipment.

5.2. Limitations and Considerations

Despite that the space technologies are extremely conservative and the reliability is the first priority, there is a new trend today -using Commercial of the Shelf (COTs) in space due to their performance and cost advantages. However, one should need to be aware of the risks by using the commercial-grade GaNFETs on space. One should also need to take special precautions in the circuit designs due to new concepts of the GaNFET itself. The main points to be considered with the commercial GaNFETs are listed below.

➢ Because the GaNFETs are faster devices compared to MOSFETs, the rising and the falling edges of the current and voltage waveforms becomes quite shorter. Besides, the gate threshold voltages of the GaNFETs are about 1V and they are almost ready to be triggered immediately even by the noises on the ground. Therefore, the parasitic inductors and the capacitors on the board become noteworthy. A designer should pay special attention to the gate drive current paths and the main circuit current paths. Thus, the layout design becomes a complicated

issue and designers should carefully spend more on the new design. This means that old layout designs are almost garbage.

➤ The majority of the commercial parts are not hermetically sealed; therefore, they need to be stored in appropriate conditions for long-term with low-humidity to avoid oxidation which is resulted in electrical performance disruption, solderability problems and mechanical degradation for the component. It would be confident to store them in a dry-pack condition.

➤ The fact that they have some plastic and outgassing materials is another risk. Therefore, the packages need to be baked before the mounting for pre-releasing the gas in it.

➤ Parts without a space heritage always pose a risk. Therefore, they can be used in the missions with short operation lifetime or non-critical functions to gain a space experience as the first step.

➤ The high vibration condition of the launch phase should be considered. The device needs to withstand the expected vibration level. They need to be tested individually or at the board level.

➤ They need to be used in the operation by appropriately derated to decrease the failure risk by lower stress. They should be used away from the limits of the specifications.

➤ Their thermal capabilities should also be screened as possible, for example by the component level or board level thermal cycling.

5.3. Future Works

Commercial GaNFETs have revealed exciting results after the radiation tests. These results encourage the designer to use this material in space applications. However, before using the GaNFETs completely as the basic switching element instead of MOSFETs in space power designs, it will be useful for GaNFET to gain space heritage as the next stage. In space applications, the space heritage for a component is one of

the most important reassuring cornerstones. If a part has a successful space heritage in the past, that component is one of the parts that the designer can safely use in future designs. Therefore, as a next step, the commercial GaNFETs will be added to the next designs of future missions and to be used in non-critical functions in order to gain space history. For this purpose, the heritage board will be designed as in Figure 5.3.
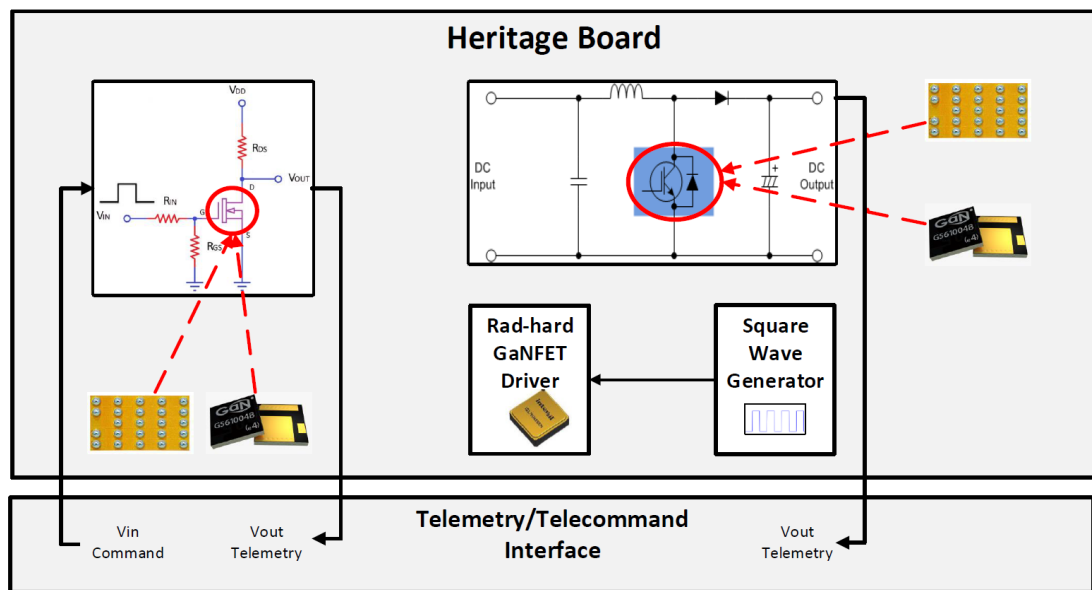

Figure 5.3 GaNFET heritage board design

In this design, two main blocks are planned. In the first, the GaNFETs will be used in the simple boost converter designs with constant duty. The constant duty signal will be produced by the square wave generator circuit having a rad-hard timer IC or the proper circuit with a rad-hard op-amp. Then, the low-side radiation-hardened GaNFET driver [53] will drive the GaNFET. The output signal value will be sent as a telemetry signal to the ground station on the earth. Over the years during the mission lifetime, this voltage level will be examined to see if GaNFET maintains its health in real space. In the second design, the GaNFET will be used as an on-off switch. The pulse signal will be sent by the telecommand and the V_{out} signal will be monitored as

a response (when the command is high, the output becomes low) to check if the GaNFET is healthy. The second design is more easily applicable to more samples because it is quite straightforward and low-cost. Besides, power loss would be lower in total compared to the boost converter design. On the other hand, the boost converter is more reliable in terms of the ability to continuously test the part under both current and voltage. Therefore, the first design will be used for the test the part under higher stress while the second one will be used to have more samples to be tested.

REFERENCES

[1]   Standards, *Space engineering spacecraft propulsion hardware,*. November. 2008, pp. 1–72.

[2]   M. R. Patel, *Spacecraft Power Systems*, vol. 29. 2004.

[3]   M. R. Hayhurst, R. E. Bitten, and E. M. Mahr, 'Space Power Heritage Study Final Results', 2019.

[4]   TI, 'LC Filter Design Application Report', 2000.

[5]   D. Graovac, M. Pürschel, and K. Andreas, 'MOSFET Power Losses Calculation Using the Data- Sheet Parameters', 2006.

[6]   G. Lakkas, 'MOSFET power losses and how they affect power-supply efficiency', *EngineerIT*, no. April, pp. 22–26, 2016.

[7]   NASA, 'COTS Components in Spacecraft Systems : Understanding the Risk', 2014.

[8]   T. Zednicek, 'Commercial versus COTS+ versus Qualified Passive Components in Space Applications', *Proc. ESA Sp. Passiv. Compon. Days*, October, p. 17, 2016.

[9]   E. Applebaum, 'Powershield: A novel approach to radiation tolerant power MOSFETs', *Eur. Sp. Agency, (Special Publ. ESA SP*, no. 589, pp. 199–203, 2005.

[10]   A. Lidow and J. Strydom, 'Gallium Nitride (GaN) Technology Overview EFFICIENT POWER CONVERSION', pp. 1–12, 2012.

[11]   K. Bernard, A. Engineer, I. Analog, P. Group, and R. E. Corp, 'Advantages of Using Gallium Nitride FETs in Satellite Applications Characteristics of GaN FETs', pp. 1–7, 2018.

[12] D. R. A. Lidow, J. Strydom, M. de Rooij, *GaN Transistors for Efficient Power Conversion*. 2014.

[13] A. Esposito, 'Advantages Of GaN FETs Versus " Best Of Breed " Silicon MOSFETs', 2015.

[14] N. Mehta, 'GaN FET module performance advantage over silicon', *Texas Instruments*, March 2015, pp. 1–7, 2015.

[15] O. E. Mansilla *et al.*, 'Low side gan fet driver for space applications', *ESPC*, vol. 12006, no. 1, pp. 2–5, 2017.

[16] C. Delepaut and N. Le Gallou, 'Power Switching Breadboard Based on Gallium Nitride Transistor ', no. 1, pp. 6–10, 2011.

[17] A. Kalavagunta *et al.*, 'Electrostatic Mechanisms Responsible for Device Degradation in Proton Irradiated AlGaN / AlN / GaN HEMTs', vol. 55, no. 4, pp. 2106–2112, 2008.

[18] B. D. White *et al.*, 'Electrical , Spectral , and Chemical Properties of Structures as a Function of Proton Fluence', vol. 50, no. 6, pp. 1934–1941, 2003.

[19] J. Chen *et al.*, 'Proton-Induced Dehydrogenation of Defects in AlGaN / GaN HEMTs', *IEEE Trans. Nucl. Sci.*, vol. 60, no. 1, pp. 4080–4086, 2013.

[20] A. G. Hemts *et al.*, 'RF Performance of Proton-Irradiated', *IEEE Trans. Nucl. Sci.*, vol. 61, no. 1, pp. 2959–2964, 2014.

[21] T. Roy *et al.*, 'Process Dependence of Proton-Induced Degradation in GaN HEMTs', *IEEE Trans. Nucl. Sci.*, vol. 57, no. 1, pp. 3060–3065, 2010.

[22] B. D. Weaver *et al.*, 'On the Radiation Tolerance of AlGaN / GaN HEMTs', vol. 5, no. 7, pp. 208–212, 2016.

[23]   European Space Components Coordination, 'Single Event Effects Test Method and Guidelines - ESCC Basic Specification No . 25100', *Ecss*, no. 25100, pp. 1–24, 2002.

[24]   ESCC, *TOTAL DOSE STEADY-STATE IRRADIATION TEST METHOD ESCC Basic Specification No . 22900*, no. 22900. 2007, pp. 1–22.

[25]   L. Scheick, 'Determination of single-event effect application requirements for enhancement mode gallium nitride HEMTs for use in power distribution circuits', *IEEE Trans. Nucl. Sci.*, vol. 61, no. 6, pp. 2881–2888, 2014.

[26]   C. Abbate *et al.*, 'Microelectronics Reliability Experimental study of Single Event Effects induced by heavy ion irradiation in enhancement mode GaN power HEMT', *MR*, pp. 6–10, 2015.

[27]   S. Dhawan *et al.*, 'Buck Converter Development for the Inner Detector Environment of the SLHC Upgrade', pp. 1–6, 2007.

[28]   J. I. Vette, 'The space radiation environment', *IEEE Trans. Nucl. Sci.*, vol. 12, no. 5, pp. 1–17, 1965.

[29]   J. W. J. Howard and D. . Hardage, 'Space Radiation and Its Effects on Electronic Systems', July, 1999.

[30]   N. Ya'acob, A. Zainudin, R. Magdugal, and N. F. Naim, 'Mitigation of space radiation effects on satellites at Low Earth Orbit (LEO)', *Proc. - 6th IEEE Int. Conf. Control Syst. Comput. Eng. ICCSCE 2016*, no. November, pp. 56–61, 2017.

[31]   K. K. Robert Baumann, *Radiation Handbook for Electronics*. 2019.

[32]   USADefenceDepartment, *Test Method Standard for Semiconductor Devices: MIL-STD-750E*, FEBRUARY 1995. 2006, p. 685.

[33]   N. Ikeda, S. Kuboyama, and S. Matsuda, 'Single-event burnout of super-junction power MOSFETs', *IEEE Trans. Nucl. Sci.*, vol. 51, no. 6 II, pp. 3332–3335, 2004.

[34]   M. V. O'Bryan *et al.*, 'Compendium of current single event effects results from NASA goddard space flight center and NASA electronic parts and packaging program', *IEEE Radiat. Eff. Data Work.*, vol. 2017–July, 2017.

[35]   M. G. Faruk *et al.*, 'Proton and neutron radiation effects studies of MOSFET transistors for potential deep-space mission applications', *IEEE Aerosp. Conf. Proc.*, pp. 1–13, 2012.

[36]   M. Wind, J. V. Bagalkote, P. Beck, M. Latocha, and M. Poizat, 'TID and SEGR radiation characterisation of european COTS power MOSFETs with respect to space application electronics', *Proc. Eur. Conf. Radiat. its Eff. Components Syst. RADECS*, vol. 2015–Decem, pp. 1–3, 2015.

[37]   EPC, 'EPC2034 – Enhancement Mode Power Transistor', 2016.

[38]   NASA, *Parts Assurance Standard Measurement System Identification :* 2017, pp. 1–39.

[39]   A. Gencer, B. Demirköz, I. Efthymiopoulos, and M. Yi, 'Nuclear Instruments and Methods in Physics Research A Defocusing beam line design for an irradiation facility at the TAEA SANAEM Proton Accelerator Facility', vol. 824, pp. 202–203, 2016.

[40]   D. of Defence, *Test method standard microcircuits*, no. July. 2018, p. 208.

[41]   ESA, *TERMS, DEFINITIONS, ABBREVIATIONS, SYMBOLS AND UNITS ESCC Basic Specification No.21300*, no. 21300. 2013, pp. 1–20.

[42]   GaNSystems, 'EVG100E15 100 V enhancement mode GaN transistor Preliminary Datasheet', 2017.

[43]   ECSS, 'Space product assurance Derating -EEE components ECSS Secretariat ESA-ESTEC Requirements & Standards Division Noordwijk, The Netherlands', 2011.

[44]   S. Liu, C. Dicienzo, M. Bliss, M. Zafrani, M. Boden, and J. L. Titus, 'Analysis of commercial trench power MOSFETs' responses to Co60 irradiation', *IEEE Trans. Nucl. Sci.*, vol. 55, no. 6, pp. 3231–3236, 2008.

[45]   Texas Instruments, 'UCC27611 5-V , 4-A to 6-A Low Side GaN Driver', 2018.

[46]   Texas Instruments, 'LM555 Timer', 2015.

[47]   C. Particle, T. W. Hertel, and G. S. Smith, 'Pulse radiation from an insulated antenna: An analog of Cherenkov radiation from a moving', *IEEE Trans. Antennas Propag.*, vol. 48, no. 2, p. 165172, 2000.

[48]   A. M. Sanchez, V. Brisan, and A. Difonzo, 'TID irradiation facility utilizing novel alanine dosimetry', *IEEE Radiat. Eff. Data Work.*, pp. 1–5, 2017.

[49]   Vishay, 'Power MOSFET Basics : Understanding the Turn-On Process', 2015.

[50]   nexperia, 'Designing in MOSFETs for safe and reliable gate-drive operation', 2017.

[51]   L. Dobrescu, M. Petrov, D. Dobrescu, and C. Ravariu, 'Threshold voltage extraction methods for MOS transistors', *Proc. Int. Semicond. Conf. CAS*, vol. 1, no. 2, pp. 371–374, 2000.

[52]   EXXELIA, 'PM 907 - PM 907 S Datasheet', 2015.

[53]   Intersil, 'Isl70040seh, isl73040seh Radiation Hardened Low-Side GaN FET Driver Datasheet', 2019.

APPENDICES

## A. Encountered Grounding Problem Before the Proton Irradiation Test and Its Solution

When the DUT1 on PCB1 was switched individually, waveforms were well enough appropriate as in Figure 3.5. However, when the DUT2 was switched together with DUT1 or individually, the waveforms turned into abrupt and unexpected forms. As can be seen in Figure A.1- (a) and (b), a 2 V peak to peak oscillation came out in the sensed V_{gs} signal of the DUT2 which is supposed to be constant at around 2.3 V level. This oscillation also affects the V_{gs} signal of the DUT2, which can be seen in Figure 3.5- (c).
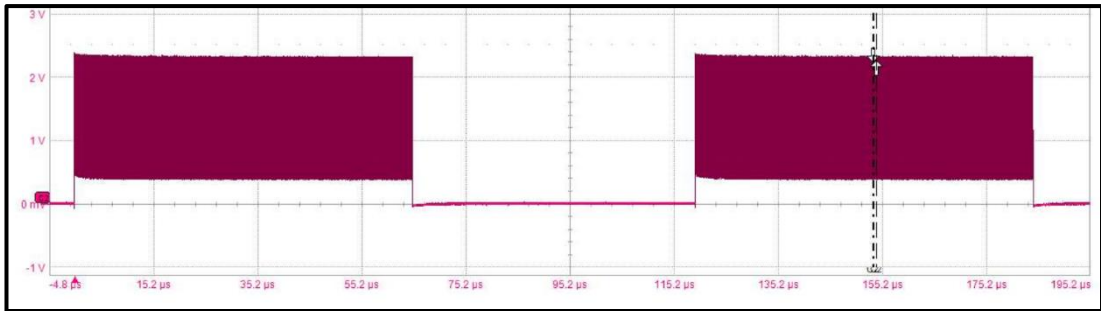
(a)
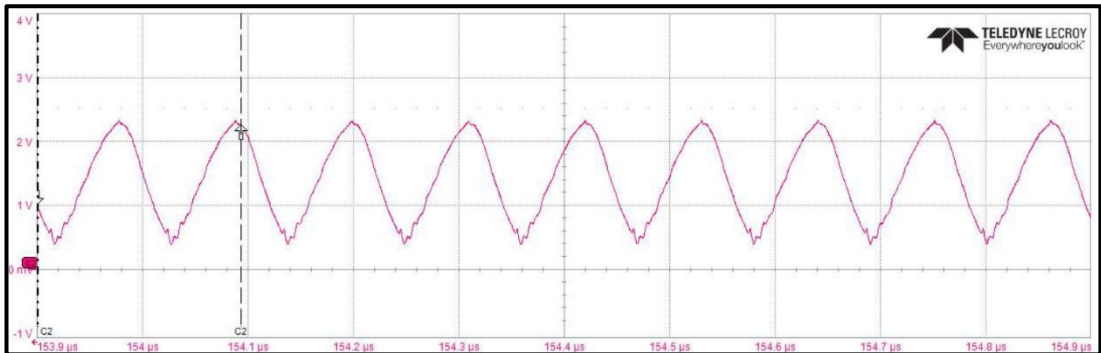
(b)
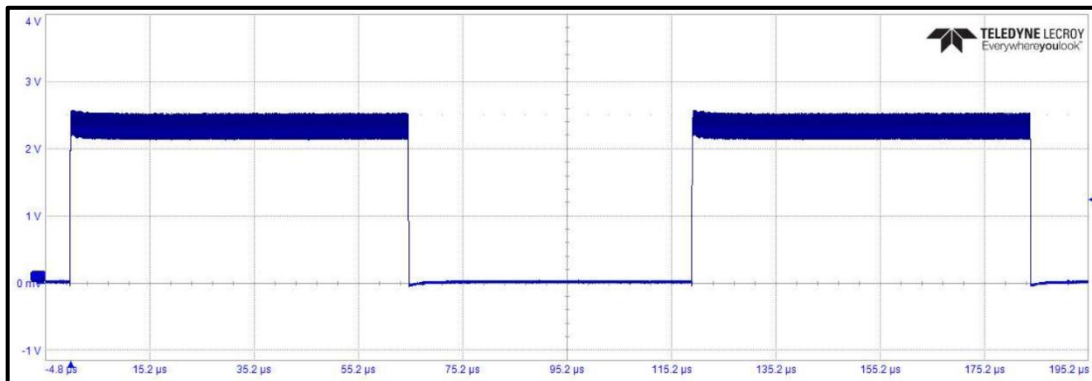
(c)

Figure A.1 Grounding Problem: (a): Sensed Vgs signal of DUT2 on test PCB1 (b) Sensed Vgs signal of DUT2 on test PCB1 (zoomed) (c): Sensed Vgs signal of DUT1 on test PCB1

When the possible causes of the problem were pondered, it was realized that the source of the problem could be the grounding strategy. The circuit designed in a way that it has two grounds (signal and power ground, namely) which are connected at a single star point through the 0 Ohm resistor, which can be seen in Figure A.2. When the GaNFET is turning on, it draws current from the driver to charge its gate to source capacitor. This current is basically drawn from decoupling (or supply) capacitor connected to the supply pin of the driver IC. Turn on the current path can be investigated in Figure A.2 – left (red). Because the decoupling capacitor is referenced to signal ground, the current had to travel quite a long path to return to the signal ground again. When the gate current charges C_{gs} and pass to power ground (to which the GaNFET source is referenced), it needs to return to capacitor's negative (signal ground) through the 0 Ohm jumper resistor.
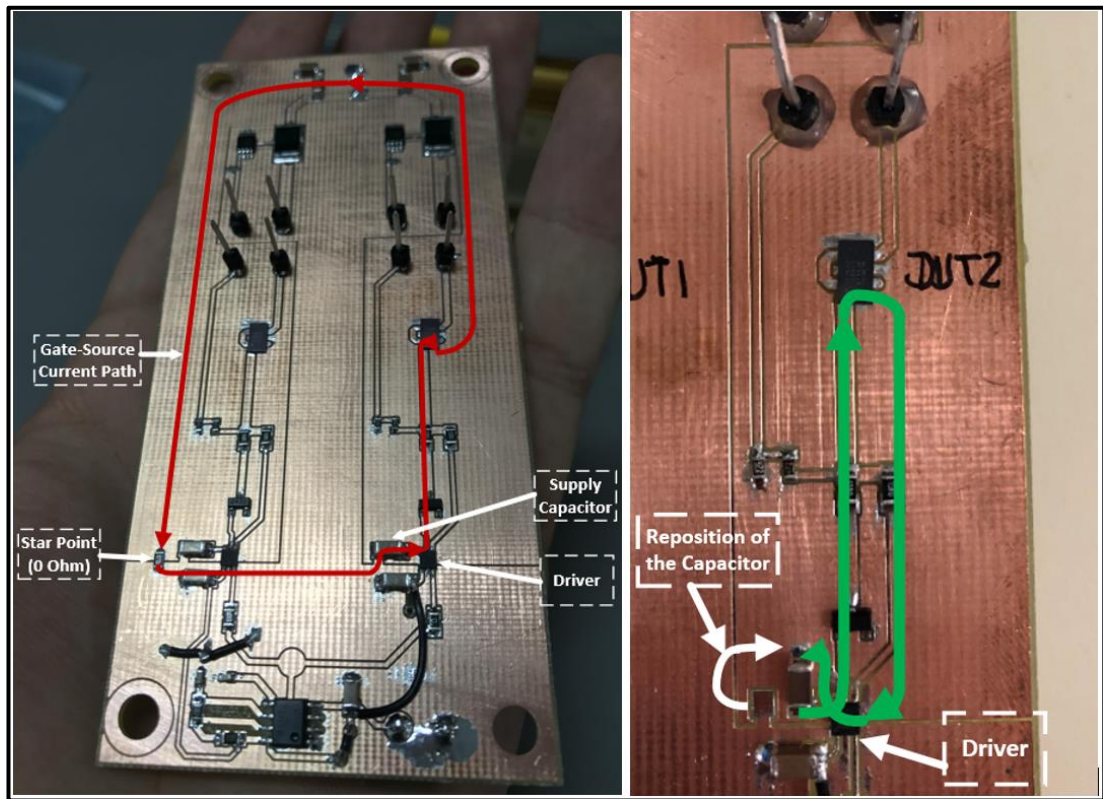
Figure A.2 GaNFET Vgs current path – Left: initial configuration, Right: final configuration

As a solution to a problem, supply capacitor's reference is changed from signal ground to power ground by reposition of the capacitor as in Figure A.2- right. In this way, the current route was turned out the new green path shown in the same figure. This is rather a short way comparing to the previous path (red). Problem was solved by this shorter gate current path, and both DUTs on the same PCB were started to switch properly at the same time. Both the V_{ds} and I_{ds} waveforms belonging to DUT1 and DUT2 became smooth square waves.

B. Detailed Proton Irradiation Test Procedure

1. **Preparation:** METU-DBL applied its own procedure and made necessary preparation. (Current/flux adjustment by proper dosimetry measurements, PCB holder X-Y positioning control, beam stopper control, relay control, etc.)

2. **Pre-Irradiation phase:** Before the irradiation, supply voltages were turned on for PCB-1 and DUTs started to switch. For 5 seconds, Vgs and Ids signals were recorded for both DUTs (5 Msample for each signal with a sampling rate of 1Msample/second).

3. **Irradiation phase:** Then, beam stopper was opened, and DUTs were irradiated with given flux while the DUTs were switching. When the aimed fluence level was reached in 12.5 seconds, beam stopper was closed to stop the irradiation. The total fluence level of 10^{11} protons/cm^2 was reached. V_{gs}-I_{ds} measurements for both DUTs were recorded for also irradiation time interval of 12.5 seconds. (12.5 Msample for each signal with a sampling rate of 1 Msample/second).

4. **Post-irradiation phase:** After beam stopper was closed and irradiation was stopped, post-irradiation measurements were also recorded for 5 seconds by switching on the GaNFETs. (5 Msample for each signal with a sampling rate of 1Msample/second).

5. **PCB2 phases:** When recording is finished for test PCB-1, test PCB-2 was moved to the irradiation window by the remote control of PCB carrier apparatus. Same procedure, applied to test PCB-1 so far, was also implemented for test PCB-2 and same measurements were saved for 2 DUTs on it.

6. **Destructive irradiation phase:** Lastly, after the measurement of the mentioned phases finished in the written order, destructive irradiation was performed for 30 minutes with the same flux level for only two DUTs on test PCB-1. The scope was monitored during the destructive phase to see if there would be a problem on signals indicating the device is short-circuited or open-circuited in its internal structure. It was planned to stop irradiation if the failure was detected by monitoring of the waveforms on the scope. No anomaly was observed on the scope screen and during 30 minutes of a destructive phase. The total fluence level of 1.476×10^{13} protons/cm^2 was reached. Last 10 seconds of switching waveforms of destructive irradiation phase were recorded. (10 Msample for each signal with a sampling rate of 1Msample/second).

C. Detailed Gamma-Ray Irradiation Test Procedure

1. Pre-Test and Characterization
- Nine test samples and one reference sample for each brand, a total of 20 components were switched at 50 V-Vds and 1 A-Ids at 2 kHz frequency (exact value: 1.93 kHz) on an individual basis in the irradiation test site at room temperature before the irradiation starts. For 1,5 milliseconds time interval having 3 switching cycles, V_{ds}-I_{ds}-V_{gs} waveforms were recorded with an oscilloscope with 2.5 GS/s sampling rate in LabNotebook file format. Besides, for 100 nanoseconds time interval, the V_{ds}-I_{ds}-V_{gs} turn-on waveforms were recorded as well.

2. Irradiation Setup
- Irradiation room cards were positioned in a way that they were perpendicular to gamma-ray radiation direction.
- Three of the devices from each brand, a total of 6 devices, were biased with 50V from their drain pins, and their gate and source pins were grounded. 3 GaNFETs from each brand, a total of 6 devices, were biased with 4.7 V from their gate pins and their drain and source pins were grounded. Remaining three devices from each brand, a total of 6 devices, were remained unbiased. Additionally, gate, source, and drain terminals of these components were grounded.
- Radiation dose was adjusted to 12,5 kRad (Si)/hour. With the proper dosimetry methods, the dose rate was correlated.

3. Irradiation
- All devices on both irradiation room cards were irradiated for 1 hour to reach the total exposure level of 12,5 kRad (Si). Irradiation start time was recorded.

4. Device Health Check Test
- Irradiation was stopped, and biases on gates and drains were cut off. Irradiation stop time was recorded.
- Irradiation room PCBs were transported from irradiation room to test room for post-irradiation electrical tests. Time was recorded.
- Gate-drain-source terminals of each device under test shorted together individually at the test desk.
- Reference samples were switched at the same electrical conditions as in Step-2: Pre-Test and Characterization (50 V-V_{ds} and 1 A-I_{ds} at 2 kHz).

- Nine test samples and one reference sample for each brand, a total of 20 parts were switched at 50 V-V_{ds} and 1 A-I_{ds} at 2 kHz on an individual basis in the test room at room temperature. For 1.5 milliseconds time interval having 3 switching cycles, V_{ds}-I_{ds}-V_{gs} waveforms were recorded with an oscilloscope with 2.5 GS/s sampling rate. Besides, for 100 nseconds time interval, the V_{ds}-I_{ds}-V_{gs} turn-on waveforms were recorded as well. Health check test start and finish times were recorded.
- It was assured that the time interval between the completion of the irradiation and the beginning of the health check test was shorter than the 10 minutes.

5. Reirradiation
- Steps 3-4-5 were repeated for 25-50-100 kRad (Si) levels, meaning that 1-2-4 hours of reirradiation time intervals were applied.
- It was assured that the time between two consecutive irradiations did not exceed 2 hours.

6. Annealing at Room Temperature
- Components were kept at irradiation room temperature $\pm$ 5 °C and not to exceed 30 °C for 24 hours.
- During 24 hours of room temperature annealing, devices were biased with the same conditions applied in the irradiation.
- Devices were tested as in step-2 just after the 24 hours of room temperature annealing, and necessary recordings were retaken with the same switching conditions